2019

Detection of DDH in Infants and Children Using Audible Acoustics

Tanvir Hassan
University of Central Florida

DETECTION OF DDH IN INFANTS AND CHILDREN USING AUDIBLE ACOUSTICS

by

TANVIR HASSAN
B.S Bangladesh University of Engineering and Technology, 2014

A thesis submitted in partial fulfillment of the requirements
for the degree of Master of Science
in the Department of Mechanical and Aerospace Engineering
in the College of Engineering and Computer Science
at the University of Central Florida
Orlando, Florida

Fall Term
2019

Major Professor: Hansen A. Mansy

ABSTRACT

Detection of developmental dysplasia of the hip (DDH) in infants and children is important as it leads to permanent hip instability. Current methods for detecting DDH, such as ultrasound and x-rays, are relatively expensive and need qualified medical personnel to administer the test. Furthermore, x-ray ionizing radiation can have potential harmful effects. In the current study, an acoustic non-invasive and simple approach was investigated for detection of DDH. Different benchtop simplified models and pig models were constructed and tested. Models were stimulated with band-limited white acoustic noise (10-2500 Hz) and the response of the models was measured. The power spectrum density, transfer function, and coherence were determined for different hip dysplasia levels and for normal cases. Results showed that the power spectrum density, transfer function, and coherence were affected by dysplasia occurrence. Effects appear larger for more severe dysplastic hips. This suggests that the proposed approach may have potential for DDH detection.

ACKNOWLEDGMENTS

I would like to express my sincere gratitude towards my advisor Dr. Hansen Mansy for supporting me throughout this research with his patience, ideas, and guidance. He has taught me the methodology to carry out research and to present the research works as clearly as possible.

Besides my advisor, I would like to thank the rest of my thesis committee: Dr. Alain Kassab and Dr. Sang-Eun Song for their valuable inputs in my research.

My sincere thanks also goes to Dr. Richard Sandler, and Dr. Charles Price for helping me in my research through their enthusiasm, and immense knowledge.

In addition, I would like to thank Logan Mckinney and Gregory Fobes as well as my other fellow lab mates in Biomedical Acoustic Research Laboratory for their continuous support.

Last but not the least; I would like to take the opportunity to thank my family and friends for their spiritual support throughout my life.

TABLE OF CONTENTS

LIST OF FIGURES

LIST OF TABLES

CHAPTER 1: INTRODUCTION

Developmental dysplasia of the hip (DDH) in neonates is common with approximately 2-3 per thousand neonates suffering from the condition [1]. It is widely acknowledged that early intervention of patients with DDH can lead to decreased rate of late presentation [2], while delayed detection may cause deferred and less effective treatment resulting in chronic disability in these children. Current screening methods in infants include certain physical examination techniques (e.g., the Ortolani and Barlow maneuvers), but these require significant skill and training to perform reliably. While ultrasonography can be used as screening tool, it utility is limited by unavailability in low resource settings, and reliance on highly trained professionals [3, 4]. Therefore, for primary care providers in the USA, especially for developing regions, it would be useful to develop new non-invasive, easy to use, and accurate tools for DDH detection.

Sound transmission in the human body can be affected by the tissue composition along the sound path and the surrounding structures. Therefore, acoustic transmission may correlate with pathologies involving structural changes. Previous studies utilized sound transmission to detect a variety of pulmonary, gastrointestinal, vascular, and cardiac conditions [5-10].

DDH may also be detectable using sound transmission because this condition involves anatomical changes that may affect sound transmission through the hip joint. Previous studies suggested the utility of sound transmission measurements for detection of bone and joint changes. For example, Richardson et al. [11] used sound attenuation of a 256-Hz tuning fork to diagnose DDH. The tuning fork was placed on the patella and the sound transmission was detected with a stethoscope over the lower abdomen. In all of 56 observations made on 18 children with congenital dislocation of

the hip, a unilateral reduction in sound transmission was noted in 53 cases. When a normal hip is flexed the sound detected remained the same or decreased, if the hip is dislocated the sound amplitude increased.

Kwong et al. [12] used an excitation system that generated pink noise at the sacrum. A hand-held shaker (Bruel & Kjaer, Type 5961) with a mild vibration force (<0.7 N RMS) was used to detect transmission differences between normal neonates and those with unilateral DDH. Results showed that the coherence of sound transmitted to the two hips was high (0.89-0.96) for preschoolers, neonates and adults. The highest coherence was found in the adult group, whereas the lowest coherence was found in the preschool group. Overall, the neonate's coherence was slightly lower than the adults in that study. A second study [13], used the same technique and found a significant difference between the normal neonates and patients with unilateral DDH. A discrepancy parameter was calculated and a cut-off discrepancy of 2.0 dB achieved a sensitivity of 100% in detecting DDH. Frequency bands that were most effective were around 200, 250, and 315 Hz.

Safa et al. [14] used an electroacoustic exciter with a range of 20Hz to 20 KHz and two microphones to differentiate between normal and abnormal hips. The study reported that dysplastic hips had lower sound transmission values than normal hips in a study of 22 patients (average age 5.9 years; range 0.3-14 years). In that study, patients were tested in four positions: a) hips and knees neutrally positioned and measurements performed between the patella and the pubis symphysis, b) hips and knees neutrally positioned and measurements performed between the patella and the anterior superior iliac spine (ASIS), c) hips and knees positioned at 45 degree and 90 degree of flexion, respectively, and measurements performed between the patella and pubis symphysis, and d) hips and knees positioned at 45 degree and 90 degree of flexion, respectively,

and measurements performed between the patella and the ASIS. In each position, the sound generator was placed on the patella and the receiver was applied on the pubis symphysis and ASIS. It was shown that sound transmission values of dysplastic hips were always lower than that of normal hips when the hip and knee were flexed. It was also shown that sound transmission values decreased with age. While previous studies have provided useful insights, the measurement system involved varied significantly among studies. It can be concluded, however, that accurate quantification of acoustic transmission in the body requires robust systems for sound generation and detection.

1.1 Research Objective

The main focus of this study was to build and test an acoustic system and technique for DDH screening in neonates. Simplified benchtop models and pig models were developed. Subjects were stimulated with acoustic signals, and sound transmission was measured. The power spectrum density, transfer function, and coherence, were determined for s normal hip geometry and for hip dysplasia. Another objective of this study is to design and test a system for measuring sound transmission in the body. The study aims include determining: (1) the static load needed to reach a target SNR (>20 dB) at the measurement points and a coherence (>0.8) between excitation and measurement points; (2) the exciter sensitivity to static load changes; (3) the exciter input maximum power and corresponding acceleration that results in acceptable signal to noise ratio. These results will help guide the choice of optimal exciter that can: (1) withstand sufficient static load (~500g), which would provide coupling to the bone to reach a target SNR and coherence; (2) has low sensitivity to load (low variability for a load change ~100 gm); (3) provide sufficient acoustic excitation energy to maintain the target SNR and coherence; (4) available at a reasonable

cost (~<$500); (4) insures patient comfort, such that no subject discomfort would be reported for a contact area of ~ 3 cm^2).

CHAPTER 2: SOUND TRANSMISSION: BENCHTOP MODELS

2.1 Hardware and Analysis

A computer-controlled system was constructed to generate and measure acoustic signals in order to quantify acoustic transmission across joints. The computer was connected to a data acquisition module (Model: NI USB-6211, National Instruments, Austin, TX). A MATLAB code was written to generate a white noise (50-2500 Hz) signal, to acquire three acoustic signals, and to calculate the transfer function, phase and coherence between the any two of the acquired signals.

The stimulus signal generated by the computer was amplified using a power amplifier that drove an electromagnetic shaker. The shaker then introduced the stimulus signal into the model to be tested. Initially a large shaker (Model: 2007E, the Modal Shop Inc., Cincinnati, OH.) and amplifier (Model: TS200, Accel Instruments Corp., Irvine, CA) were used. Smaller amplifiers and shakers were also used in order to build a more compact system (Chapter 3).

Three uniaxial accelerometers (Model 352C65, PCB Piezotronics, Depew, NY) were used to detect the stimulus and the transmitted signals at the excitation and the two measurement points. A multi-channel charge amplifier (Model: 480B21, PCB Piezotronics, Depew, NY) was also used to amplify the accelerometer output. The above accelerometers had a sensitivity of 100 mV/g and do not allow measurement of acceleration > 50g. For cases when the acceleration was > 50g, an accelerometer (Model 3220A, Dytran Instruments Inc., Chatsworth, CA) with a sensitivity of 10 mV/g was used.

2.1.1 Power Spectral Density Function (PSD)

The power spectral density function (PSD) is a measure of the strength of the vibrations (energy) as a function of frequency [15]. The unit of PSD is energy per frequency (Hz). Calculations of PSD were done by Fast Fourier Transform (FFT).

2.1.2 Transfer Function (TF)

The following equation was used to calculate the transfer function ($TF_{xy}(f)$) [16].

$$TF_{xy}(f) = \frac{P_{xy}(f)}{P_{xx}(f)} \quad (1)$$

Here, P_{xy} is the cross power spectrum between the two signals, P_{xx} is the power spectrum of the first signal.

2.1.3 Phase

The following equation was used to calculate phase delay ($\varphi_{xy}(f)$) [17] between two signals *x*, *y*:

$$\varphi_{xy}(f) = tan^{-1}\left(\frac{Imaginery\ P_{xy}(f)}{Real\ P_{xy}(f)}\right) \quad (2)$$

2.1.4 Coherence

The following equation was used to calculate the coherence ($\gamma_{xy}(f)$) between two signals *x*, *y*:

$$\gamma_{xy}(f) = \frac{(|P_{xy}(f)|)^2}{(P_{xx}(f))(P_{yy}(f))} \quad (3)$$

Coherence [18] quantifies the association between the two signals as a function of frequency. It is bound by 0 and 1 where a higher value indicates stronger association.

2.2 Calibration

The accelerometers were calibrated before performing all experiments. Calibration was done by attaching the two accelerometers to the shaker as shown in Figure 1. Then the transfer function, coherence and phase were determined.

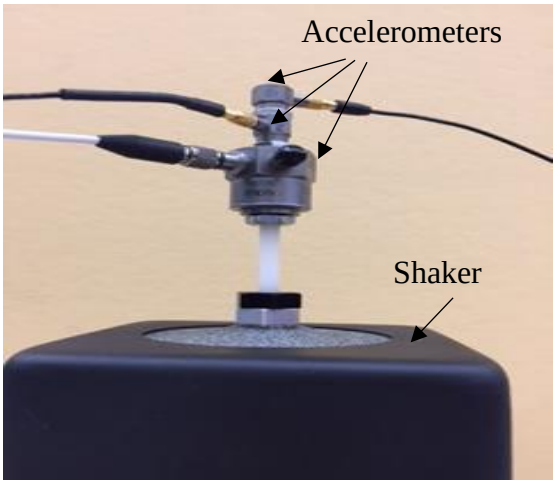

Figure 1: Example calibration set up showing a shaker and three sensors

2.3 Benchtop Models

2.3.1 Two Aluminum Bars

Figure 2 shows the setup utilizing two aluminum bars. Here the lower bar bottom edge was stimulated by the shaker. These aluminum bars were used to simulate the connection between the femoral head and acetabulum at different tilt angles. By changing the angle between the two rods, the surface contact between the rods was altered. This allows quantification of the effects of these geometrical changes on acoustic transmission. Three different angles between the bars were considered: 35, 50, and 90 degrees. To measure the acoustic signal at the stimulus and detection

locations, one accelerometer was affixed at the stimulus point (bottom of the lower bar) while the other accelerometer was affixed at the upper end of the top bar. Accelerometer wax (PCB Piezotronics, Depew, NY) was used to couple the accelerometers to their respective locations. Thin tape was used to stabilize the top bar.

(a)Aluminum bars with 0 degree angle

(b) Aluminum bars with 35 degree angle

(c) Aluminum bars with 50 degree angle

(d) Aluminum bars with 90 degree angle

Figure 2: Setup of aluminum bars with different angles

2.3.2 3D Printed Model of A ball and Socket Joint

(a) Case 0: Femoral head completely inside acetabulum

(b) Case 1: Femoral head partially inside acetabulum

(c) Case 2: Femoral head outside the acetabulum

(d) Case 3: Femoral head completely outside the acetabulum.

Figure 3: Setup of different simulated hip joints for the 3D printed model with different connecting points between the simulated femoral head and simulate ilium. These include cases where the femoral head is inside and outside the acetabulum

Figure 3 shows the 3D printed model of a simplified hip joint. The model consisted of two parts. One part was the simplified femur and the other was the simplified acetabulum and ilium. Since the femur is typically tilted by 33-38 degrees when measuring the acetabular index [19], the simulated femur was tested at a tile angle of 35 degrees. Tests were done with the simulated femur in (a) case 0: the normal position (femoral head fully inside the acetabulum) and (b), (c), (d) case 1-3: at 3 different displaced stages. In all cases, the accelerometer wax was used to affix the simulated femur to the desired contact point of the simulated ilium. The accelerometer locations were at the top and bottom points of the model as can be seen in Figure 3.

2.3.3 3D Printed Model of Femur and Ilium Including the Acetabulum:

Figure 4 shows a more realistic model of the femur, ilium and an acetabulum. The femoral head and acetabulum were polished to better simulate the real case.

The model dimensions were extracted from an actual CT. Four different cases were studied in this model: (a) case 0: normal hip, (b) case 1: the smallest level of dysplasia where the femoral head is touching the acetabulum but not throughout the contact surface, which corresponds to the International Hip Dysplasia Institute (IHDI) [20] Grade 1 dysplasia, (c) case 2: femoral head rests on the rim of the acetabulum (IHDI grade 3), and (d) case 3: femoral head is completely outside the acetabulum and touching the ischial body of the ilium (IHDI grade 4). The first accelerometer was placed at the distal articulating surface of the femur (since there is no patella in this model) while the second accelerometer was placed at the iliac crest.

(a) Case 0: normal (no dysplasia)

(b) Case 1: onset of dysplasia (IHDI grade 1)

(c) Case 2: moderate dysplasia (IHDI grade 3)

(d) Case3: severe dysplasia (IHDI grade 4)

Figure 4: Setup of different hip joints for realistic model with different angles.

2.4 Results and Findings

Calibration:

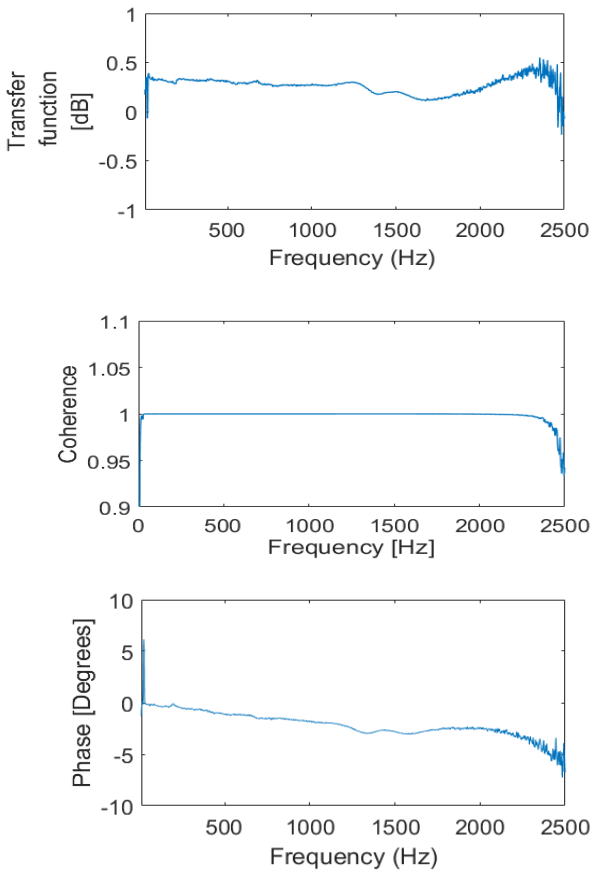

Figure 5: Transfer function, coherence, and phase delay between two accelerometers during calibration

Calibration results are shown in Figure 5 where the transfer function, coherence and phase between two accelerometers are displayed. The results of the calibration showed that in the frequency range of interest (10-2000 Hz), the transfer function (TF) was within ±0.5 dB, coherence was > 95 %, and the phase was 0±5 degrees.

First Simplified Model:

The results of the first model are shown in Figure 6 for four different angles. It can be seen in Figure 6a that the transfer function was close to 0 dB (±0.5 dB, 50Hz<f<2000Hz) when rods were fully touching (angle = 0). This suggests equally efficient transmission at all frequencies (as expected) because of optimal coupling between the two rods at this angle. When the angle increased, there was a gradual loss of transmission in the 50-600 Hz frequency band. The peaks that appear in the spectrum at higher frequencies are probably due to system resonances. The coherence was high for most cases signifying high correlation between the input and output signals. This suggests a strong association between the stimulus and the transmitted signal. This is possibly due to the high model simplicity that allows efficient transmission and relatively low nonlinear effects and resonances, except at the 90 degree case, where low transmitted signal amplitudes resulted in loss of coherence. Figure 6c shows the Phase angle between the two accelerometer signals. The phase was nearly zero (±5 degrees, 50Hz<f<2000Hz) when the two bars were aligned. A very small phase delay is expected in this case since the speed of sound is significantly high. At higher angles, the angle remained small but phase delay became noticeable at high frequencies, which suggests additional delay at the connection between the two rods possibly due to nonlinearities. For the 90 degree case, the phase delay may not be reliable since the transmitted signal was significantly inhibited.

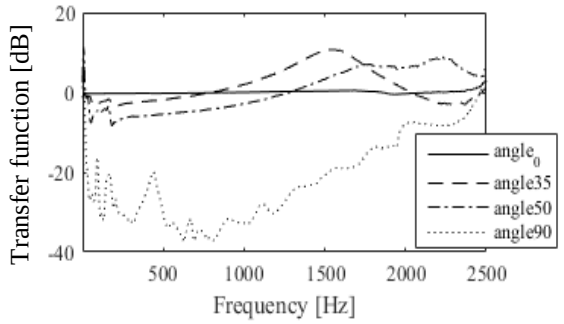

(a) Transfer function comparison for model 1 at different tilt angles (geometry shown in Fig 2). When rods were fully touching (angle=0), transmission was equally efficient at all frequencies as expected. When angle increased, there was a gradual loss of transmission in the 50-600 Hz frequency band.

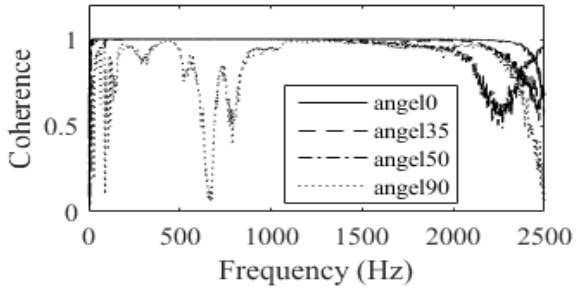

(b) The coherence function for model 1. Coherence was close to 1 for most cases except the case with the largest angle; where heavily attenuated transmitted signals lead to lowered coherence.

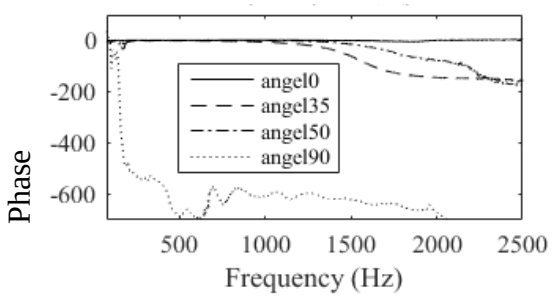

(c) Phase angle between the two accelerometer signals for model 1. The phase was close to zero when the two bars were aligned. A very small angle is expected in this case due to the high speed of sound. At higher angles, the angle remained small but the phase delay became noticeable at higher frequencies which suggests additional delay at the connection between the two rods possibly due to nonlinearities. For the 90 degree case, the delay may not be reliable since the transmitted signal was significantly inhibited.

Figure 6: (a) Transfer function, (b) Coherence, and (c) Phase delay of first simplified model.

3D Printed Model of Simplified Hip Joint:

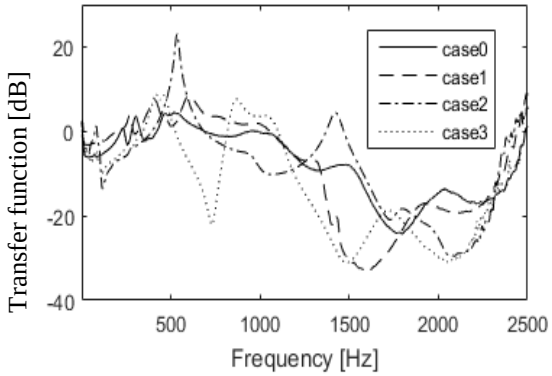

(a) Transfer function comparison for model 2 for the normal and displaced cases. The complexity of the transfer function is likely due to the models complex geometry. However, there was a drop in transfer function for the dysplasia cases in most of 100- 2300 Hz frequency band. The drop in TF was small (0-20 dB) but noticeable at certain frequencies.

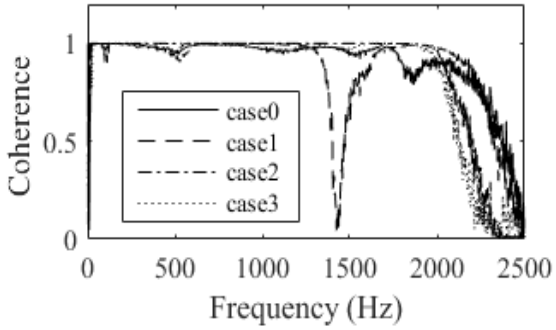

(b) Coherence function for model 2 (shown in Figure 3). The coherence was close to 1 except for high frequencies and around 1400 Hz, where the signal experienced low amplitudes.

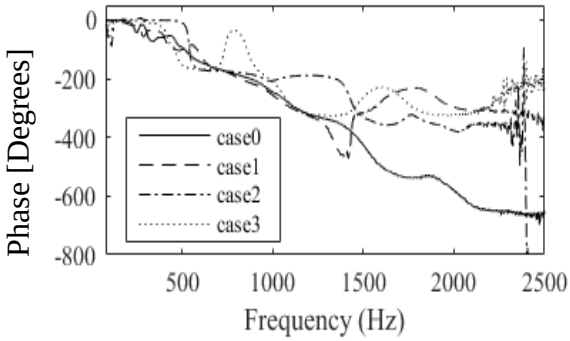

(c) Phase angle between the two accelerometer signals for model 2. The phase (especially for case 0) appears linear with frequency which is consistent with a fixed time delay (i.e., fixed speed of sound of about 150 m/s).

Figure 7: (a) Transfer function, (b) Coherence, and (c) Phase delay for the 3D printed model

The results of the second model are shown in Figure 7 for four different cases (case: 0-3). It can be seen in Figure 7a that when severity of dysplastic hips increased, there was a loss of transmission in most of the 100-2300 Hz frequency band. Case 2 exhibited noticeable resonances around 500 and 1500 Hz. The coherence was high for most cases suggesting strong association between the stimulus and the transmitted signal except for a drop in coherence around 1400 Hz for case 1. The reason is possibly due to the low signal amplitudes resulted in loss of coherence. Figure 7c shows Phase angle between the two accelerometer signals. The phase appears linear with frequency which is consistent with an almost constant time delay (and hence frequency independent speed of sound).

3D Printed Model of Simplified Femur and ilium:

The results of the first model are shown in Figure 8 for 4 different cases. It can be seen in Figure 8a that the there was a drop in the transfer function for the dysplastic cases in most of the 600-2500 Hz frequency band. The coherence was close to 1 except for high frequencies (>2300 Hz) and at around 2000Hz (case: 2) that experienced low signal amplitudes resulted in loss of coherence. Figure 8c shows the phase angle between the two accelerometer signals. Phase delay was noticeable and tended to approach 180 degrees at high frequencies (1100-1600 Hz), which has similarity to the response of some systems containing inertia and stiffness.

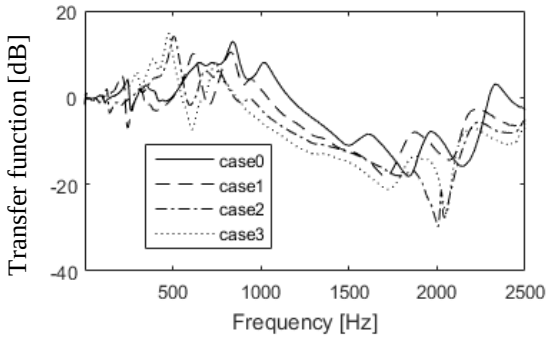

(a) The transfer function comparison for model 3 for the normal and displaced cases (Geometries are shown in figure. 4). There was a drop in the transfer function for the dysplastic cases for most of the 600-2500 Hz frequency range. The TF drop was small (0-20dB) but noticeable at certain frequencies

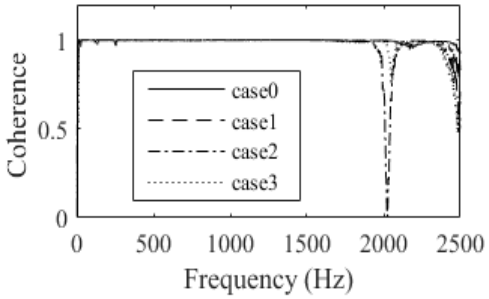

(b) Coherence function for model 3. The coherence was close to 1 except for high frequencies and around 2000Hz where the signals experienced low amplitudes.

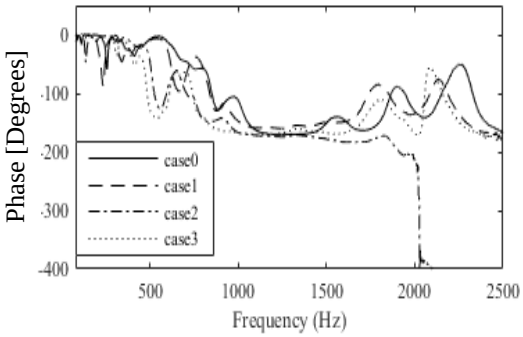

(c) Phase angle between the two accelerometer signals for model 3. Phase delay tended to increase with frequency and approached 180 degrees at high frequencies (1100 -1600 Hz).

Figure 8: (a) Transfer function, (b) Coherence, and (c) phase delay of 3D printed model of simplified femur and ilium of Figure 4.

2.5 Conclusions

The following conclusions are drawn based on the discussion in this chapter:

- The transfer function, coherence, and phase were determined for simulated normal hip geometry and for simulated hip dysplasia
- Results showed that simulated hip dysplasia inhibited sound transmission, which was demonstrated by changes in the transfer function, coherence and phase. The magnitude of these changes appear to correlate with the simulated degree of hip dysplasia.

CHAPTER 3: EXCITERS TO MEASURE SOUND TRANSMISSION THROUGH JOINTS

3.1 Objectives

The objectives of this study is to document the following for each available exciter:

- Static load needed to reach a target SNR (>20 dB) at measurement points and a target coherence (>0.8) between excitation and measurement points.
- Exciter sensitivity to static load changes.
- Exciter input power and corresponding acceleration at the desired SNR and coherence.

The results of this study will help guide the choice of optimal exciters that:

- Can withstand sufficient static load (~500g), which would provide coupling to the bone to reach a target SNR and coherence.
- Has low sensitivity to load (i.e., low variability for a load change ~100 gm).
- Provide sufficient acoustic excitation energy to maintain the target SNR and coherence.
- Available at a reasonable cost (~<$500).
- Insures patient comfort (i.e., no subject discomfort reported for ~1 cm^2 contact area).

3.2 Available exciters

(a) Small exciter (b) Medium exciter

(c) Large exciter (d) iLouder exciter

Figure 9: Available exciters in our experiments

Four exciters were considered (Figure 9). The smallest exciter was a speaker (Model: MX 2, Massive Audio, Los Angeles, CA; weight: 120g; diameter: 2 inch; power rating: 40W max; 5W max input power in our experiment). The medium size exciter was also a speaker (Model: 40-1325A, Radio Shack, Fort Worth, TX; weight: 400g; max diameter: 3.5 inch; power rating: 20W max; 2.5 W max input in our experiment). The largest exciter was a shaker (Model: SF-9324, PASCO Scientific, Roseville, CA; weight: 900g; diameter: 3.54 inch; power rating: 5W max). A 0.5 Watt max was inputted into this exciter and corresponded to an acceleration of about 50 g (about 490 m/s2). The fourth exciter (iLouder, Model: QY40R-Z, Dongguan Qian Yin Electroacoustic Co., Ltd., China, weight: 199g; max diameter: 1.73 inch; power rating: 20W max; 0.75 W max input in our experiment) was a contact speaker.

3.3 Methods

3.3.1 Benchtop Static Force Loading Test

(a) (b) (c) (d)

Figure 10: Experimental set up to study the effect of static load using the benchtop model of soft tissue on (a) small exciter, (b) medium exciter, (c) large exciter, and (d) iLouder exciter

The experimental setup for testing the effect of static load is shown in Figures 10 and 11. A soft cylinder (d=25mm, thickness= 5 mm, elastic modulus 30 kPa) was placed on top of exciters (one at a time). A static load was applied on top of the soft cylinder by a force gauge (Model DS2-4, Imada, Japan). An accelerometer (Model 352C65, PCB Piezotronics, Depew, NY, or Model 3220A, Dytran Instruments Inc., Chatsworth, CA) was rigidly connected to the exciter. The static load for the small exciter was: 0, 50, 100, 150 and 200g. The static load for the medium exciter was: 0, 50, 100, 150, 200, 300, 400 and 500g. The static load for the large exciter was: 0, 100, 200, 500, 800, and 1000g. The static load for the iLouder exciter was: 300, 600, 900, 1200, and 1500g.

The maximum loads were chosen such that the maximum static displacement is small (a few mm). The stimulus signal (electrical input to amplifier) was acquired by Channel 1 of the analogy to digital converter. The accelerometer output signal was acquired by Channel 2.

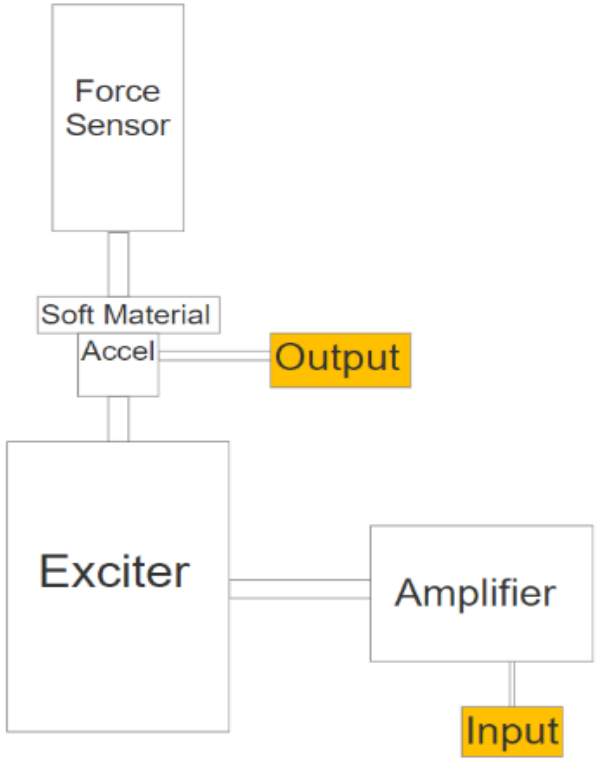

Figure 11: Schematic diagram of set up for benchtop model

3.3.2 Human Subject for Testing Effect of Static Force Loading

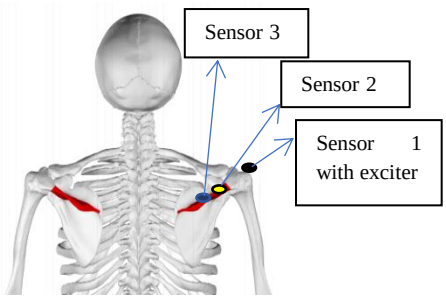

Figure 12: Location of sensors on human subject

Sensor 1 (with exciter) was placed on the greater tubercle. Sensor 2 and 3 were placed on the spine of scapula. Sensor 1, 2, 3 signals were acquired by channel 1, 2 and 3, respectively. Sensor locations are shown in Figure 12 and 13.

Figure 13: Experimental set up for testing the effect of static force loading in humans

3.4 Results: Effect of applied static load

3.4.1 Small exciter- benchtop test

Input Power spectrum density [dB]

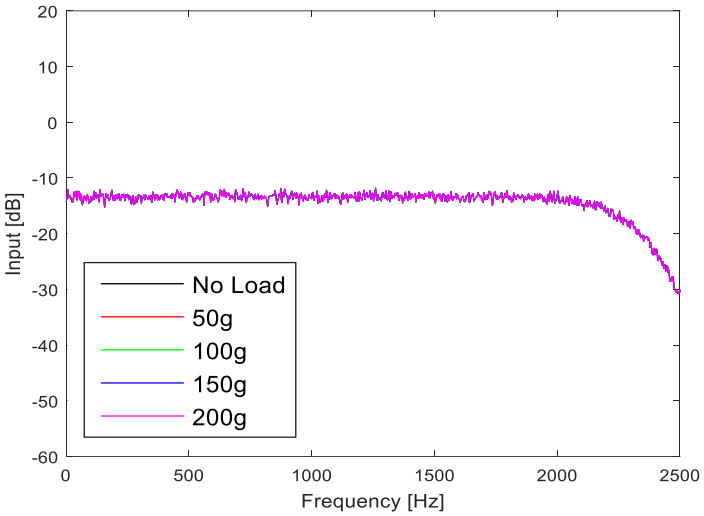

Output Power spectrum density [dB]

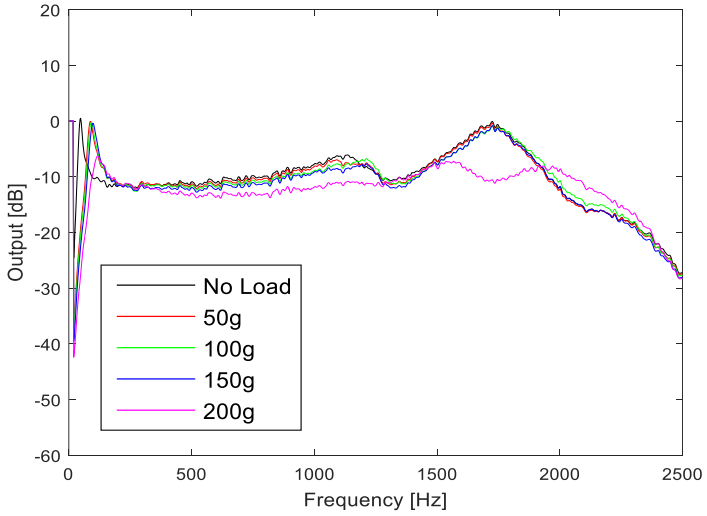

Figure 14: Electrical input, and accelerometer output for benchtop test of the small exciter

Figure 14 shows the input and output PSD for the small exciter at different static loading conditions. While the input stayed consistent, the output signal was affected by the load. Here, it

was observed that for loads between zero and 150g, the PSD signal was similar for frequencies > about 200 Hz. However, for a load of 200g, the PSD showed noticable differences compared to lower loads. The maximum PSD difference was ~10 dB at around 1750 Hz. This suggests that this exciter is less sensitive to loading changes in the 0-150g range. It should be noted, however, that low loading conditions (such as zero loading) may not be preferred as coupling to the bone would be low under these conditions. It also to be noted that there were loading effect at low frequencies (< 200 Hz) for almost all loads.

3.4.2 Small exciter- human subject

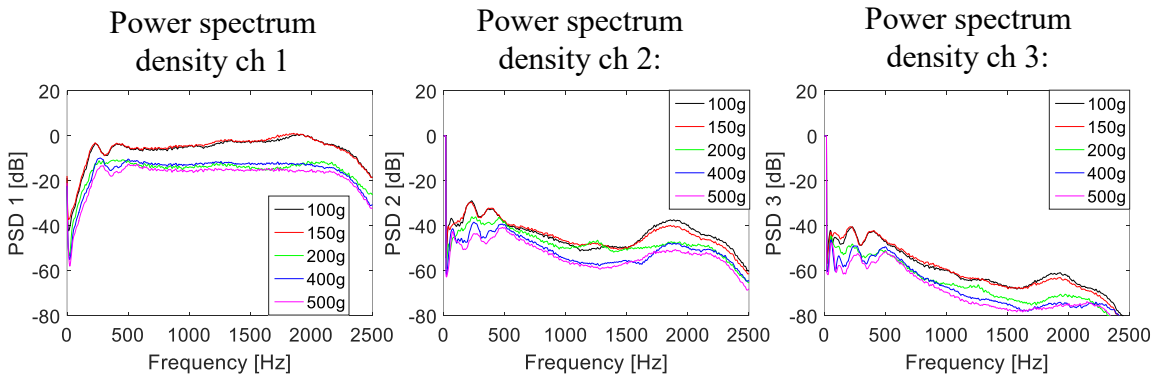

Figure 15: Effect of applied static load on small exciter for human subject at excitation and measurement points PSD for sensor 1, sensor 2, and sensor 3

Figure 15 shows the PSD of sensor 1, 2 and 3 (see Figure 12 for sensor locations) for the small exciter at different static loading conditions. Here, it was observed that for loads of 100g and 150g, the PSD of all 3 sensors were similar for almost all frequencies. However, for loads of 200g, 400g and 500g, the PSD dropped compared to lower loads. The maximum PSD drop was ~15 dB at around 400 Hz for the 500g load. This suggests that the small exciter is less sensitive to loading changes in the 50-150g range. The transfer function between channels was similar for all applied

loads with more similarity for loads of 100g and 150g (Figure 16). This suggests small coupling differences at the stimulus point.

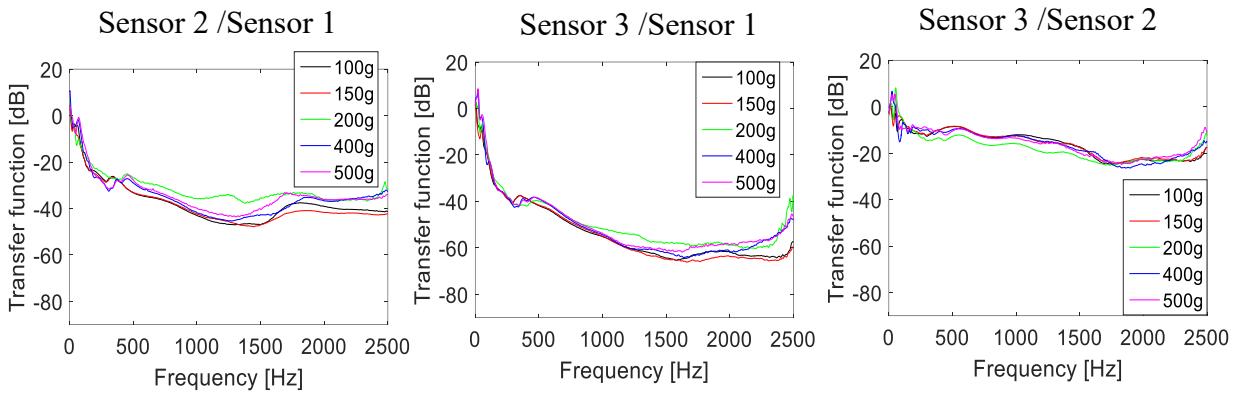

Figure 16: Effect of applied static load on small exciter for human subject at excitation and measurement points TF for sensor (2/1), sensor (3/1), and sensor (3/2).

3.4.3 Medium exciter- benchtop test

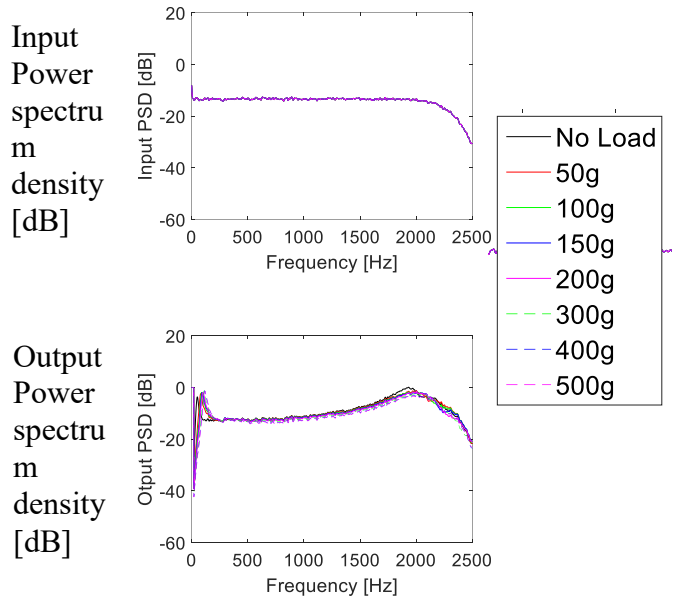

Figure 17: Electrical input, and accelerometer output for benchtop study of medium exciter

Figure 17 shows the input and output PSD for the medium exciter at different static loading conditions. While there was no noticeable change on the input PSD, the output signal was affected by the load. Here, for loads between zero and 400g, the PSD of the signal was similar for loads between 200-1750 Hz. However, for a load of 500g, the output PSD showed slight difference compared to lower loads, where the maximum PSD difference was ~2 dB at ~2000 Hz. This suggests that this exciter is less sensitive to loading changes in the 0-500g range (200<f<1750Hz). There were some loading effects at low frequencies similar to what was observed for the small exciter.

3.4.4 Medium exciter- human subject

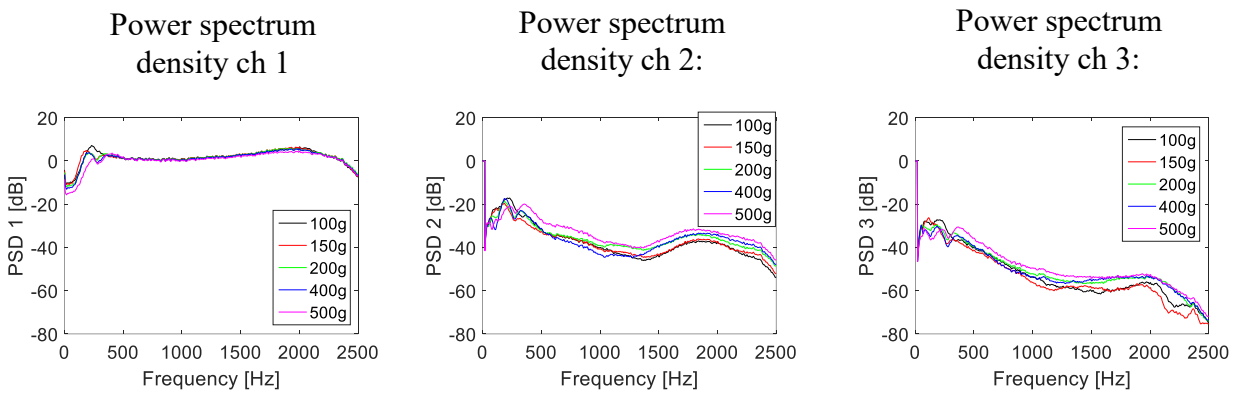

Figure 18: Effect of applied static load on medium exciter for human subject at excitation and measurement points PSD for sensor 1, sensor 2, and sensor 3

Figure 18 shows the PSD of sensor 1, 2 and 3 for the medium exciter at different loading conditions. Here, it was observed that for static loads of 100g- 400g, the PSD signals were similar for sensor 1 at frequencies > about 300 Hz. However, for a load of 500g, the PSD showed a noticeable amplitude decrease below 300Hz. For sensor 2 and 3, there was no consistent load effect trend for f< 300Hz. But the PSD differences for a load of 500g tended to be higher for f> 300 Hz.

This suggests that the medium exciter is less sensitive to loading changes in the 100-400g range. Transfer function between channels was similar for applying 100-400g load (Figure 19). Slight change was visible (<5 dB) for applying 500g load. This may be indicative of increased acoustic coupling at the stimulus point.

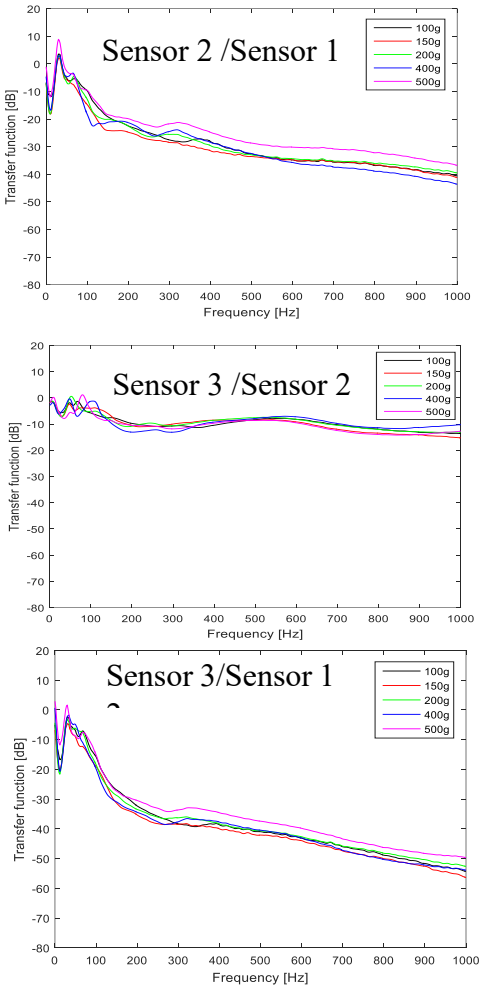

Figure 19: Effect of applied static load on medium exciter for human subject at excitation and measurement points TF for sensor (2/1), sensor (3/2), and sensor (3/1)

3.4.5 Large exciter- benchtop test

Input Power spectrum density [dB]

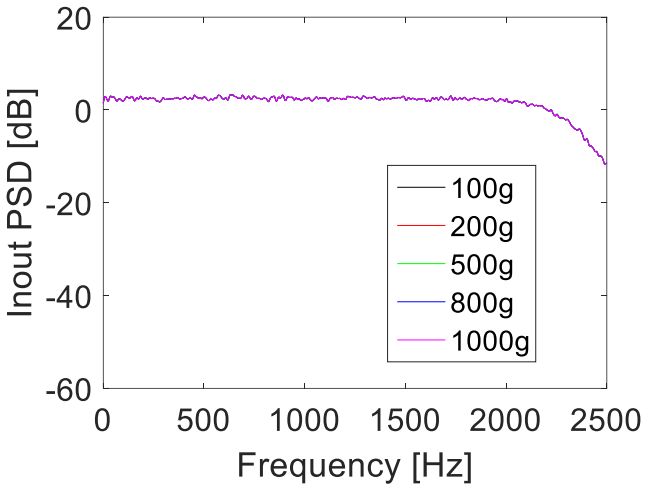

Output Power spectrum density [dB]

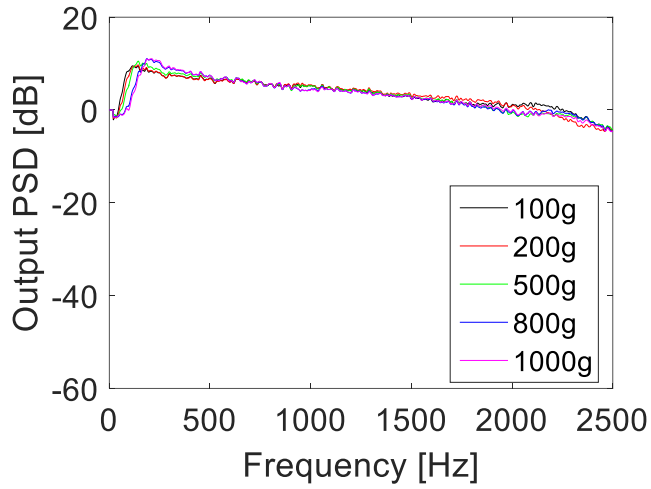

Figure 20: Electrical input, and accelerometer output for benchtop study of large exciter

Figure 20 shows the input and output PSD for the large exciter at different static loading conditions. Similar to the other exciters, the output signal was affected by the load. Here, it was observed that for loads between 100g and 1000g, the PSD signal was similar except in the 50-150Hz where PSD was lower for a load of 800g and above. This suggests that this exciter is less

sensitive to loading changes in the 100-1000g range (except between 50-150 Hz). At low frequencies (<200Hz) the effect of load was not noticeable for loads of 100-500 grams.

3.4.6 Large exciter- human subject

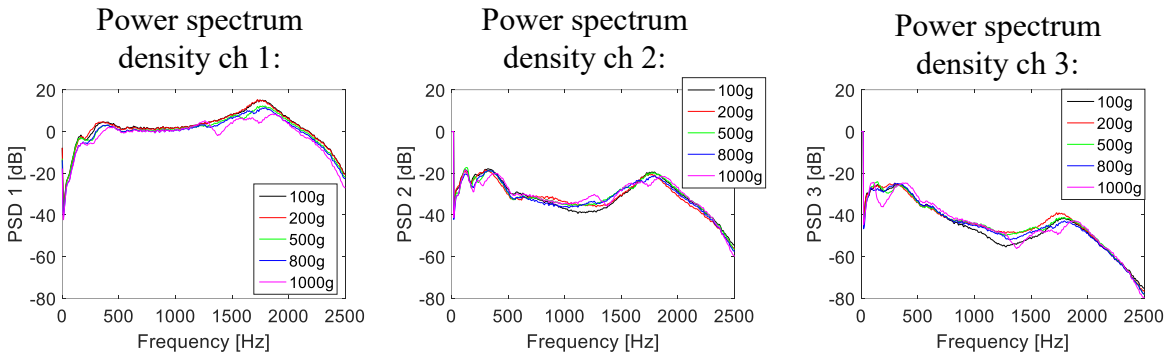

Figure 21: Effect of applied static load on large exciter for human subject at excitation and measurement points PSD for sensor 1, sensor 2, and sensor 3

Figure 21 shows the PSD of sensor 1, 2 and 3 for the large exciter at different static loading conditions. Here, it was observed that for loads of 100-1000g, the PSD signals were similar for all frequencies for sensor 1 and 2. However, for a load of 1000g, the PSD showed a very small drop compared to lower loads for sensor 3. This suggests that the large exciter is minimally sensitive to loading changes in the 100-800g range. It should be noted, however, that applying more than 500g load may cause patient discomfort. Transfer function between channels was similar for loads of 100-1000g. Slight change was visible (~5 dB at 200-300) for applying 1000g load (Figure 22).

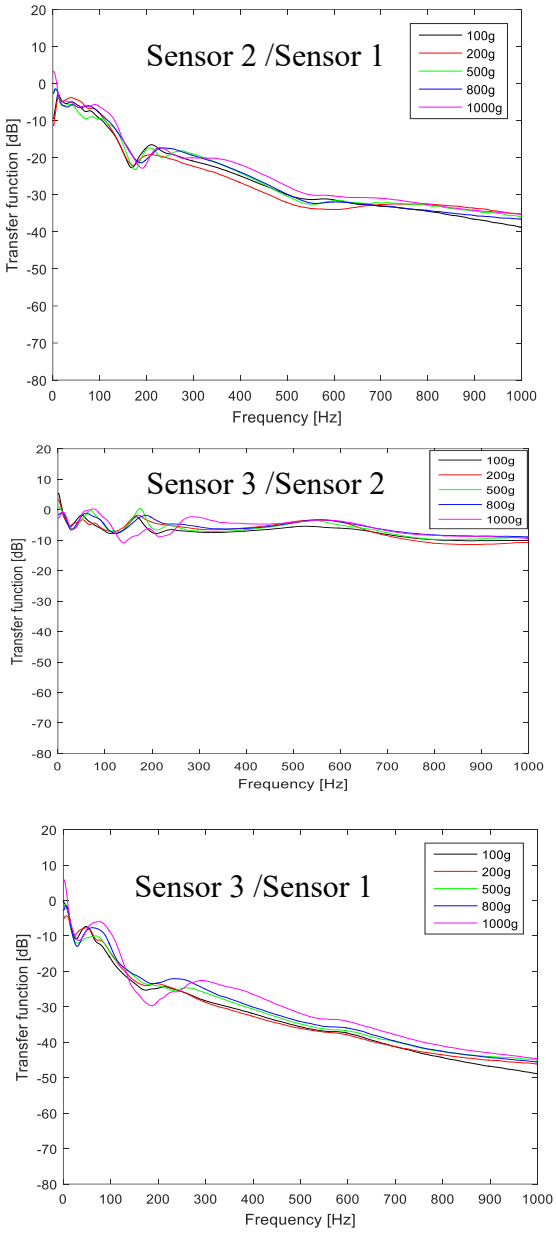

Figure 22: Effect of applied static load on large exciter for human subject at excitation and measurement points TF for sensor (2/1), sensor (3/2), and sensor (3/1)

3.4.7 iLouder exciter- benchtop test

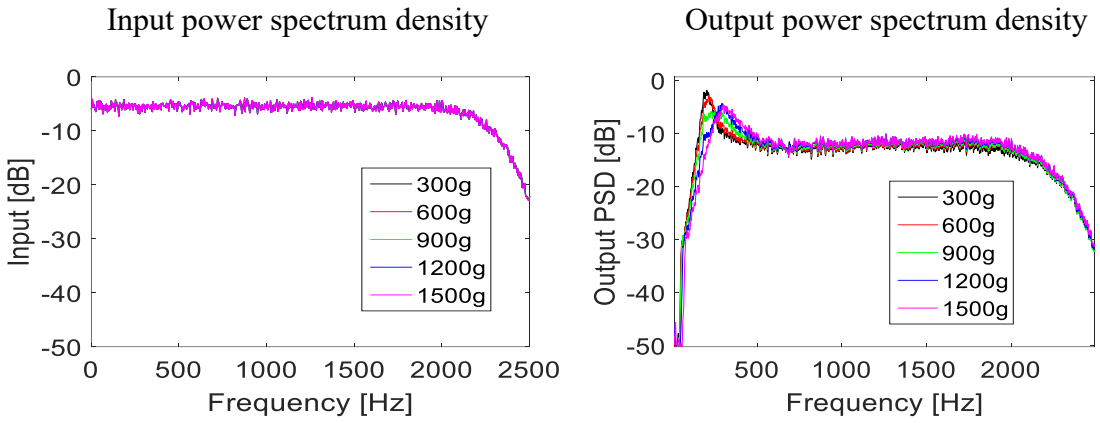

Figure 23: Electrical input, and accelerometer output for benchtop study of iLouder exciter

Figure 23 shows the input and output PSD for the iLouder exciter at different static loading conditions. Similar to the other exciters, the output signal was affected by the load. Here, it was observed that for loads between 100g and 1500g, the PSD signal was similar except in the 50-150Hz where PSD was lower for a load of 900g and above. This suggests that this exciter is less sensitive to loading changes in the 100-1500g range (except between 50-150 Hz). At low frequencies (<200Hz) the effect of load was not noticeable for loads of 100-600 grams.

3.4.8 iLouder exciter- human subject

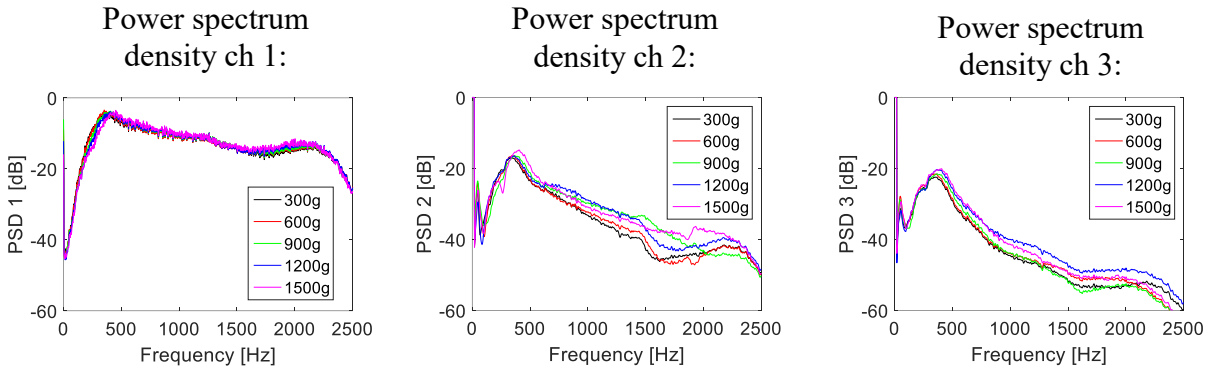

Figure 24: Effect of applied static load on iLouder exciter for human subject at excitation and measurement points PSD for sensor 1, sensor 2, and sensor 3.

Figure 24 shows the PSD of sensor 1, 2 and 3 for the iLouder exciter at different static loading conditions. Here, it was observed that for loads of 100-600g, the PSD signals were similar for all frequencies for sensor 1 and 2. However, for a load of 900g and higher, the PSD showed a small increase compared to lower loads for sensor 2 and 3. This suggests that the iLouder exciter is minimally sensitive to loading changes in the 100-600g range. Increase in PSD may be indicative of increased acoustic coupling at the stimulus point. Transfer function between channels was similar for loads of 100-600g (Figure 25). Slight change was visible for a load of 900g and higher.

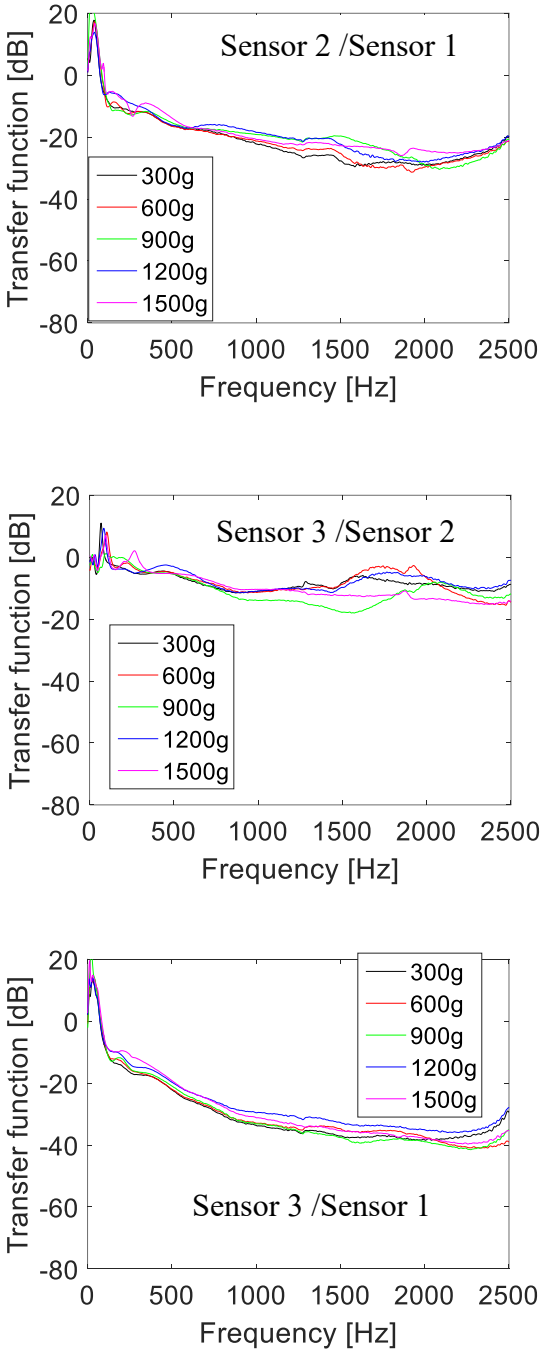

Figure 25: Effect of applied static load on iLouder exciter for human subject at excitation and measurement points TF for sensor (2/1), sensor (3/2), and sensor (3/1)

3.5 Stimulus amplitude requirements at 500 and 1000 gm of static load

3.5.1 Objective

The objective of this study is to determine the excitation acceleration amplitude required to achieve appropriate (> 20 dB) signal to noise ratio.

3.5.2 Methods

The stimulus amplitude requirements were tested in a human subject using broadband excitation. The test protocol steps were as follows:

- Place the "iLouder" exciter at left humeral head and apply 500 gm of static force (repeat for 1000 gm)
- Place two "3523C65" accelerometers at the left scapular spine (5-10 cm away from exciter). Secure accelerometer using a 3M medical grade double sided tape.
- Use a broad band signal from 50-2500 Hz.
- Vary the input excitation amplitude (peak to peak value) between about 0 g and 70 g.
- Calculate the frequency-dependent signal to noise ratio at each excitation level. This is done by calculating signal to noise ratio at different frequencies and then calculating the mean of all the values of SNR.

Prior to this experiment, the relation between the "Amplification factor" in the computer program and stimulus acceleration for the iLouder exciter (with the amplifier volume midway, e.g., at the 12 0'clock position) was documented.

3.5.3 Results and Findings:

Figure 26 shows amplification factor vs SNR channel 1, 2 and 3 at 500g, and 1000g.

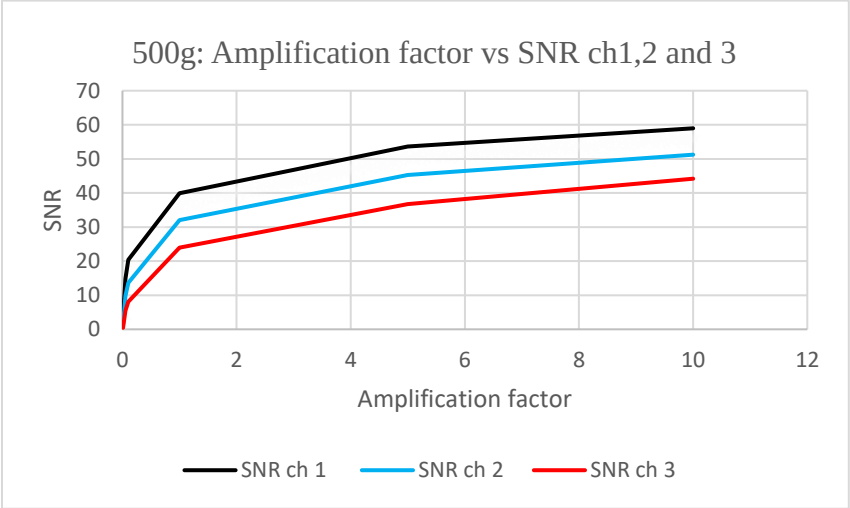

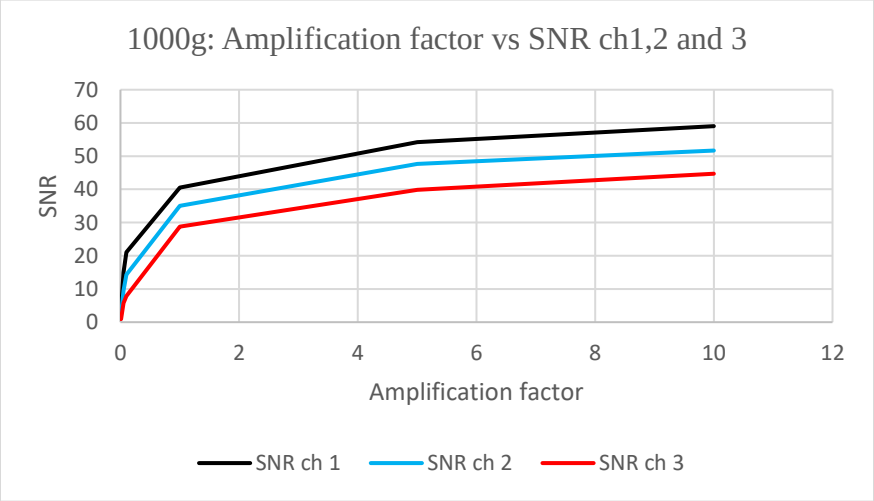

Figure 26: Amplification factor vs SNR channel 1, 2 and 3 at 500g, and 1000g

The data suggests that relatively high SNR (> 25dB) were achieved for amplification factors ≥1.

Figure 27 shows input acceleration vs SNR channel 1, 2 and 3 at 500g, and 1000g.

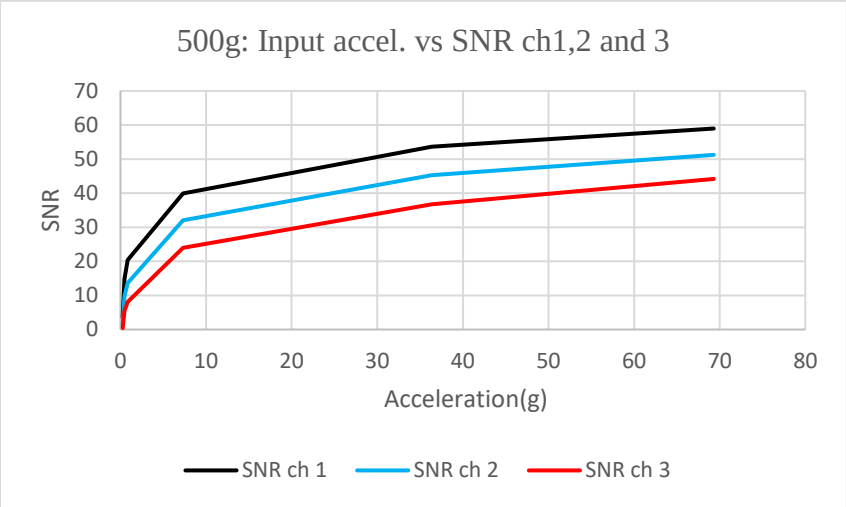

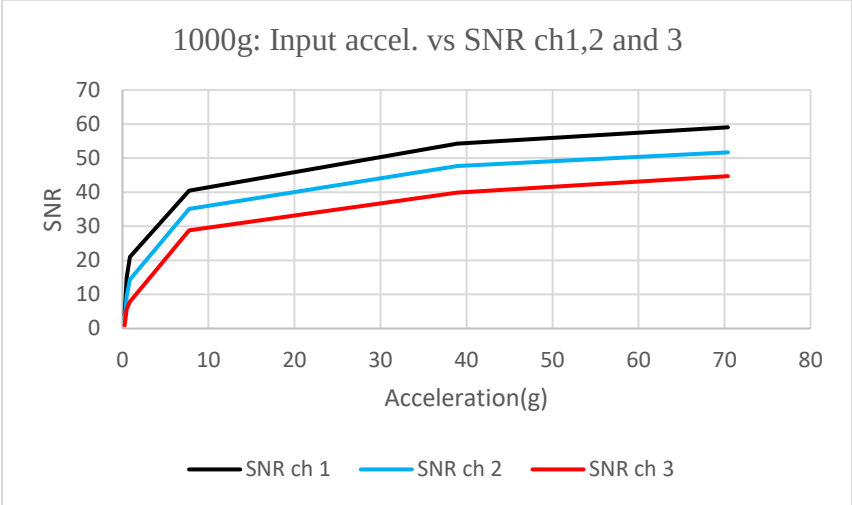

Figure 27: Excitation acceleration vs SNR channel 1, 2 and 3 at 500g, and 1000g

The data suggests that acceptable SNR (>25dB) were achieved for input acceleration of ≥ 8g. Hence, an input acceleration of about 8g would be recommended to achieve this SNR level.

3.6 Comparison of signal to noise ratio for different exciters

Objective:

The objective of this study is to compare signal to noise ratio for different exciters.

Methods:

To compare the possible signal to noise ratio, tests were performed in a human subject to measure the background noise as well as the signal at stimulus and other two measurement locations. The sensor placement are shown in Figure 12 and discussed in section 3.3.2. The experimental conditions were as follows:

- Applied static loading: 100g load was applied to each exciter during the test.
- Input acceleration for exciters were: Small exciter: 22g; medium exciter: 22g; large exciter: 369g and iLouder exciter: 64g.

The tests for each exciter were done in different days, which increase variability, possibly due to changes in senor locations.

The test steps were:

- Apply a static load to the exciter, and place exciter at the stimulus location (Sensor 1).
- Acquire the acceleration signal from all 3 sensors (Figure 12) simultaneously without any stimulus signal.
- Send an excitation signal to the exciter and reacquire the 3 acceleration signal.

The analysis steps were:

- Calculate the spectra for each acceleration signal
- Calculate the transfer function, coherence, and phase difference between each sensor pair (i.e., Sensor 1 and 2; Sensor 1 and 3).

Results and Findings: The spectra for each acceleration signal and the transfer function between sensor pairs are shown in Figure 28. This data suggests the following:

- All of the exciters showed ability to achieve high SNR (> 50dB) at the stimulus point and (> 25dB) at the measurement points.
- The large exciter (PASCO shaker) had the highest SNR at excitation and measurement points. This is consistent with the fact that the input acceleration used for this exciter was also highest.
- The transfer function between the measurement and excitation point was higher for iLouder exciter. This is not expected if the stimulus and measurement points as well as coupling with the skin is unchanged. It is, then, suspected that this observed differences between the transfer functions may be due to experimental setup differences as the experiments for that exciter were done on the different day. Another reason may be differences between input acceleration level. Hence, it is recommended to repeat the experiment for all exciters on the same day to have comparison that is more accurate.
- The transfer function for the "No excitation" case should be ignored since the coherence (see the next section) was low.

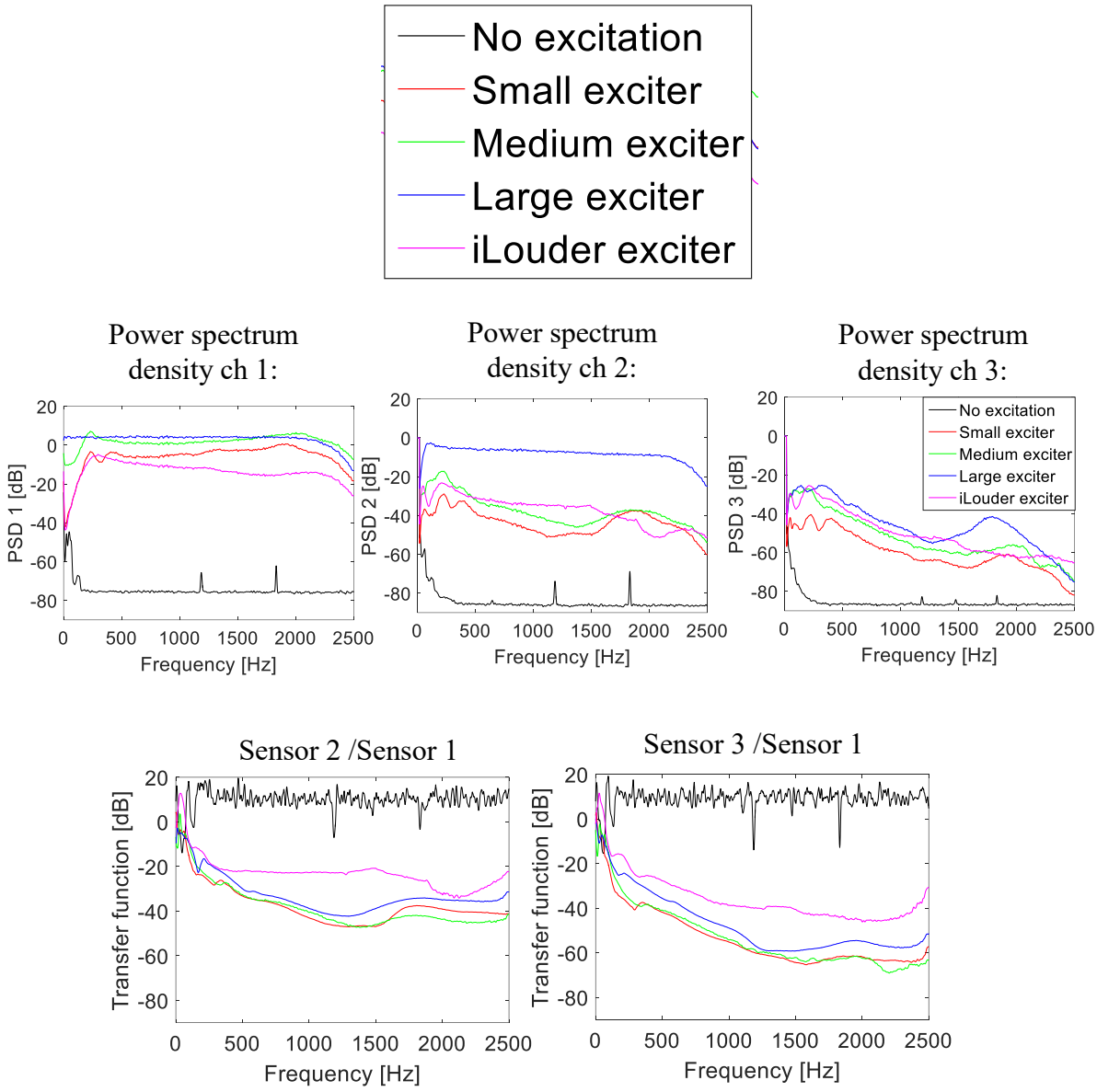

Figure 28: Power spectrum density for different exciters at excitation and measurement points. Transfer function between excitation and measurement points for different exciters.

3.7 Coherence between excitation and measurement points for different exciters

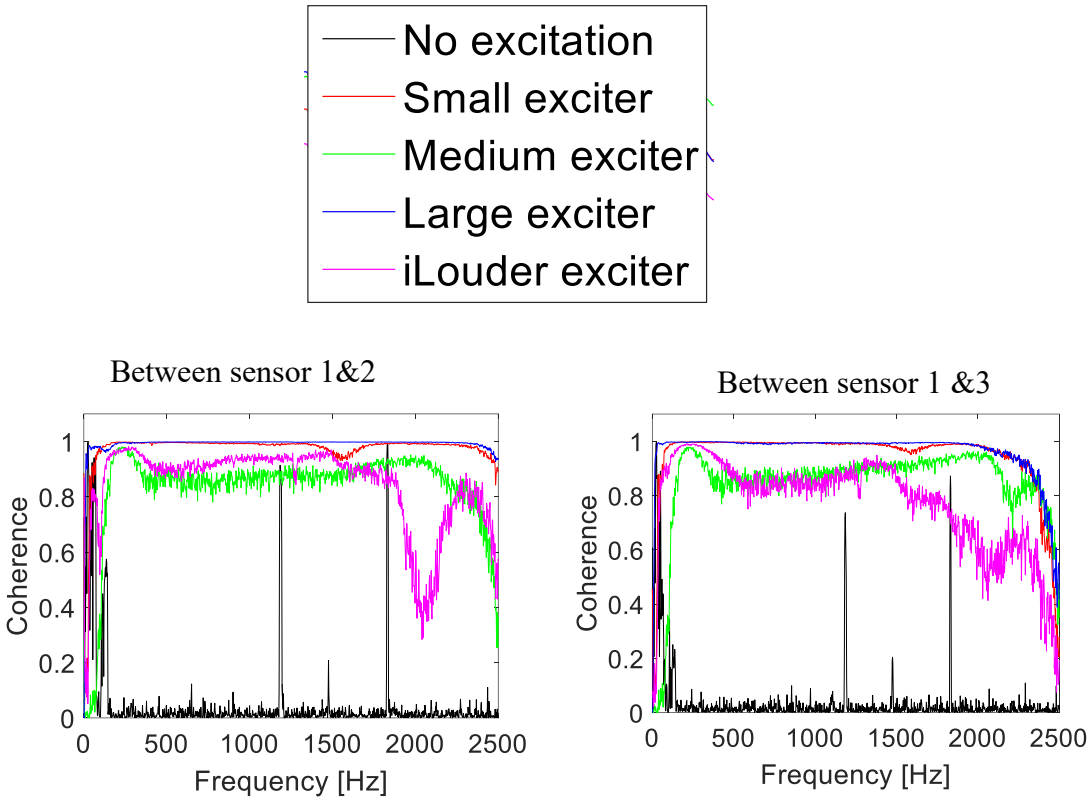

Figure 29: Coherence between excitation and measurement points for different exciters.

Results and Findings: The coherence between the stimulus and measurement points are shown in Figure 29. The data shown suggests the following:

- Coherence was >0.8 for all exciters for frequencies up to 1500 Hz.
- Coherence was higher for the small and large exciter.
- Coherence for the “No excitation” case was very low since noise appears uncorrelated.

3.8 Tuning fork performance

3.8.1 Objective

The objective of this study to quantity the signal to noise ratio when a regular and an electronic fork are used for excitation and the transmitted sounds. Another objective is to explore the utility of using a low cost sensor (piezo disc violin pickup, Model: WCP-60V, Cherub Technology Co Ltd, China) as well as the use of a cell phone microphone (both internal and external microphones will be tested) for the detection of transmitted sounds.

3.8.2 Methods:

The tuning fork was tested on a bench top set up and in a human subject. The experimental set ups for both situations are shown in Figure 30.

Benchtop test: The experimental steps were as follows:

- Place "soft tissue" simulator over the force gauge. Here a heavy memory foam layer (thickness= 5 mm, diameter= 2cm approximately) was used.
- Place an accelerometer (Model 3220A, Dytran Instruments Inc., Chatsworth, CA) above the soft tissue and the tuning fork above the accelerometer.
- Connect stimulus accelerometer (Accel 1) to Channel 1. Accelerometers 2&3 are not used in this experiment.
- Apply as static load of 150, 250, 500 and 1000 gm (one at a time). The contact area for the tuning fork was (2.5 cm^2).
- Measure the stimulus acceleration while the fork is not stimulated.

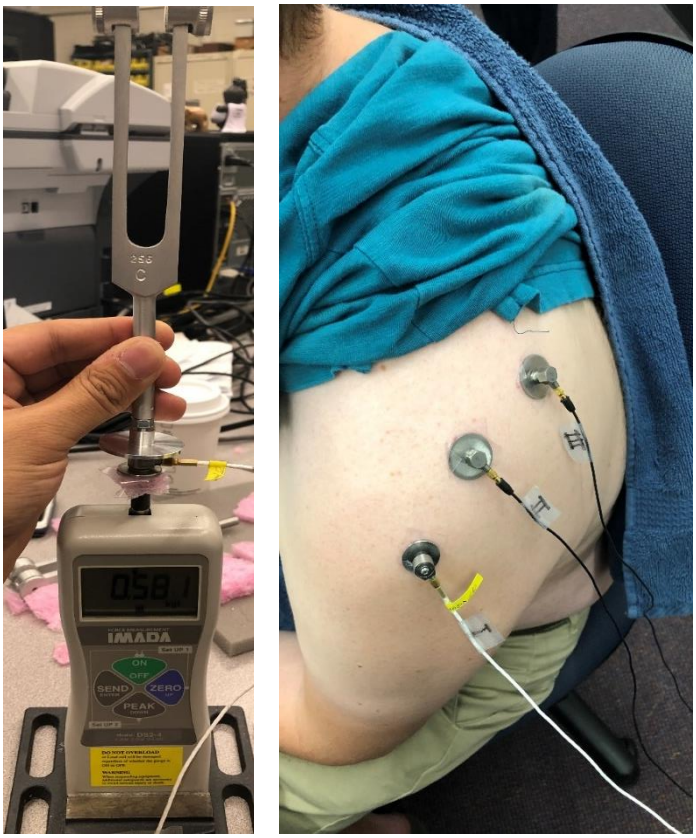

Figure 30: Experimental set up to study the effect of static load on tuning fork using the benchtop test of soft tissue (left) and human subject (right).

- Strike the fork (with its small "hammer") to cause it to "ring" and measure the stimulus acceleration.
- Repeat the experiment for the electronic fork. In this case the stimulus acceleration will be recorded while the fork is on or off and no hammer is needed.
- Quantify the frequency-dependent signal to noise ratio at the stimulus point as the ratio between the spectral value when the form is stimulated divided by the spectral value without stimulation.

Human subject: The experimental steps were as follows:

- Place the fork at left humeral head and apply an approximate static force of 200 gm.
- Place accelerometer 1 between the tuning fork and the skin. Place accelerometer 2, 3 over the scapular spine as shown in Figure 30.
- To test the utility of low cost piezo sensor for transmitted sound detection, place the piezo sensor at the left scapular spine where accel 2 is usually placed. Record excitation and transmitted sounds when the fork is ringing and when it is not.
- To test the utility of using a cell phone microphone (Model: V20, LG Electronics, South Korea) for transmitted sound detection, record sound at measurement point by phone internal microphone, then by the external microphone (Model: PV510+, PoP Voice, USA), respectively. The external microphone was placed in a 3D printed stethoscope head (2cm diameter) with a diaphragm.
- Calculate the signal to noise ratio by dividing the signal amplitude by the amplitude of the amplitude of the case without stimulus, which represents background noise.

3.8.3 Results and Findings

Effect of load on SNR for electronic tuning fork: 128 Hz – benchtop model:

Figure 31 shows output PSD for benchtop study of 128 Hz rated electronic tuning fork.

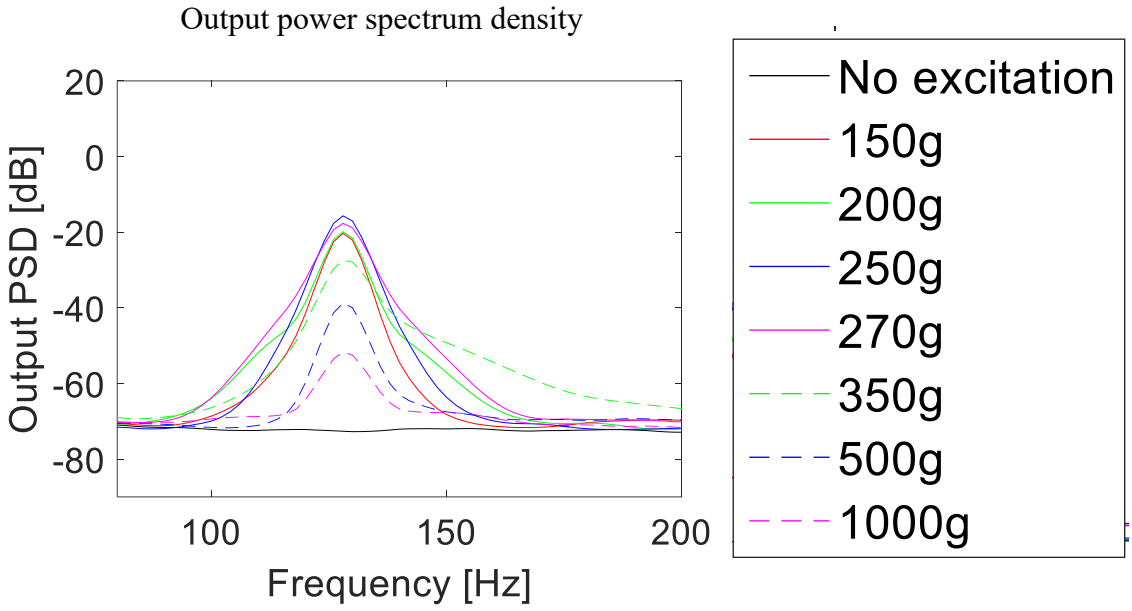

Figure 31: Output power spectrum density for benchtop study of electronic tuning fork

Findings: The data of Figure 31 suggests the following:

- Acceleration of stimulus signal was 6.94g.
- SNR was ~ 60 dB for loads of ≤ 250g.
- SNR starts to decrease for applied loads of ≥ 300g.

Hence, it can be concluded that the electronic tuning fork may be used for loads 100-300g because of the lower SNR at higher loads.

Signal to noise ratio and effect of load on SNR for manual tuning fork: 128 Hz – benchtop model:

Figure 32 shows output PSD for benchtop study of 128 Hz rated manual tuning fork.

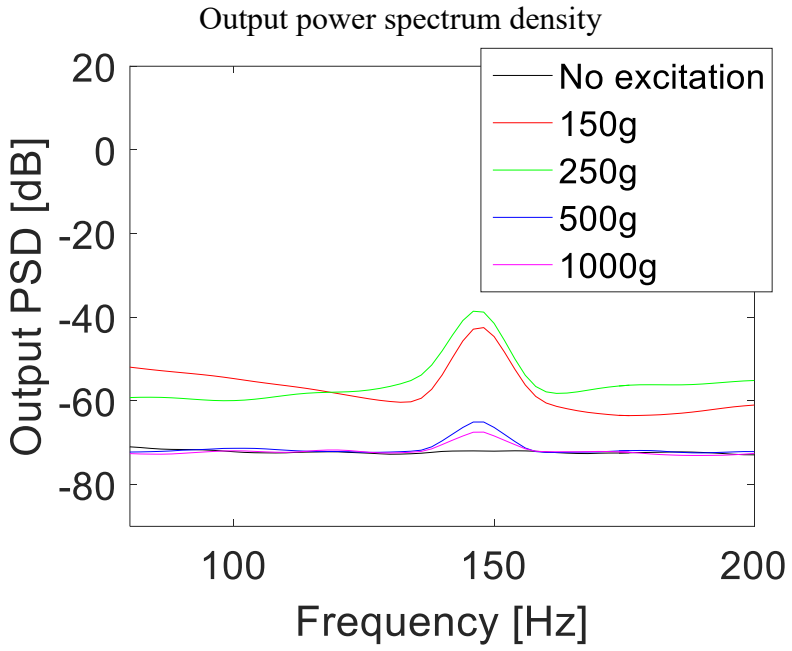

Figure 32: Output power spectrum density for benchtop study of the manual tuning fork

Findings: The data of Figure 32 suggests the following:

- Acceleration of stimulus signal was 0.42g.
- SNR was 35 dB (100-300g load).
- SNR starts to decrease for applied load ≥ 300g.
- Ideal range for load when using manual tuning fork: 100-300g to keep a relatively high SNR.

Effect of load on SNR for electronic tuning fork: 128 Hz – human subject:

Figure 33 shows PSD at excitation and measurement points of a human subject when using a 128 Hz electronic tuning fork.

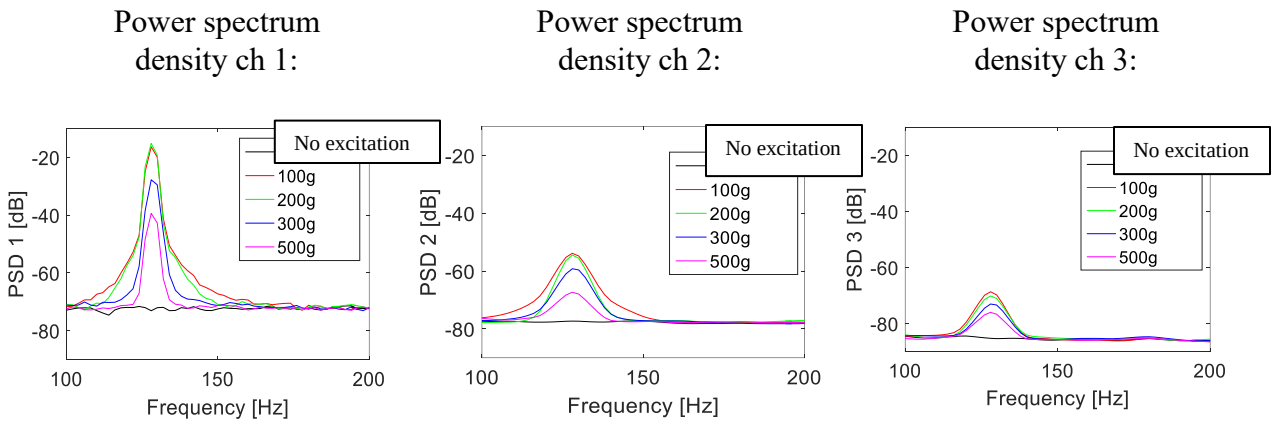

Figure 33: Power spectrum density at excitation and measurement points of a human subject for the electronic tuning fork of 128 Hz

Findings: The data of Figure 33 suggests the following:

SNR at excitation and measurement points:

- Excitation point (ch 1): 60 dB for a 100g load.
- Measurement point (ch 2): 20 dB for a 100g load.
- Measurement point (ch 3): 15 dB for a 100g load.

SNR starts to decrease for a load of $\geq$ 200g.

Ideal range for load when using electronic tuning fork: 100-200g to avoid decreasing SNR.

Signal to noise ratio at different frequencies for manual tuning fork – human subject:

Figure 34 shows PSD at excitation and measurement points of a human subject for applying 128, 256, 512, 1024, 2048 Hz rated manual tuning fork.

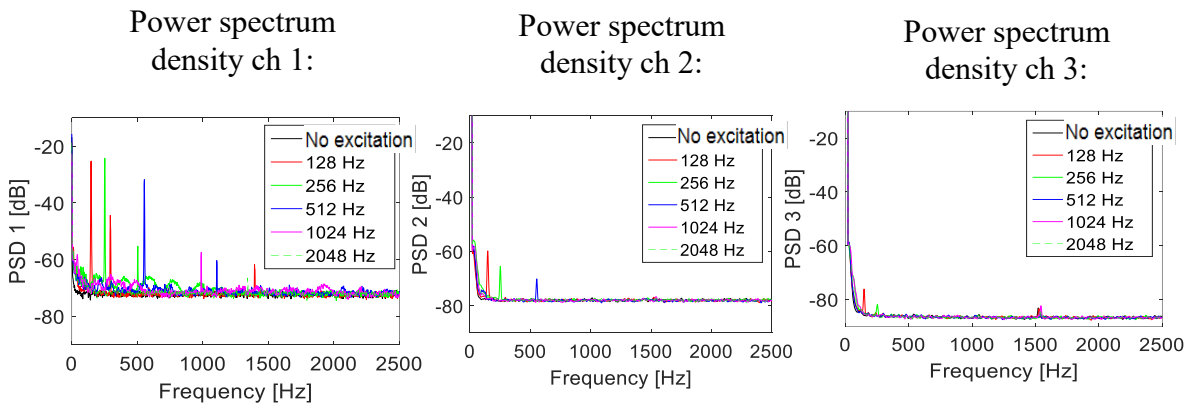

Figure 34: Power spectrum density at excitation and measurement points for a human subject with excitation using manual tuning forks.

Findings: The data of Figure 34 suggests that SNR was higher at excitation points and measurement points for 128 Hz and 256 Hz tuning fork.

Signal to noise ratio for the piezo sensor and PCB accelerometer at a measurement point (Electronic tuning fork: 128 Hz)

Figure 35 shows PSD at measurement point of piezo sensor or PCB accelerometer on human subject for applying 128 Hz rated electronic tuning fork.

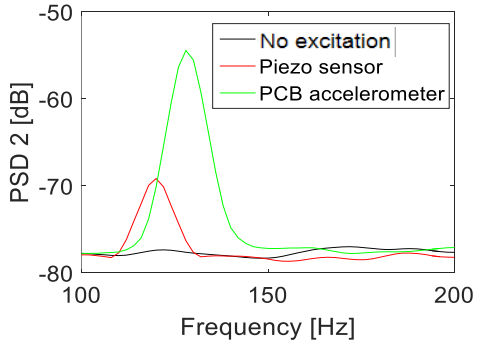

Figure 35: Power spectrum density at measurement point of piezo sensor or PCB accelerometer of human subject for electronic tuning fork of 128 Hz.

Findings: The data of Figure 35 suggests that the piezo sensor can detect the signal at 128 Hz but amplitude is 15 dB less than PCB accelerometer.

Signal to noise ratio for the phone internal microphone and external piezo microphone at measurement point (Electronic tuning fork: 128 Hz)

Figure 36 shows PSD at measurement point of phone internal microphone or external piezo microphone on human subject for applying 128 Hz rated electronic tuning fork.

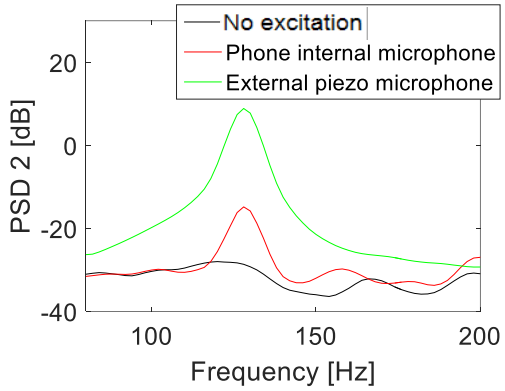

Figure 36: Power spectrum density at measurement the point for the phone internal and external microphone on human subject for electronic tuning fork of 128 Hz

Findings: The data of Figure 36 suggests that the external piezo microphone signal amplitude was about ~ 20 dB higher.

3.9 Benchtop study: The frequency content of the tapping and scratching stimuli

Tapping and scratching at the sacrum was used as an acoustic stimulus. To help interpret the results benchtop tests were carried out to study the spectral content of these signals.

3.9.1 Methods

The experimental set up is shown in Figure 37. The experimental steps were as follows:

- Tapping was done in two ways: first on topping with the middle finger directly of a disc that is connected to an accelerometer (accel 1). Secondly, tapping was also done with a metal bar on a coin that was placed above the accelerometer.
- Scratching was done on top of paper disk placed above the accelerometer.
- Acoustic stimulus (tapping and scratching) was acquired by accelerometer 1 at the stimulus point.

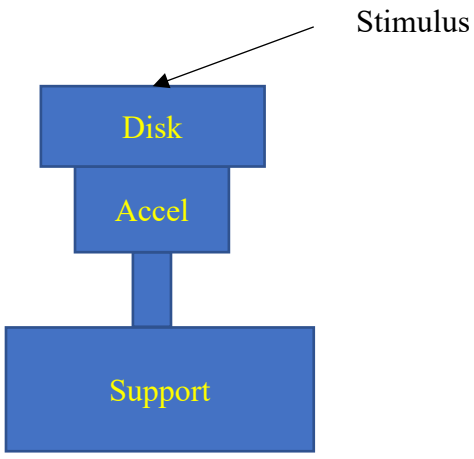

Figure 37: Schematic diagram of set up for benchtop model using tapping and scratching

3.9.2 Results and Findings

Finger tapping on a disc over the accelerometer:

Figure 38 shows PSD for the full frequency (left) range and for low frequencies (right) for finger tapping on accelerometer.

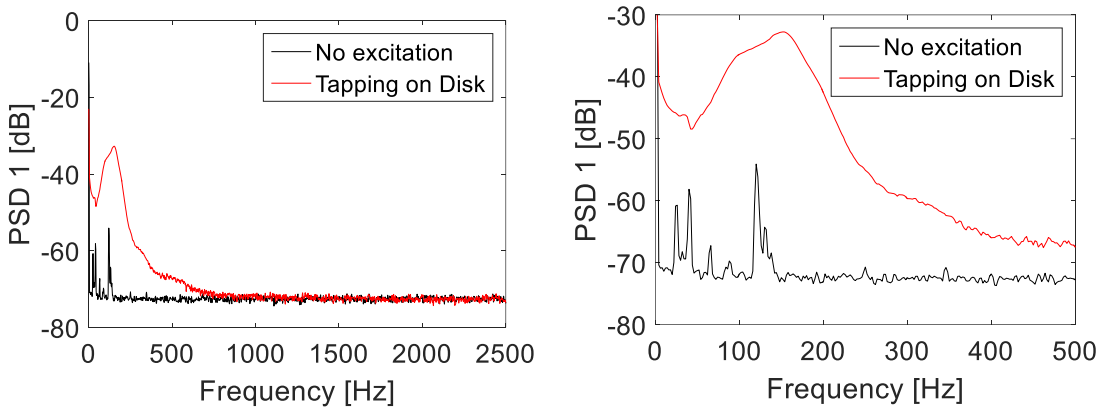

Figure 38: Power spectrum density for the full frequency range and for low frequencies (0-500 Hz).

Findings: The data of Figure 38 suggests the following:

- Direct tapping on a soft surface primarily excites low frequencies (< about 500 Hz).
- Input signal to noise ratio (SNR) > 10 dB for f<300 Hz.
- Maximum SNR around (~40 dB) was at around 150 Hz.
- This stimulus may not be effective to DDH detection since higher frequency stimulation (up to 1200 Hz) as suggested by animal studies results (next paragraph).

Scratching a paper disk (placed over accelerometer 1 over the stinger):

Figure 39 shows PSD for the full frequency range and for low frequencies (0-500 Hz) for scratching a paper disk.

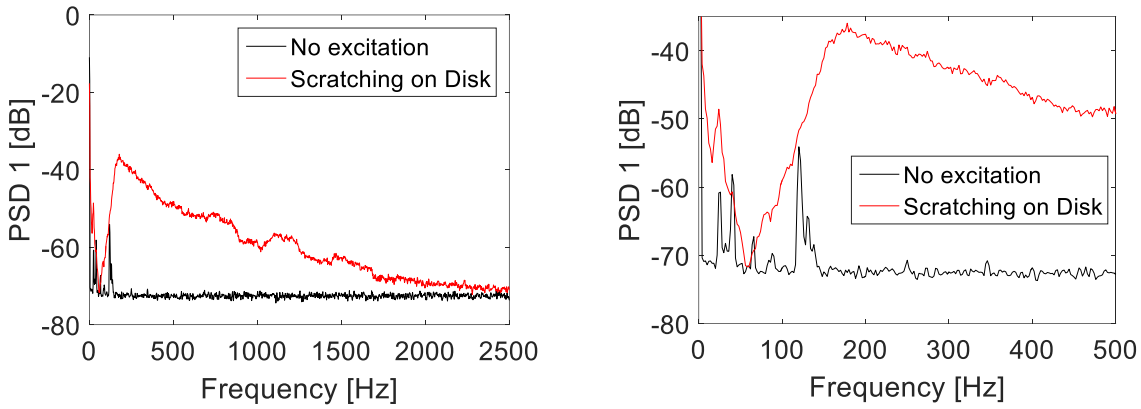

Figure 39: Scratching input: Power spectrum density for the full frequency range and for low frequencies (0-500 Hz).

Findings: The data of Figure 39 suggests the following:

- Input SNR was > 10 dB, and 20 dB for f< 500 and 1000 Hz, respectively.
- Maximum SNR of 35 dB was achieved at around 200 Hz.
- This stimulus has potential utility but output SNR need to be measured as it is likely lower than at the stimulus point.

Tapping a coin with a metal bar (placed over the accelerometer):

Figure 40 shows PSD for the full frequency range and for low frequencies (0-500 Hz) for tapping with a metal bar a coin.

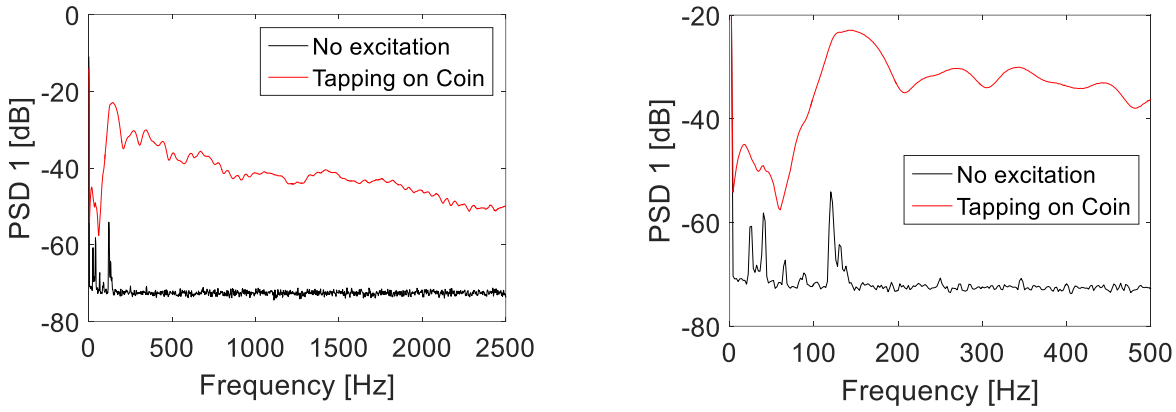

Figure 40: Power spectrum density for the full frequency range and for low frequencies (0-500 Hz).

Findings: The data of Figure 40 suggests the following:

- Input SNR was > 30 dB for frequencies below 2500 Hz.
- This stimulus has high potential utility, but output SNR need to be measured as it is lower at than that at the stimulus point.

Scratching on plastic container while exciter is touching the sacrum:

Figure 41 shows PSD for the full frequency range and for low frequencies (0-500 Hz) for scratching on plastic container.

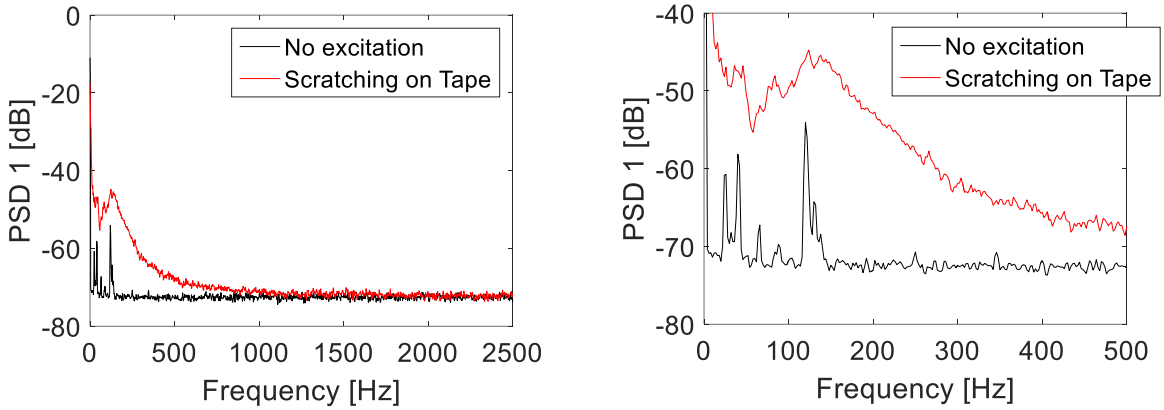

Figure 41: Power spectrum density for the full frequency range and for low frequencies (0-500 Hz).

Findings: The data of Figure 41 suggests the following:

- Input SNR was > 10 dB, and 20 dB for f< 500 and 1000 Hz, respectively.
- Maximum SNR of 35 dB was achieved at ~ 200 Hz.
- This stimulus has low potential utility.

3.10 Conclusions

Broadband exciters: Based on the discussion on section 3.4 and 3.6 and Figures 14-25 and 28, the following conclusions are drawn:

- All the exciter shows good SNR(> 20 dB) and coherence higher than 0.8 in the frequency domain of 150-1500 Hz (Figure 28 and 29).

- Large exciter and iLouder exciter are less sensitive to static load (for loads < 500 gm).

Tuning Fork: Based on the discussion on section 3.8 and Figure 31-34, the following conclusions are drawn:

- Electronic tuning fork shows higher SNR than manual fork.
- Static load should not be applied more than 200g because of lower SNR at higher loads (Figure 31-34).
- Only 128 and 256 Hz rated manual tuning fork shows enough SNR ratio at excitation and measurement points.

Tapping and scratching: Based on the discussion on section 3.9 and Figure 38-41, the following conclusions are drawn:

- Tapping on a coin with a metal bar and scratching a paper disk shows utility.

CHAPTER 4: SOUND TRANSMISSION IN A PIG MODEL

4.1 Pig 1 experiment: iLouder exciter

4.1.1 Objectives

The objective of this study is to document the effect of left hip dysplasia in an animal model.

4.1.2 Approach

One preserved pig (Carolina Biological Supply Company, Burlington, North Carolina) was used in this experiment. This pig is called "pig 1" as it was the first pig to be tested. Surgery was performed where the ligaments holding the left hip joint were cut. This allows the left hip to be displaced at different levels. No surgery was performed to the right hip. Two different approaches for causing dysplasia were implemented.

Approach 1: (a) Both femur heads are held in the acetabulum by hand (this will be called "Full contact" or "control" case) to simulate the healthy state and (b) the dysplasia state is simulated by actively pulling the left femur head out of the acetabulum (this state will be called full DDH). This approach is meant to provide more control of the contact between the femur head and acetabulum. However, holding the thighs by hand may introduce noise and variability as it involves human control of the displacement. Hence experiments without hand holding the hips were also performed.

Approach 2: Here the left femur head is (a) let to sit in the acetabulum (while supported by a string to help increase contact between the head and socket) and (b) the femur head is let to fall out of

the socket under its own weight. This approach may offer more repeatability but also more uncertainty about the contact between the femur head and acetabulum.

4.1.3 Methods

The experimental set up is shown in Figure 42. The experimental steps were as follows:

- Place the pig (pig 1) supine in the plastic container.
- Tie the upper extremities to the side of the container to help keep the pig supine.
- Secure sensor (accelerometer) 2 and 3 over the left and right condyles, respectively, using double sided tape.
- Excite at the sacrum from the bottom of the container where a hole (~ 4 cm diameter) was made to allow direct access to the sacrum.
- Use the iLouder exciter to introduce a stimulus acoustic signal with sensor 1 placed at the exciter tip. Tapping and scratching were also used as acoustic stimuli.
- Sound transmission measurements were performed for the displaced and non-displaced cases.

Full contact both hips (control): Left full dysplasia (DDH): Left full dysplasia(DDH) (Zoom in)

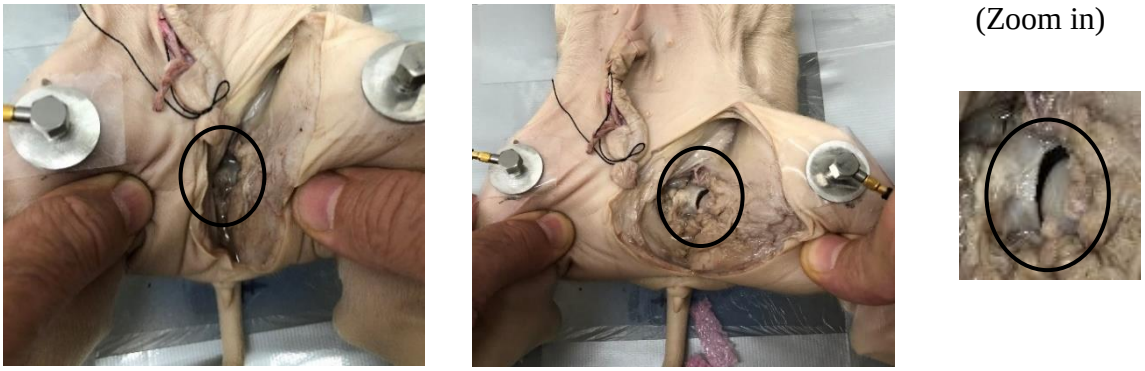

Figure 42: Photographs showing the setup. The circles show the joint location.

4.1.4 Results and Findings

Effect of dysplasia on transmission from the scrum to the left and right condyles. Hand-held thighs and broadband excitation.

Transfer function (TF):

The transfer function between left and right condyles for three runs is shown in Figure 43.

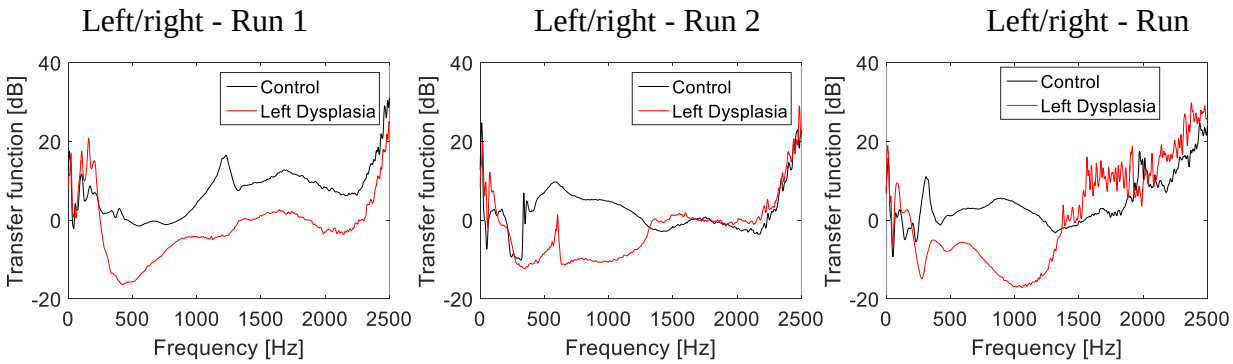

Figure 43: The transfer function between sensor 2 (left condyle) and sensor 3 (right condyle). This was repeated for three runs. The "Control" refer to the case of no dysplasia for both hips. Thighs were held by hand.

Average transfer function (TF) between left and right signals is shown in Table 1.

Table 1: Average transfer function (TF) between left and right signals in two frequency bands and the ratio of TF between the two bands.

	Joint state	Average TF in Band 1 (5-240 Hz)	Average TF in Band 2 (300-1200 Hz)	TF ratio between Band 1 and 2
Run 1	Control	6.51	2.18	4.32
	Left Hip Dysplasia	10.72	-9.02	19.74
Run 2	Control	1.46	4.84	-3.37
	Left Hip Dysplasia	3.41	-9.65	13.06
Run 3	Control	-0.62	3.15	-3.77
	Left Hip Dysplasia	2.50	-10.86	13.37

Findings:

The transfer function (Figure 43) remained closer to zero in the control case indicating more bilateral sound transmission to both hips.

- Transfer function changes with DDH are summarized below (Table 1):
  - Below 240 Hz: Smaller TF average increase (~2 to 4 dB) was seen. Hence, the low frequency sounds appear to more effectively transmit around the displaced hip.
  - 300-1200 Hz: Larger TF average drop (~11 to 14 dB). There was more TF loss in the higher frequency band compared to the gain at the lower frequency band.
  - The maximum TF drop with DDH was ~ 20 dB at ~300 Hz (Run 3).
- The transfer function ratio between the above two frequency bands (Table 1) were:

Control: -3.4-4.3 dB

DDH: 13.1-19.7 dB

A threshold on this ratio may be an important feature for detecting bilateral DDH as a control hip measurement would not be needed for this calculation.

Coherence (between left and right condyle signals):

The coherence between left and right condyles for three runs is shown in Figure 44.

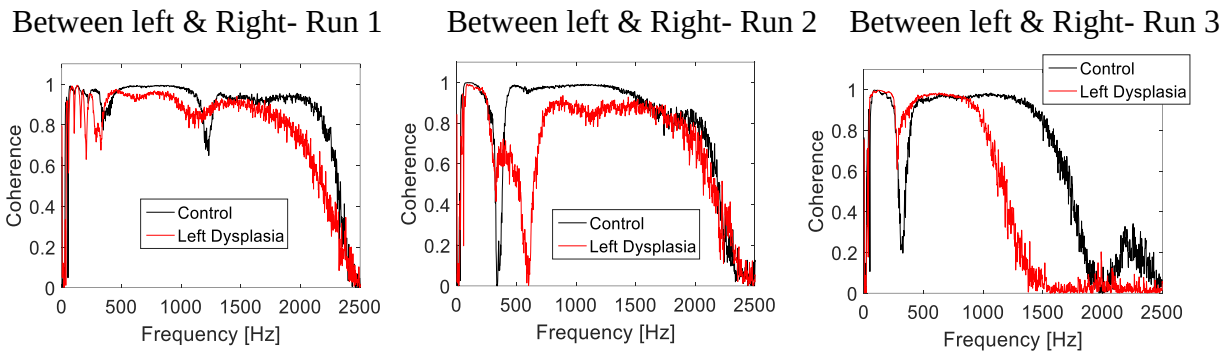

Figure 44: The coherence between sensor 2 (left hip) and sensor 3 (right hip). This was repeated for three runs. The "Control" refer to the case of no dysplasia for both hips. Thighs were held by hand.

Findings: The data of Figure 44 suggests the following:

- Small coherence changes below 240 Hz with DDH was seen. This is a sign of efficient bilateral transmission around the displaced joint.
- More noticeable drop in coherence with DDH for frequencies above 300 Hz. This consistent with loss in transmission.
- The sharp drop in coherence occurs at different frequencies for the control and DDH cases. This is likely due to different frequencies for resonance and anti-resonance.

Phase (between left and right condyle signals):

The phase between left and right condyles for three runs is shown in Figure 45.

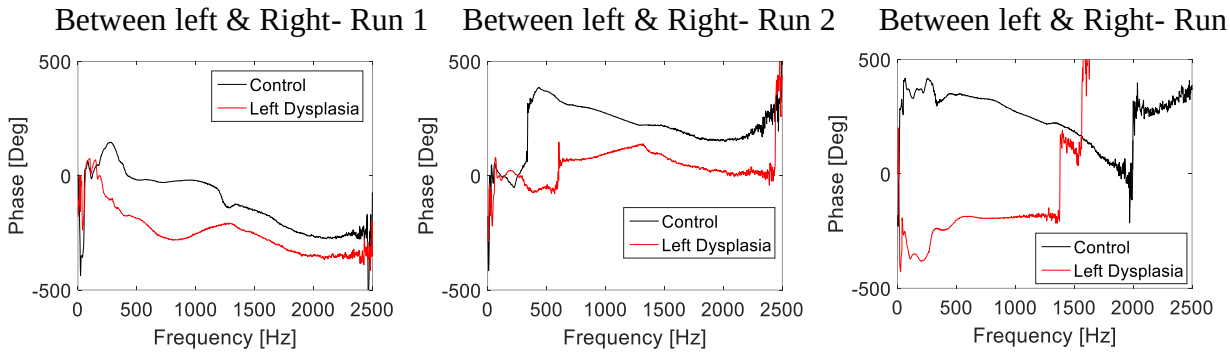

Figure 45: The phase angle between sensor 2 (left hip) and sensor 3 (right hip). This was repeated for three runs. The "Control" refer to the case of no dysplasia for both hips. Thighs were held by hand.

Findings: The data of Figure 45 suggests the following:

- The most reliable results were for run 1 since coherence stayed relatively high. Will focus on this case for this discussion.
- There was relatively larger phase delay at higher frequencies.
- There was small change in phase with DDH for frequencies below 200 Hz.
- There were larger phase change for DDH. Hence, phase changes between frequency bands may be a useful feature for DDH detection.

Power spectral density (PSD) and transfer function (TF) – run 1:

PSD for the left and right hips and for the sacrum, and TF for sacrum to left and sacrum to right are shown in Figure 46.

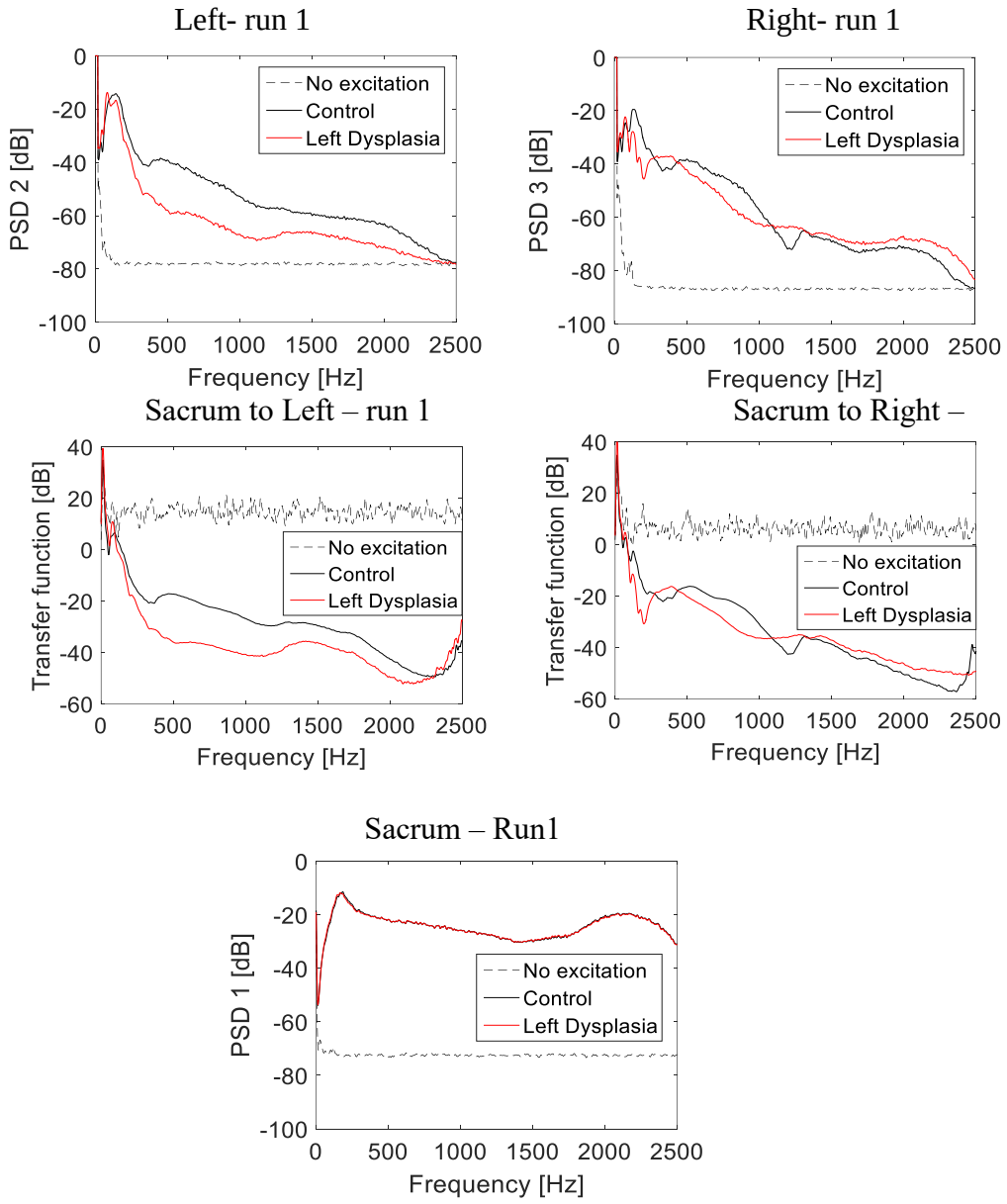

Figure 46: The power spectral density (PSD) for the left and right hip (PSD 2 and PSD3, respectively) and for the sacrum (PSD 1). Transfer function for sacrum to left and sacrum to right. This was repeated for three runs. The "Control" refer to the case of no dysplasia for both hips. This figure shows the first run.

Average PSD of sensor 2 and 3 in 2 frequency bands and the PSD ratio between bands is shown in Table 2.

Table 2: Average PSD of sensor 2 and 3 in 2 frequency bands and the PSD ratio between bands

	Joint state	Average PSD in Band 1 (5-240 Hz)	Average PSD in Band 2 (300-1200 Hz)	PSD ratio between Band 1 and 2
Left (PSD 2)	No excitation	-69.26	-78.10	8.84
	Control	-21.47	-46.57	25.10
	Left hip Dysplasia	-23.26	-61.41	38.16
Right (PSD 3)	No excitation	-73.91	-86.80	12.89
	Control	-26.25	-48.57	22.32
	Left hip Dysplasia	-31.92	-51.99	20.07

Average TF of sensor 2 and 3 in 2 frequency bands and the TF ratio between the bands is shown in Table 3.

Table 3: Average transfer function sensor 1 to sensor 2 and sensor 1 to sensor 3 in 2 frequency bands and the TFE ratio between bands (run 1)

	Joint state	Average TFE in Band 1 (5-240 Hz)	Average TFE in Band 2 (300-1200 Hz)	TFE ratio between Band 1 and 2
Transfer function: Sacrum to left (2/1)	No Excitation	15.26	14.83	0.43
	Control	0.86	-22.75	23.61
	Left Hip Dysplasia	-0.53	-37.30	36.77
Transfer function: Sacrum to right (3/1)	No Excitation	9.70	6.29	3.41
	Control	-3.89	-24.68	20.79
	Left Hip Dysplasia	-9.22	-28.15	18.92

Findings: The data of Figure 46, Table 2, and Table 3 suggests the following:

- PSD 3 (right hip) was similar for both control and DDH, which is expected since no surgery was done to the right hip. There was a small drop in the 500-1000 Hz range, possibly due to minor displacement of the right hip or operator variability (Figure 46 and Table 2).
- PSD 2 (left hip) dropped with full dysplasia indicating sound transmission loss. The maximum drop was ~ 20 dB at 500 Hz (Figure 46 and Table 2).
- Transfer function between sacrum to left shows the drop from -22.75 dB to -37.30 in the frequency band of 300-1200 Hz with full dysplasia (Figure 46 and Table 3).
- The noise floor in the right was lower than the left. This is related to our set up (likely the accelerometer amplifier noise differences).

Power spectral density (PSD) and transfer function (TF) – run 2:

PSD for the left and right hip, and TF for sacrum to left and sacrum to right are shown in Figure 47.

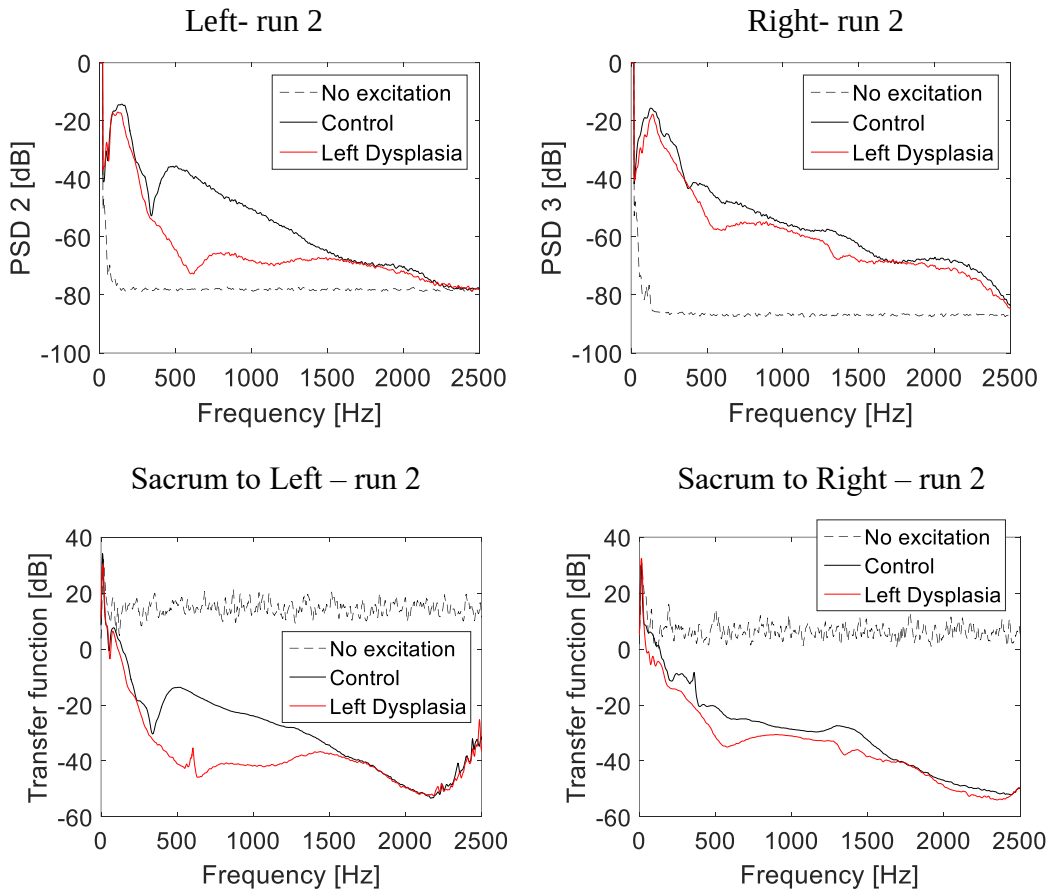

Figure 47: The power spectral density (PSD) for the left and right hip (PSD 2 and PSD3, respectively) and for the sacrum (PSD 1). Transfer function for sacrum to left and sacrum to right. This was repeated for three runs. The "Control" refer to the case of no dysplasia for both hips. This figure shows the second run.

Findings: The data of Figure 47, Table 4, and Table 5 suggests the following:

- PSD 3 (right hip) was similar for both cases, which is expected (Figure 47 and Table 4).
- PSD 2 (left hip) showed sound transmission loss with full dysplasia. The maximum drop was around 35 dB at 500 Hz (Figure 47 and Table 4).
- Transfer function between sacrum to left shows the drop from -21.10 dB to -40.34 in the frequency band of 300-1200 Hz with full dysplasia (Figure 47 and Table 5).

Average PSD of sensor 2 and 3 in 2 frequency bands and the PSD ratio between bands is shown in Table 4.

Table 4: Average PSD of sensor 2 and 3 in 2 frequency bands and the PSD ratio between bands

	Joint state	Average PSD in Band 1 (5-240 Hz)	Average PSD in Band 2 (300-1200 Hz)	PSD ratio between Band 1 and 2
Left (PSD 2)	No excitation	-69.26	-78.10	8.84
	Control	-21.36	-45.25	23.88
	Left Hip Dysplasia	-23.78	-65.76	41.98
Right (PSD 3)	No excitation	-73.91	-86.80	12.89
	Control	-20.90	-49.22	28.32
	Left Hip Dysplasia	-25.32	-54.05	28.73

Average TF of sensor 2 and 3 in 2 frequency bands and the TF ratio between bands is shown in Table 5.

Table 5: Average transfer function sensor 1 to sensor 2 and sensor 1 to sensor 3 in 2 frequency bands and the TFE ratio between bands (run 2)

	Joint state	Average TFE in Band 1 (5-240 Hz)	Average TFE in Band 2 (300-1200 Hz)	TFE ratio between Band 1 and 2
Transfer function: Sacrum to left (2/1)	No Excitation	15.26	14.83	0.43
	Control	0.71	-21.10	21.81
	Left Hip Dysplasia	-2.62	-40.34	37.72
Transfer function: Sacrum to right (3/1)	No Excitation	9.70	6.29	3.41
	Control	0.75	-24.55	25.31
	Left Hip Dysplasia	-3.85	-30.22	26.37

PSD for the left and right hip, and TF for sacrum to left and sacrum to right are shown in Figure 48.

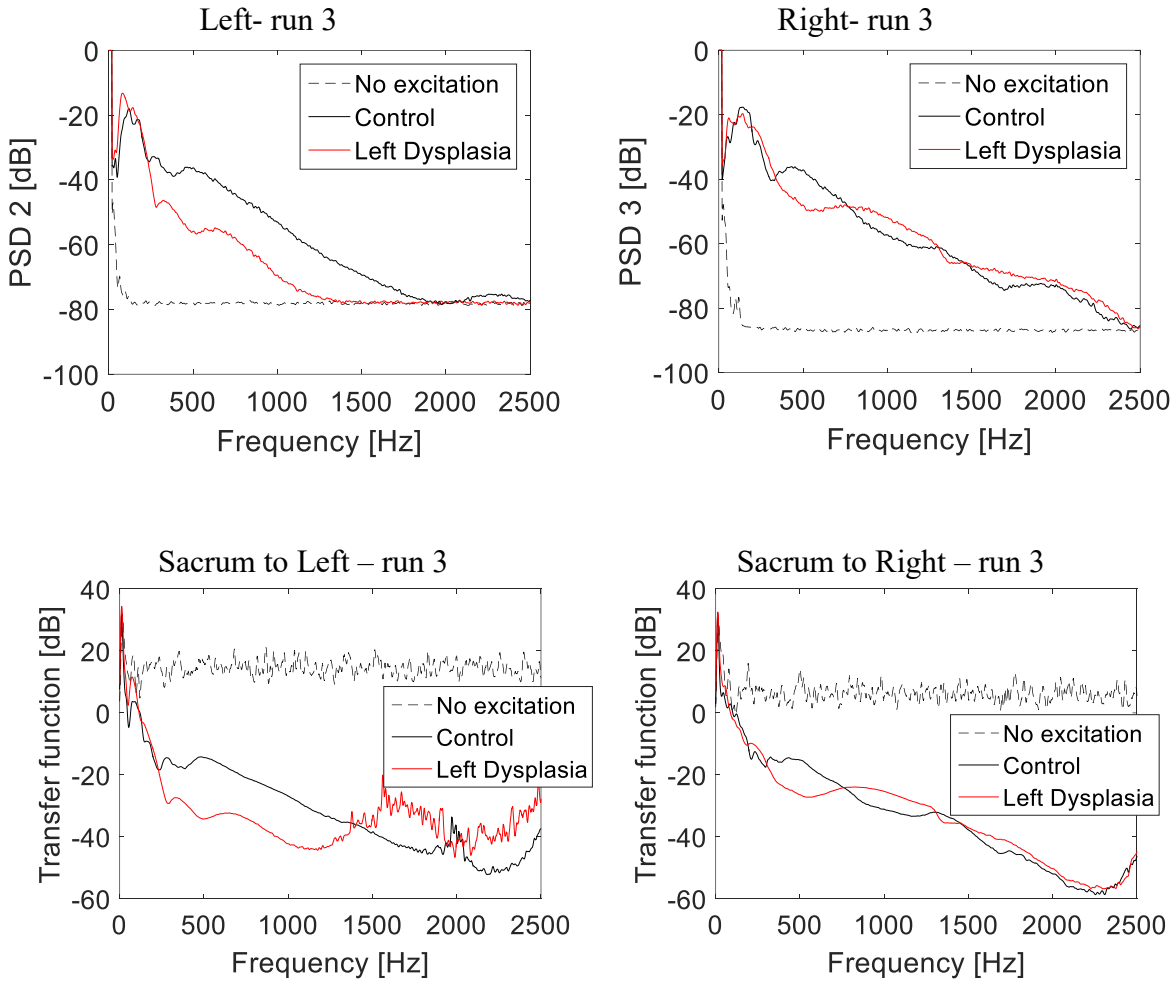

Figure 48: The power spectral density (PSD) for the left and right hip (PSD 2 and PSD3, respectively). Transfer function for sacrum to left and sacrum to right. This was repeated for three realizations. The "Control" refer to the case of no dysplasia for both hips. Thighs were held by hand. This figure shows the third run.

Findings: The data of Figure 48, Table 6, and Table 7 suggests the following:

- PSD 3 (right hip) was similar for both cases, which is expected (Figure 48 and Table 6).
- PSD 2 (left hip) showed sound transmission loss with full dysplasia. The maximum drop was around 20 dB at 500 Hz (Figure 48 and Table 6).
- Transfer function between sacrum to left shows the drop from -21.71 dB to -36.17 in the frequency band of 300-1200 Hz with full dysplasia (Figure 48 and Table 7).

Average PSD of sensor 2 and 3 in 2 frequency bands and the PSD ratio between bands is shown in Table 6.

Table 6: Average PSD of sensor 2 and 3 in 2 frequency bands and the PSD ratio between bands

	Joint state	Average PSD in Band 1 (5-240 Hz)	Average PSD in Band 2 (300-1200 Hz)	PSD ratio between Band 1 and 2
Left (PSD 2)	No excitation	69.26	-78.10	8.84
	Control	-25.15	-45.64	20.49
	Left Hip Dysplasia	-21.64	-60.71	39.07
Right (PSD 3)	No excitation	-73.91	-86.80	12.89
	Control	-23.17	-48.25	25.08
	Left Hip Dysplasia	-22.51	-49.21	26.70

Average TF of sensor 2 and 3 in 2 frequency bands and the TF ratio between bands is shown in Table 7.

Table 7: Average transfer function sensor 1 to sensor 2 and sensor 1 to sensor 3 in 2 frequency bands and the TFE ratio between bands (run 3)

	Joint state	Average TFE in Band 1 (5-240 Hz)	Average TFE in Band 2 (300-1200 Hz)	TFE ratio between Band 1 and 2
Transfer function: Sacrum to left (2/1)	No Excitation	15.26	14.83	0.43
	Control	-2.95	-21.71	18.76
	Left Hip Dysplasia	0.51	-36.17	36.68
Transfer function: Sacrum to right (3/1)	No Excitation	9.70	6.29	3.41
	Control	-1.13	-23.91	22.79
	Left Hip Dysplasia	-0.42	-25.18	24.75

Repeatability:

PSD for the left and right hip for the control (also called: full contact) case is shown in Figure 49.

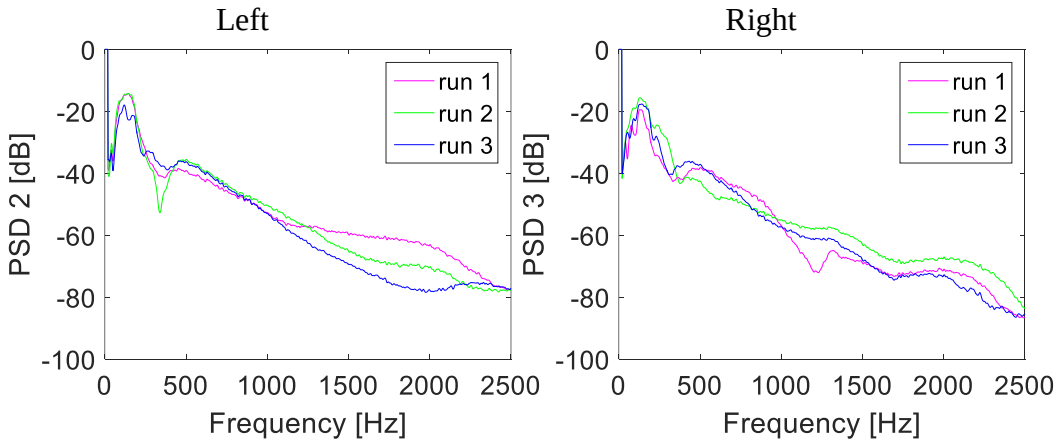

Figure 49: Full contact (Both femur heads are in contact with their respective acetabulum). The power spectral density (PSD) for the left and right hip (PSD 2 and PSD3, respectively). This was repeated for three realizations.

PSD for the left and right hip of the control (i.e., full contact) case is shown in Figure 50.

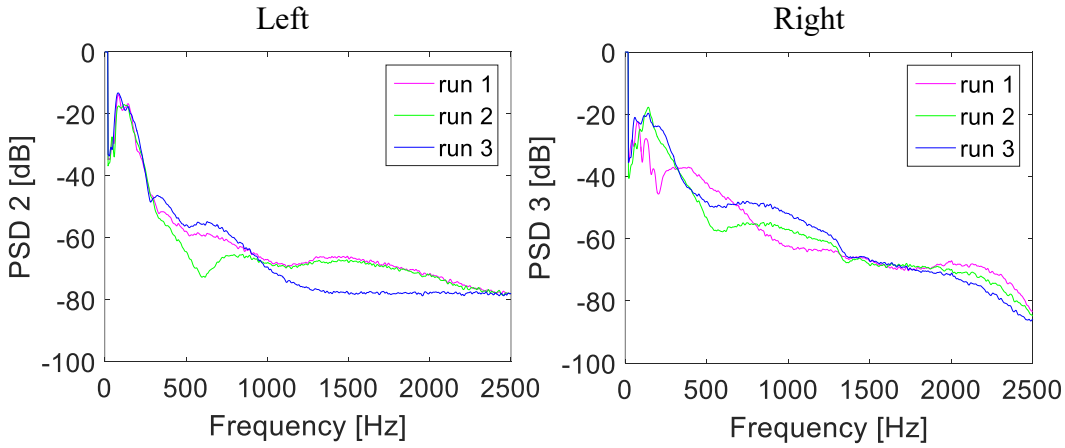

Figure 50: Full dysplasia (in left hip only). The power spectral density (PSD) for the left and right hip (PSD 2 and PSD3, respectively). This was repeated for three realizations.

Findings: The data of Figure 49, Figure 50, Table 8, and Table 9 suggests the following:

- Repeatability is slightly higher for the no-dysplasia case.
- Possible more repeatability below 1000 Hz.

Average PSD of sensor 2 and 3 in 2 frequency bands and the PSD ratio between bands for no-dysplasia case is shown in Table 8.

Table 8: Average PSD of sensor 2 and 3 in 2 frequency bands and the PSD ratio between bands (No-dysplasia)

	Repeatability case	Average PSD in Band 1 (5-240 Hz)	Average PSD in Band 2 (300-1200 Hz)	PSD ratio between Band 1 and 2
Left (PSD 2)	Run 1	-21.47	-46.57	25.10
	Run 2	-21.36	-45.25	23.88
	Run 3	-25.15	-45.64	20.49
Right (PSD 3)	Run 1	-26.25	-48.57	22.32
	Run 2	-20.90	-49.22	28.32
	Run 3	-23.17	-48.25	25.08

Average PSD of sensor 2 and 3 in 2 frequency bands and the PSD ratio between bands for dysplasia case is shown in Table 9.

Table 9: Average PSD of sensor 2 and 3 in 2 frequency bands and the PSD ratio between bands (dysplasia)

	Repeatability case	Average PSD in Band 1 (5-240 Hz)	Average PSD in Band 2 (300-1200 Hz)	PSD ratio between Band 1 and 2
Left (PSD 2)	Run 1	-23.26	-61.41	38.16
	Run 2	-23.78	-65.76	41.98
	Run 3	-21.64	-60.71	39.07
Right (PSD 3)	Run 1	-31.92	-51.99	20.07
	Run 2	-25.32	-54.05	28.73
	Run 3	-22.51	-49.21	26.70

Effect of hand holding the thighs:

To test this effect, the thighs first rested under their own weight. Excitation was applied at the sacrum using the broad band exciter. Sensors were at the left and right condyle as shown in Figure 42. Here, the effect of hand holding the thighs was investigated by comparing the case of nand holding thighs to the case where the thighs rested under their own weight without hand holding.

Results and Findings:

Transfer function between left and right sensor is shown in Figure 51.

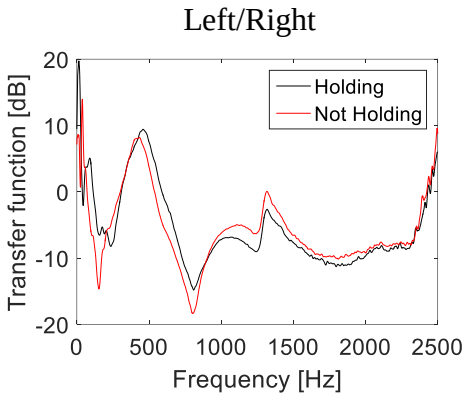

Figure 51: Transfer function between left and right sensor (i.e., L/R)

PSD for left and right sensors and TF for sacrum to left and sacrum to right is shown in Figure 52.

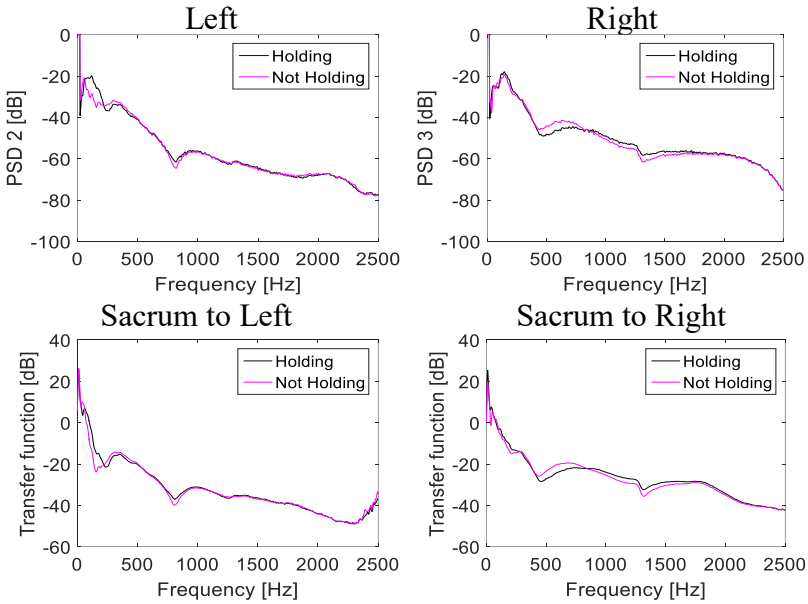

Figure 52: Power spectrum density for left and right sensors and transfer function for sacrum to left and sacrum to right

Findings: The data of Figure 51, 52, Table 10, 11, and 12 suggests the following:

- Hand holding the thighs had minimal effects on the sound transmission.
- Left hip: Similar sound transmission in all frequencies both cases except ~100-200 Hz (~10 dB) (Table 11).
- Right hip: Similar sound transmission in all frequencies both cases except ~500-700 Hz (~5 dB) (Table 11).
- The transfer function was similar (Table 10 and Table 12).

Average TF from right to left hip in 2 frequency bands and the TF ratio between bands is shown in Table 10.

Table 10: Average transfer function in 2 frequency bands and the TF ratio between bands

	Joint state	Average TF in Band 1 (5-240 Hz)	Average TF in Band 2 (300-1200 Hz)	TF ratio between Band 1 and 2
Transfer function: left/right (2/3)	Holding	-0.42	-3.91	3.49
	No holding	-3.94	-5.03	1.09

PSD for the left and right hip, and TF for sacrum to left and the sacrum to right are shown in Table 11 and Table 12.

Table 11: Average PSD of sensor 2 and 3 in 2 frequency bands and the PSD ratio between bands

	Joint state	Average PSD in Band 1 (5-240 Hz)	Average PSD in Band 2 (300-1200 Hz)	PSD ratio between Band 1 and 2
Left (PSD 2)	Holding	-25.06	-50.79	25.73
	Not holding	-28.53	-51.01	22.48
Right (PSD 3)	Holding	-22.84	-46.72	23.88
	Not holding	-23.92	-45.86	21.95

Table 12: Average transfer function sensor 1 to sensor 2 and sensor 1 to sensor 3 in 2 frequency bands and the TFE ratio between bands

	Joint state	Average TF in Band 1 (5-240 Hz)	Average TF in Band 2 (300-1200 Hz)	TF ratio between Band 1 and 2
Transfer function: Sacrum to left (2/1)	Holding	-5.02	-27.83	22.80
	Not holding	-8.78	-28.08	19.30
Transfer function: Sacrum to right (3/1)	Holding	-2.68	-23.75	21.06
	Not holding	-4.43	-22.99	18.56

Effect of dysplasia on sound transmission between sacrum and condyles:

Here, the thighs rested under their own weight (i.e. without holding the thigh by hand), and broadband excitation was implemented. Figure 53 shows the joint region when left femur head was fully in acetabulum and partially in acetabulum. Figure 54 shows the joint region when foam was placed to increase gap between femur head and acetabulum.

Left femur head fully in acetabulum

Femur head partially in acetabulum

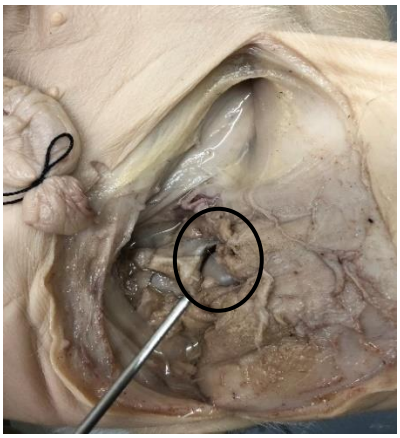

Figure 53: Photographs showing the joint region. The metal bar points to the joint location

Foam placed in joint

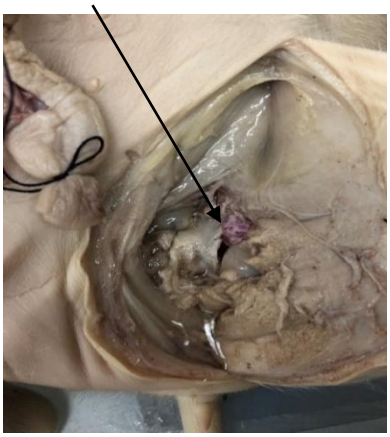

More foam placed in joint

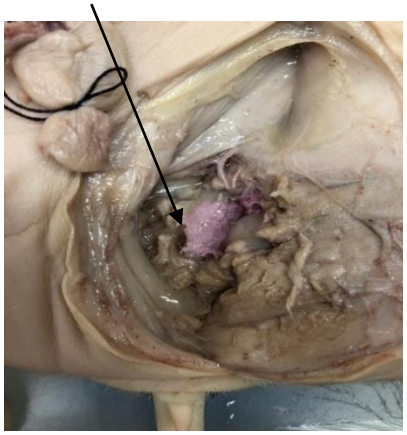

Figure 54: Photographs showing the location of foam placed in the joint. Foam was placed to increase displacement. More foam was added in the right picture.

Transfer function

Figure 55 shows TF between left and right condyles.

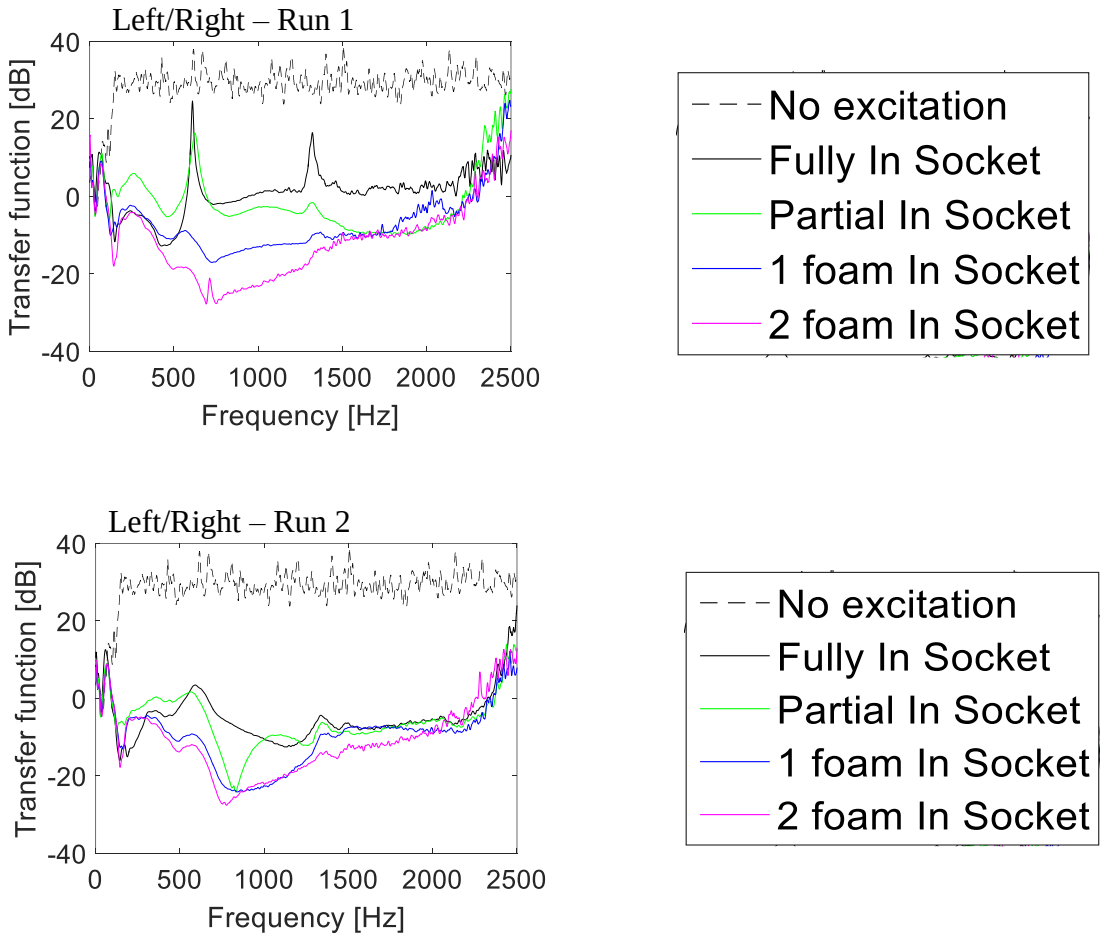

Figure 55: Transfer function between left and right condyles.

Average TF in 2 frequency bands and the TF ratio between bands for the Left/right sensors is shown in Table 13.

Table 13: Average transfer function in 2 frequency bands and the TF ratio between bands Left/right (2/3)

	Joint state	Average TF in Band 1 (5-400 Hz)	Average TF in Band 2 (600-1200 Hz)	TF ratio between Band 1 and 2
Run 1	No Excitation	22.42	29.87	-7.45
	Fully in socket	-2.39	1.03	-3.42
	Partial in socket	2.55	-1.57	4.12
	1 foam in socket	-3.32	-13.81	10.50
	2 foam in socket	-5.32	-23.27	17.95
Run 2	No Excitation	22.42	29.87	-7.45
	Fully in socket	-5.22	-7.57	2.35
	Partial in socket	-1.42	-12.12	10.70
	1 foam in socket	-4.05	-20.46	16.42
	2 foam in socket	-4.66	-21.76	17.10

Findings: The data of Figure 55, and Table 13 suggests the following:

1) The transfer function remained closer to zero in the control case indicting more bilateral sound transmission to both hips.
2) Transfer function (TF) changes with DDH:

- Below 240-300 Hz: Smaller TF changes (~5 dB) were seen.
- 600-1200 Hz: Larger TF average drop (~ 20 dB) was seen.
- The larges TF drop with DDH was > 20 dB for the foam cases. Foam insertion in the hip joinjt for this animal may have caused more dysplasia and less bone-to-bone direct contact.

3) There was more TF loss in the higher frequency band compared to the change at the lower frequency band. Hence, the low frequency sounds appear to transmit more effectively around the displaced hip.
4) Hysteresis effect: The result shows some hysteresis effects.
5) The TF for the no excitation case is higher than zero possibly due to differences in noise levels in the two channels.

Power spectral density (PSD) and transfer function between stimulus (sacrum) and output (left or right):

Figure 56 shows PSD of the sound transmitted to the left and right condyles from the sacrum and transfer function from sacrum to left and sacrum to right of run 1.

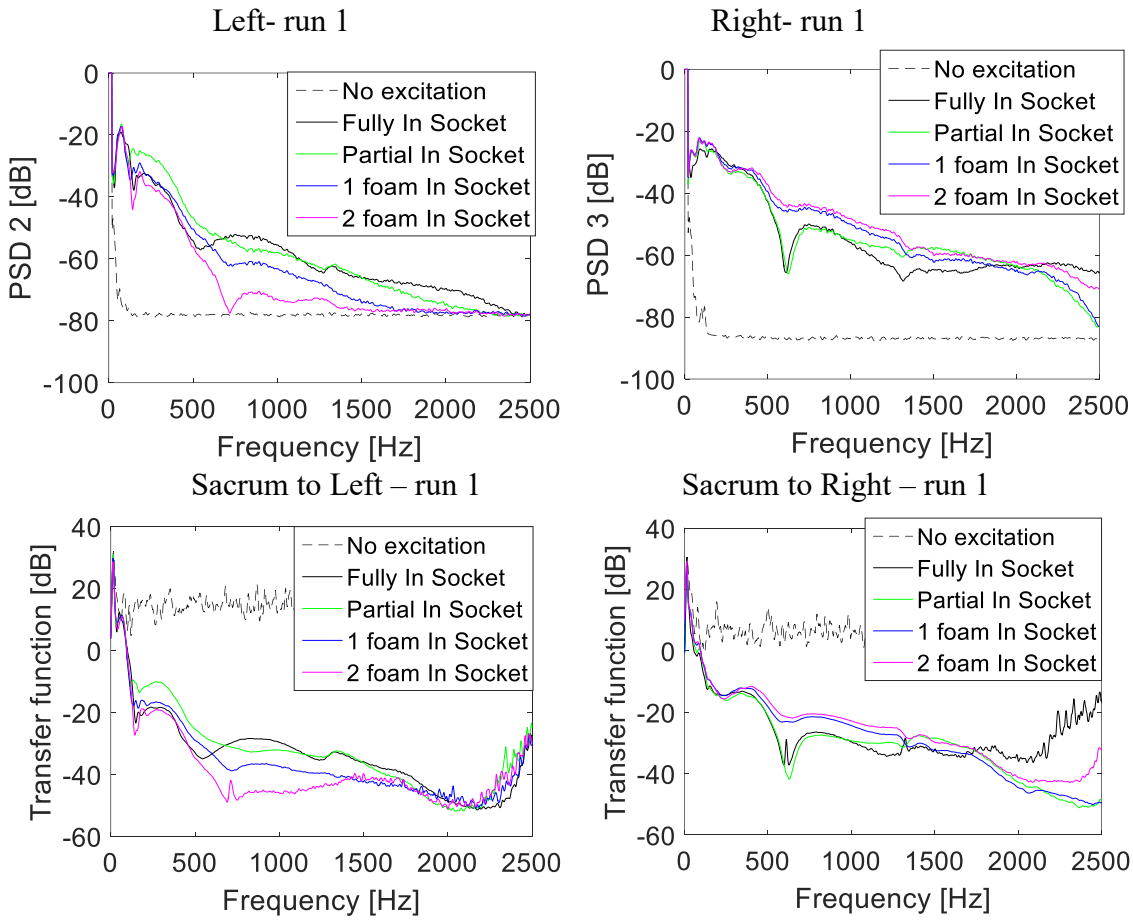

Figure 56: Power spectrum density of the sound transmitted to the left and right condyles from the sacrum and transfer function from sacrum to left and sacrum to right.

Figure 57 shows PSD of the sound transmitted to the left and right condyles from the sacrum and transfer function from sacrum to left and sacrum to right of run 2.

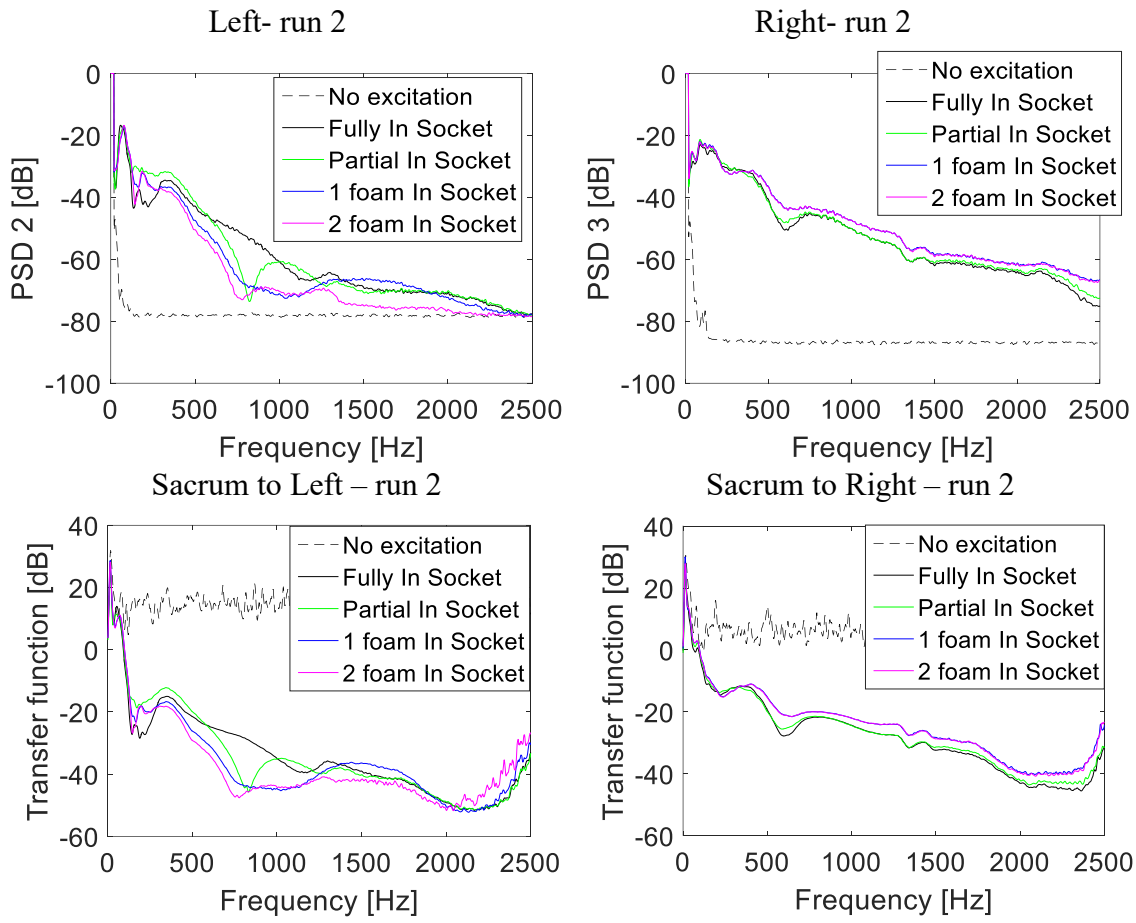

Figure 57: Power spectrum density of the sound transmitted to the left and right condyles from the sacrum and transfer function from sacrum to left and sacrum to right.

Findings: The data of Figure 56, Figure 57, Table 14, Table 15, Table 16, and Table 17 suggests the following:

- PSD 3 (right): This side was less affected by dysplasia for all cases, except around 500 Hz.
- Similarity may be higher than the hand held case, due to absence of operator hands.
- There was a slight increase in sound transmission with dysplasia possibly due inhibition of sound transmission in the contralateral side.
- For the left side (PSD2), the lowest sound transmission with dysplasia was observed when more foam was inserted into the joint. The maximum drop in transmission was around 30 dB.
- Transfer function (TF) changes with DDH:

Below 240-300 Hz: Smaller TF changes (~5 dB).

600-1200 Hz: Larger TF average drop (~ 17 dB).

The larges TF drop with DDH was > 12 dB for the foam cases. Foam in this animal may have caused more dysplasia and less bone-to-bone direct contact.

- The noise floor in the right was lower than the left. This is related to our set up (likely the accelerometer amplifier noise differences).

PSD of the sound transmitted to the left and right condyles from the sacrum and transfer function from sacrum to left and sacrum to right of run 1 and run 2 are shown in Table 14,15,16,17.

Table 14: Average PSD of sensor 2 and 3 in 2 frequency bands and the PSD ratio between bands (run 1)

	Joint state	Average PSD in Band 1 (5-400 Hz)	Average PSD in Band 2 (600-1200 Hz)	PSD ratio between Band 1 and 2
Left (PSD 2)	No Excitation	-72.83	-78.09	5.26
	Fully in socket	-31.69	-55.35	23.67
	Partial in socket	-26.72	-57.01	30.29
	1 foam in socket	-31.07	-62.47	31.40
	2 foam in socket	-33.49	-72.23	38.74
Right (PSD 3)	No Excitation	-78.95	-86.90	7.95
	Fully in socket	-28.73	-55.53	26.80
	Partial in socket	-28.90	-55.21	26.31
	1 foam in socket	-27.51	-48.48	20.97
	2 foam in socket	-27.83	-46.85	19.02

Table 15: Average transfer function sensor 1 to sensor 2 and sensor 1 to sensor 3 in 2 frequency bands and the TFE ratio between bands (run 1)

	Joint state	Average TFE in Band 1 (5-400 Hz)	Average TFE in Band 2 (600-1200 Hz)	TFE ratio between Band 1 and 2
Transfer function: Sacrum to left (2/1)	No Excitation	14.73	14.72	0.01
	Fully in socket	-11.24	-30.42	19.18
	Partial in socket	-6.13	-32.12	25.99
	1 foam in socket	-10.31	-37.52	27.21
	2 foam in socket	-12.56	-45.55	32.99
Transfer function: Sacrum to right (3/1)	No Excitation	8.25	6.39	1.86
	Fully in socket	-8.40	-29.81	21.42
	Partial in socket	-8.47	-30.24	21.77
	1 foam in socket	-6.91	-23.71	16.80
	2 foam in socket	-7.00	-22.28	15.28

Table 16: Average PSD of sensor 2 and 3 in 2 frequency bands and the PSD ratio between bands (run 2)

	Joint state	Average PSD in Band 1 (5-400 Hz)	Average PSD in Band 2 (600-1200 Hz)	PSD ratio between Band 1 and 2
Left (PSD 2)	No Excitation	-72.83	-78.09	5.26
	Fully in socket	-33.58	-56.88	23.31
	Partial in socket	-28.94	-61.27	32.32
	1 foam in socket	-31.65	-67.39	35.74
	2 foam in socket	-32.37	-68.85	36.47
Right (PSD 3)	No Excitation	-78.95	-86.90	7.95
	Fully in socket	-27.77	-49.17	21.41
	Partial in socket	-27.22	-48.73	21.50
	1 foam in socket	-27.39	-46.15	18.76
	2 foam in socket	-27.45	-46.16	18.72

Table 17: Average transfer function sensor 1 to sensor 2 and sensor 1 to sensor 3 in 2 frequency bands and the TFE ratio between bands (run 2)

	Joint state	Average TFE in Band 1 (5-400 Hz)	Average TFE in Band 2 (600-1200 Hz)	TFE ratio between Band 1 and 2
Transfer function: Sacrum to left (2/1)	No Excitation	14.73	14.72	0.01
	Fully in socket	-12.84	-31.94	19.10
	Partial in socket	-8.51	-36.11	27.60
	1 foam in socket	-10.74	-42.10	31.36
	2 foam in socket	-11.45	-43.39	31.95
Transfer function: Sacrum to right (3/1)	No Excitation	8.25	6.39	1.86
	Fully in socket	-7.34	-24.33	16.99
	Partial in socket	-6.88	-23.96	17.08
	1 foam in socket	-6.51	-21.58	15.07
	2 foam in socket	-6.63	-21.59	14.96

4.2 Pig 1 experiment: Effect of dysplasia using tapping and scratching as an input

4.2.1 Methods

Here, the animal preparations were the same as previous experiments. The experimental set up is shown in Figure 42. The experimental steps were as follows:

- The acoustic stimulation was performed by tapping and scratching (instead of the iLouder mini exciter).
- Accelerometers 2 and 3 were placed over medial left and right epicondyles, respectively.
- Finger tapping and scratching was done on sacrum. Tapping was also done by a metal bar on a coin attached to sacrum.

4.2.2 Results and Findings

Stimulus: Tapping with the finger directly on the sacrum

Power spectral density (PSD):

Figure 58 shows PSD for the left and right sensors.

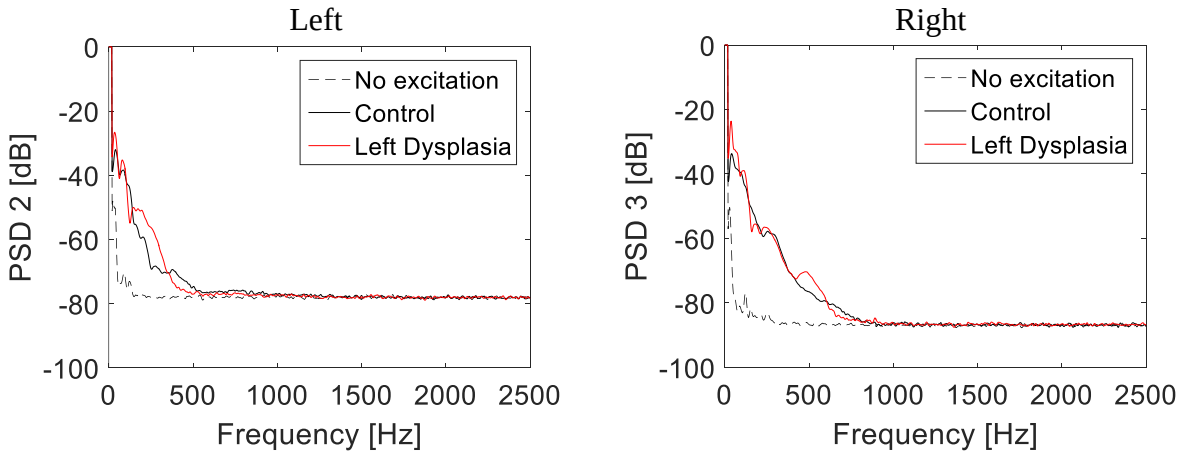

Figure 58: Power spectrum density for left and right sensors

Findings:

The data of Figure 58, and Table 18 suggests that drop in transmission with dysplasia is not clearly noticeable.

Average PSD of sensor 2, and 3 in 2 frequency bands and the PSD ratio between bands is shown in Table 18.

Table 18: Average PSD of sensor 2 and 3 in 2 frequency bands and the PSD ratio between bands

	Joint state	Average PSD in Band 1 (5-240 Hz)	Average PSD in Band 2 (300-1200 Hz)	PSD ratio between Band 1 and 2
Left (PSD 2)	No excitation	-68.04	-77.97	9.93
	Control	-45.41	-75.49	30.08
	Left Hip Dysplasia	-42.42	-76.25	33.82
Right (PSD 3)	No excitation	-74.49	-86.68	12.19
	Control	-43.76	-81.08	37.31
	Left Hip Dysplasia	-42.17	-80.61	38.44

Transfer function: Figure 59 shows the TF between left and right sensors.

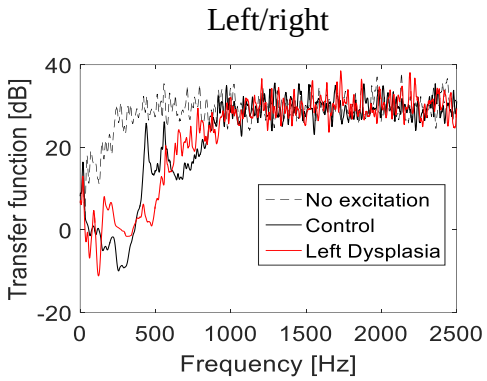

Figure 59: Transfer function between left and right sensors

Findings: The data of Figure 59, and Table 19 suggests the following:

- A drop in transfer function with dysplasia is visible around 400-500 Hz.
- Maximum loss in sound transmission was 20 dB in this region.

Average TF in 2 frequency bands and the TF ratio between bands is shown in Table 19.

Table 19: Average transfer function in 2 frequency bands and the TF ratio between bands

	Joint state	Average TF in Band 1 (5-240 Hz)	Average TF in Band 2 (300-1200 Hz)	TF ratio between Band 1 and 2
Transfer function: Left/Right (2/3)	No excitation	16.97	29.17	-12.20
	Control	-0.19	19.21	-19.40
	Left Hip Dysplasia	1.28	18.52	-17.24

Stimulus: Tapping on a coin with a metal bar

Power spectral density (PSD):

Figure 60 shows the PSD for left sensor (run 1) and right sensor (run1 and run 2).

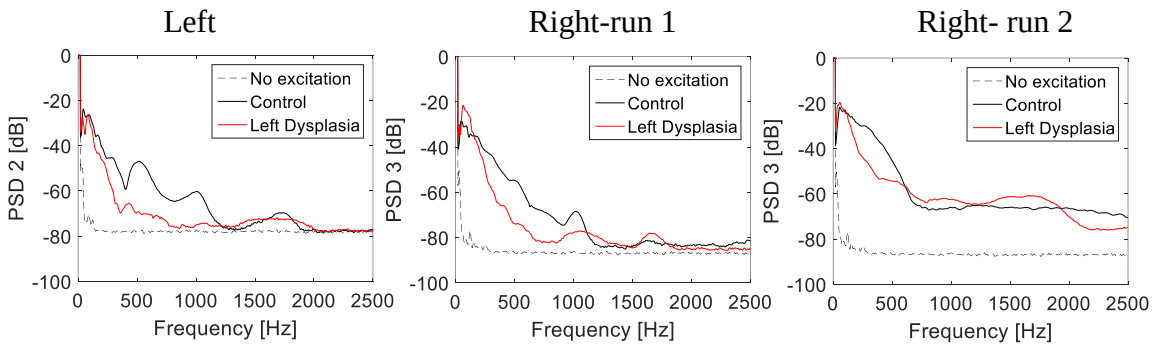

Figure 60: Power spectrum density for left sensor (run 1) and right sensor (run1 and run 2).

Findings: The data of Figure 60, and Table 20 suggests the following:

- There was a drop in transmission with dysplasia on both sensors. The drop in the right sensor was not expected. This drop may be due to small dysplasia at the joint or due to experimental error.

Average PSD of sensor 2 and 3 in 2 frequency bands and the PSD ratio between bands is shown in Table 20.

Table 20: Average PSD of sensor 2 and 3 in 2 frequency bands and the PSD ratio between bands

	Joint state	Average PSD in Band 1 (5-240 Hz)	Average PSD in Band 2 (300-1200 Hz)	PSD ratio between Band 1 and 2
Left (PSD 2)	No excitation	-68.04	-77.97	9.93
	Control	-31.42	-59.24	27.82
	Left Hip Dysplasia	-35.52	-72.32	36.81
Right-run1 (PSD 3)	No excitation	-74.49	-86.68	12.19
	Control	-32.68	-65.50	32.83
	Left Hip Dysplasia	-31.01	-76.12	45.11
Right-run2 (PSD 3)	No excitation	-74.49	-86.68	12.19
	Control	-25.07	-57.47	32.40
	Left Hip Dysplasia	-28.10	-59.29	31.19

Transfer function: Figure 61 shows TF between left and right sensors.

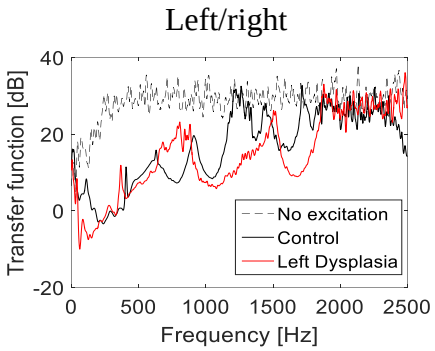

Figure 61: Transfer function between left and right accelerometers.

Findings: The data of Figure 61, and Table 21 suggests the following:

- A higher drop in transmission at the left side was noticed at between 1200-1400 Hz.
- The drop was as high as 20 dB.

Average TF in 2 frequency bands and the TF ratio between bands is shown in Table 21.

Table 21: Average transfer function in 2 frequency bands and the TF ratio between band

	Joint state	Average TF in Band 1 (5-240 Hz)	Average TF in Band 2 (300-1200 Hz)	TF ratio between Band 1 and 2
Transfer function: Left/Right (2/3)	No excitation	16.97	29.17	-12.20
	Control	3.21	10.28	-7.07
	Left Hip Dysplasia	-2.96	10.24	-13.20

Stimulus: Scratching on sacrum with a fingernail

Power spectral density (PSD):

Figure 62 shows PSD for left and right sensors.

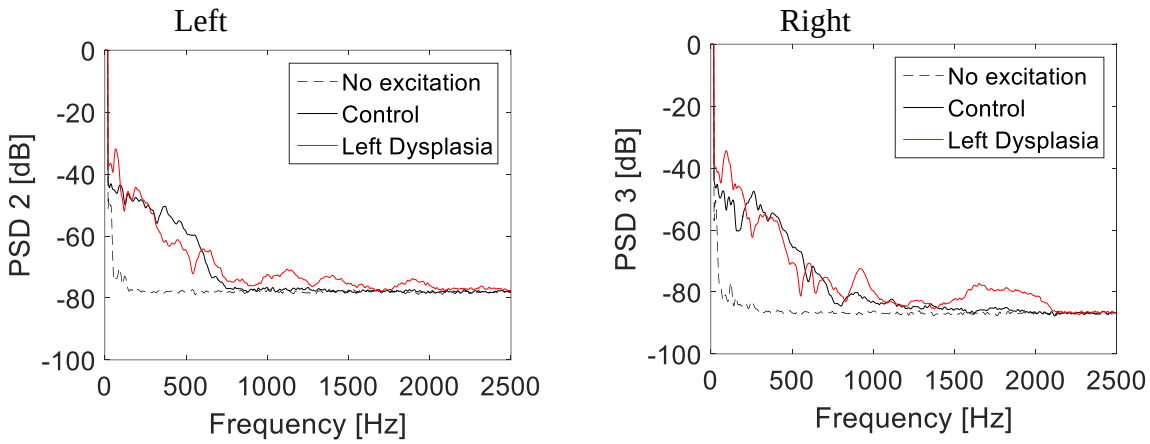

Figure 62: Power spectrum density for left and right sensors.

Findings: The data of Figure 62, and Table 22 suggests the following:

- Small drop in PSD in the left sensor.

Average PSD of sensor 2 and 3 in 2 frequency bands and the PSD ratio between bands is shown in Table 22.

Table 22: Average PSD of sensor 2 and 3 in 2 frequency bands and the PSD ratio between bands

	Joint state	Average PSD in Band 1 (5-240 Hz)	Average PSD in Band 2 (300-1200 Hz)	PSD ratio between Band 1 and 2
Left (PSD 2)	No excitation	-68.04	-77.97	9.93
	Control	-43.89	-69.52	25.62
	Left Hip Dysplasia	-40.76	-69.34	28.58
Right (PSD 3)	No excitation	-74.49	-86.68	12.19
	Control	-48.92	-74.51	25.59
	Left Hip Dysplasia	-41.69	-74.36	32.67

Transfer function: Figure 63 shows TF between left and right sensors.

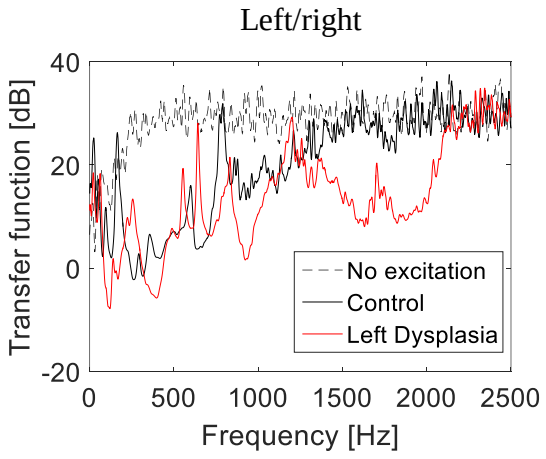

Figure 63: Transfer function between left and right sensor

Findings: The data of Figure 63, and Table 23 suggests the following:

- Drop in transfer function (~10 dB) with dysplasia was noticeable around 1300-2000 Hz.
- This stimulus may have utility but improvements are needed.

Average TF in two frequency bands and the TF ratio between bands is shown in Table 23.

Table 23: Average transfer function in 2 frequency bands and the TF ratio between bands

	Joint state	Average TF in Band 1 (5-240 Hz)	Average TF in Band 2 (300-1200 Hz)	TF ratio between Band 1 and 2
Transfer function: Right/left (2/3)	No excitation	16.97	29.17	-12.20
	Control	10.60	12.42	-1.82
	Left Hip Dysplasia	4.42	9.44	-5.02

4.3 Pig 1 experiment: tuning fork experiment

4.3.1 Methods

The experimental set up is shown in Figure 64. The experimental steps were as follows:

- Place fork at sacrum and apply 200 gm of static force.
- Place sensor 1 at the sacrum.
- Place sensor 2 and 3 at the patella. Measure transmitted sounds when the fork is ringing and when it is not.
- Calculate the signal to noise ratio
- Document transmission changes in the healthy and displaced hip.

Control Left hip dysplasia

Figure 64: Photograph showing the set up for tuning fork experiment.

4.3.2 Results and Findings

Signal to noise ratio and effect of dysplasia (Electronic tuning fork: 128 Hz)

Figure 65 shows PSD at sacrum, left hip, and right hip for applying 128 Hz electronic tuning fork.

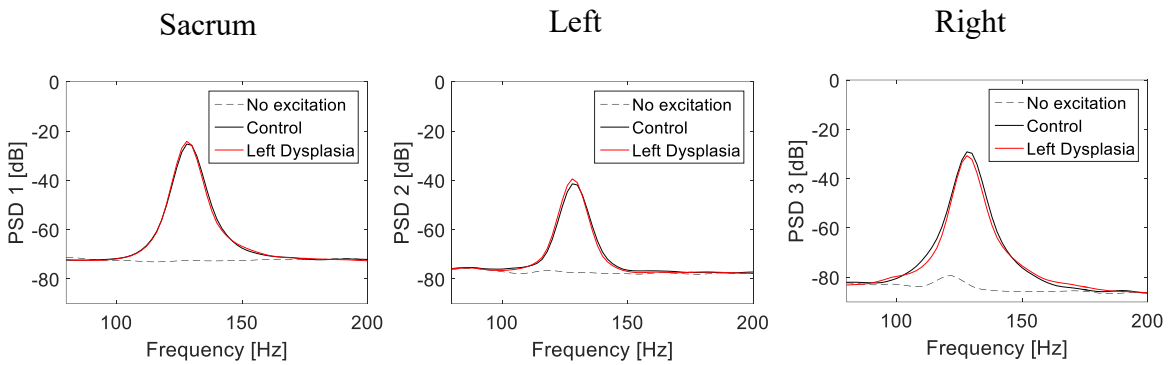

Figure 65: Power spectrum density (PSD) at sacrum, left hip, and right hip (Electronic tuning fork: 128 Hz)

Findings:

The data of Figure 65 suggests that PSD changes with left dysplasia were not noticeable.

Signal to noise ratio and effect of dysplasia (manual tuning fork: 128 Hz):

Figure 66 shows PSD at sacrum, left hip, and right hip for applying 128 Hz rated manual tuning fork.

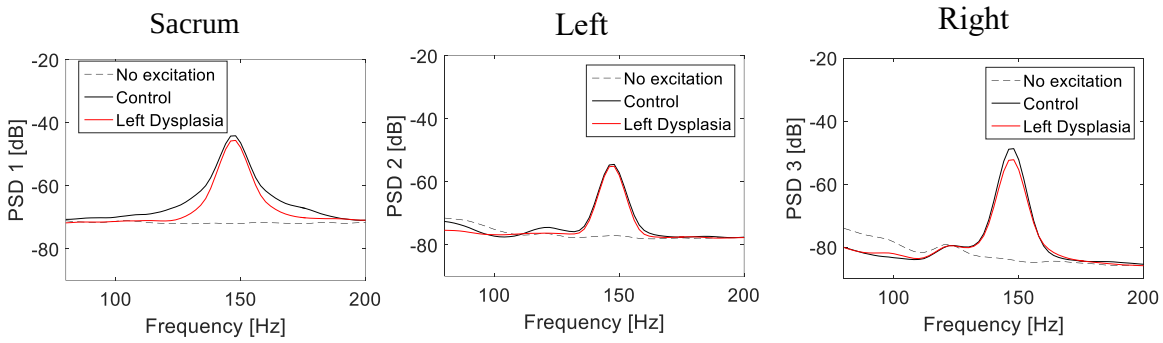

Figure 66: Power spectrum density (PSD) at sacrum, left hip, and right hip (manual tuning fork: 128 Hz)

Findings:

The data of Figure 66 suggests that the spectral changes with dysplasia were not noticeable.

Signal to noise ratio and effect of dysplasia (manual tuning fork: 256 Hz):

Figure 67 shows PSD at sacrum, left hip, and right hip for applying 256 Hz rated manual tuning fork.

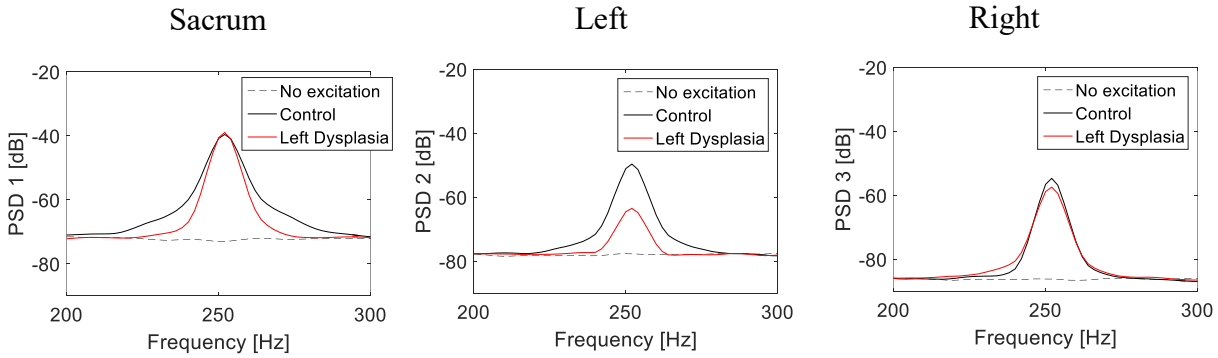

Figure 67: Power spectrum density (PSD) at sacrum, left hip, and right hip (manual tuning fork: 256 Hz).

Findings:

The data of Figure 67 suggests that spectral change with dysplasia were clearly noticeable in PSD2.

Signal to noise ratio and effect of dysplasia (manual tuning fork: 512 Hz):

Figure 68 shows PSD at sacrum, left hip, and right hip for applying 512 Hz rated manual tuning fork.

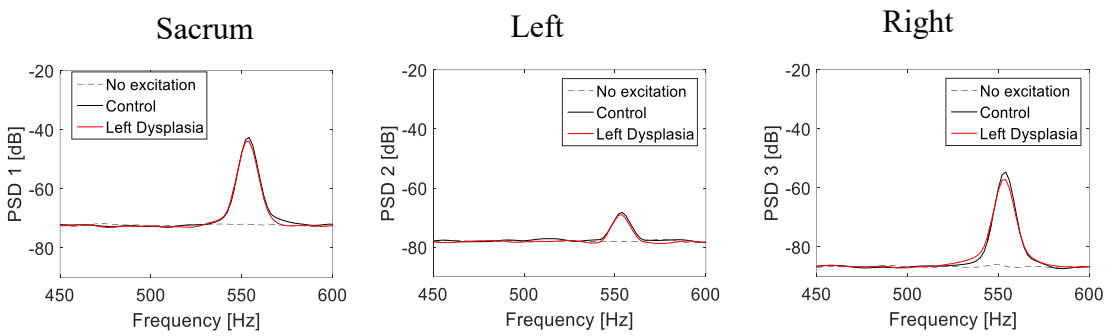

Figure 68: Power spectrum density (PSD) at sacrum, left hip, and right hip (manual tuning fork: 512 Hz)

Findings: The data of Figure 68 suggests that the spectral changes with dysplasia were not noticeable.

Signal to noise ratio and effect of dysplasia (manual tuning fork: 1024 Hz): Figure 69 shows PSD at sacrum, left hip, and right hip for applying 1024 Hz rated manual tuning fork.

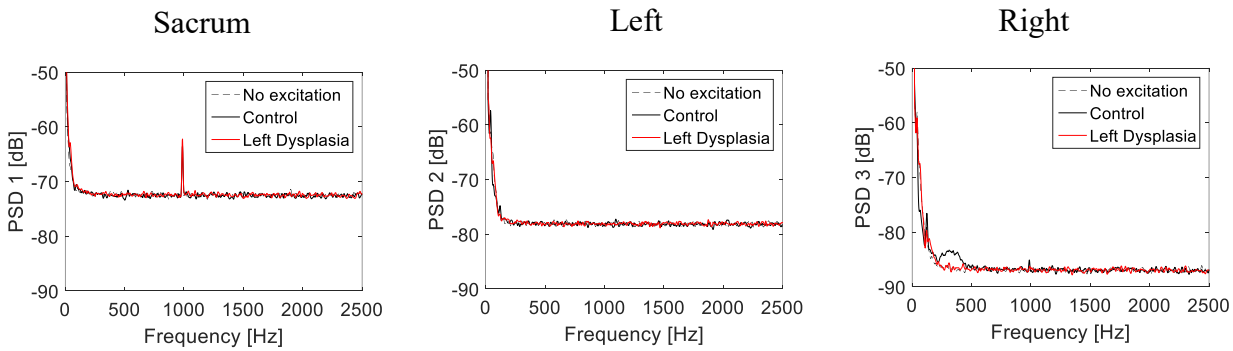

Figure 69: Power spectrum density (PSD) at sacrum, left hip, and right hip (manual tuning fork: 1024 Hz)

Findings:

The data of Figure 69 shows weak signals at measurement points. This makes it difficult to see effects of dysplasia.

Signal to noise ratio and effect of dysplasia (manual tuning fork: 2048 Hz):

Figure 70 shows PSD at sacrum, left hip, and right hip for applying 2048 Hz rated manual tuning fork.

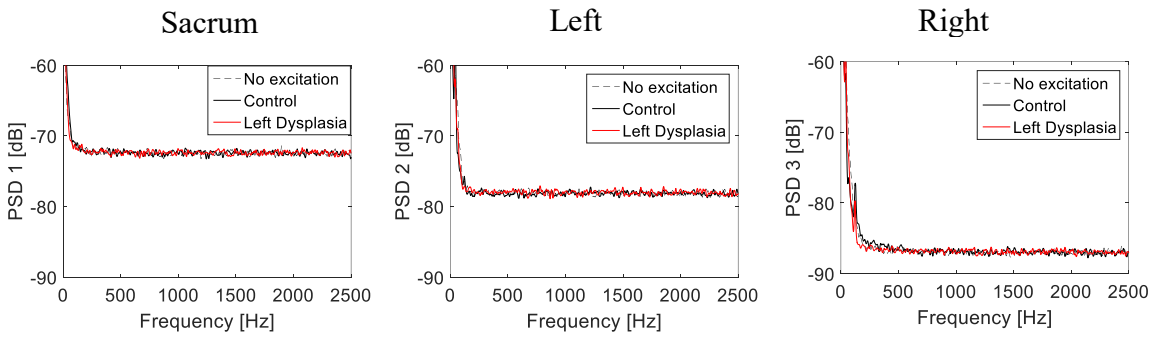

Figure 70: Power spectrum density (PSD) at sacrum, left hip, and right hip (manual tuning fork: 2048 Hz)

Findings: The data of Figure 70 shows weak signals at measurement points. This makes it difficult to see effects of dysplasia.

4.4 Pig 2 experiment: Effect of surgery and hand pulling on sound transmission

4.4.1 Methods

Here, a second pig (pig 2) was acquired. The animal preparations were the same as previous experiment described in section 4.1. The experimental set up is shown in Figure 42, and 54. The experimental steps were the same as described in section 4.1.

4.4.2 Results and Findings

Figure 71 and 72 shows PSD at the left and right hips for eight cases (below) and TF from right hip to left hip before and after surgery in the left hip.

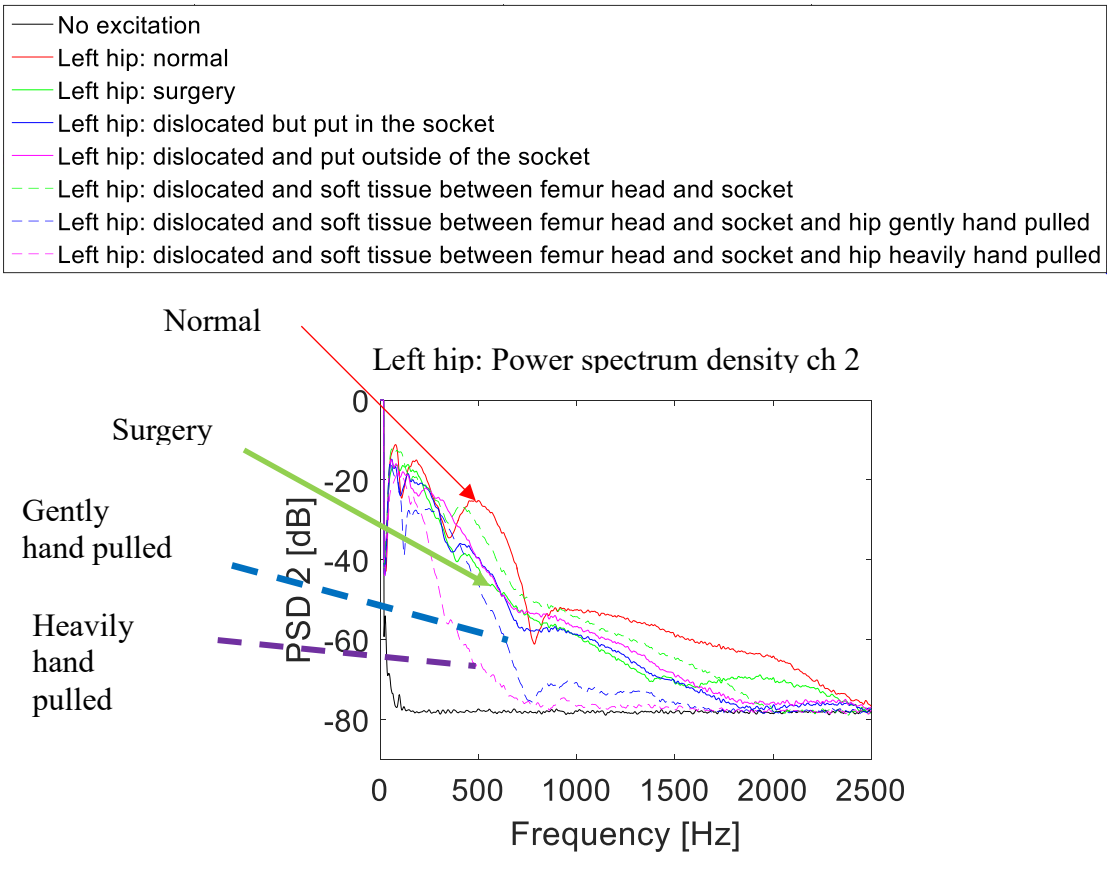

Figure 71: Description and legend for eight cases of experiment. Power spectrum density (PSD) at left hip.

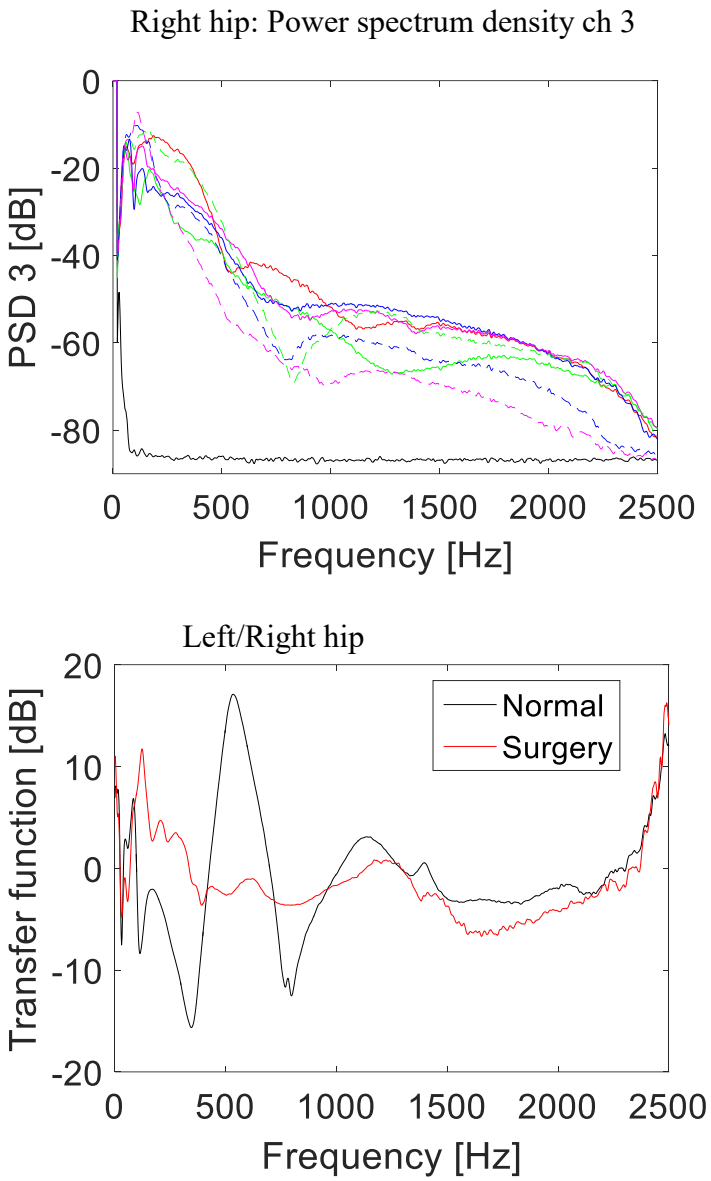

Figure 72: Power spectrum density (PSD) at right hip. Transfer function from right hip to left hip.

Findings: The data of Figure 71 and Figure 72 suggests the following:

- Effect of surgery: Drop in power spectrum density is noticeable at both left and right hips.
- Effect of hand pulling: Drop in power spectrum density is noticeable at both left and right hip. More drop was observed at left hip. Also, heavy (i.e. increased) hand pulling created more drop in PSD compared to the gently hand pulled case.

4.5 Conclusions

There was significant transmission drop (in the affected side) with dysplasia (in this pig model) for a frequency band of ~ 300-1200 Hz. This was seen in both approaches of inducing dysplasia. Certain energy ratios may correlate with dysplasia in the absence of an unaffected side. This may be useful for detecting bilateral dysplasia. Acoustic stimulation by tapping with metallic object on a coin placed at the sacrum is likely to generate acoustic stimulus in the desired frequency band. Scratching may also have utility. But both techniques may need further improvement or automation (e.g. using spring loaded thumper, etc). Broad band forcing with a mini shaker is likely more consistent and allows higher SNR. There were cases where a drop in transmission with hand pulling was seen in both left and right sensors. This needs further investigation.

CHAPTER 5: RECOMMENDATION AND FUTURE WORK

5.1 Recommendation

Table 24 shows the advantages and disadvantages of different exciters used in our experiment. Results are showing that although every exciter has some advantages, iLouder exciter has maximum advantages compared to other exciters.

Table 24: Advantages and disadvantages of exciters used in our experiment

	Advantages	Disadvantages
iLouder exciter	• Low sensitivity to load changes (up to 600g) • Light weight (~200g) • Output/Input PSD is high • Can operate on a broad frequency range • Inexpensive (<$10)	• Maximum input wattage is limited to 0.75W. However, output stimulus amplitude is sufficient.
Large exciter	• Low sensitivity to load changes (up to 800g)	• Heavy weight (907 grams) • Expensive compared to other exciters > $1000
Small exciter	• Light weight (120 g) • Can operate in a broad frequency range • Inexpensive (< $10)	• Sensitive to load changes for loads > 150g

Medium exciter	• Can operate in a broad frequency range • Inexpensive (<$10)	• Comparatively heavy weight (388g)
Electronic tuning fork	• Light weight (133g) • Easy to use	• Operates at one frequency only • Sensitive to load changes. Applied static load is limited to 100-200g • Expensive (~$400)
Manual tuning fork	• Light weight (44g) • Inexpensive (<$10)	• Operates at one frequency only • Sensitive to load changes. Applied static load is limited to 100-200g
Tapping	• No cost for excitation	• Low SNR • Stimulus frequency can be too narrow.
Scratching	• No cost for excitation	• Low SNR • Stimulus frequency can be too narrow.

5.2 Future work

The future work includes the following:

- Repeating experiments in more animals.
- Improving scratching and tapping approaches.
- Explore the coherence and phase as additional features.
- Filling the joint with fluid to have more realistic conditions.
- Test amplifier and background noise levels.
- Finding more alternatives for inexpensive sensors.

APPENDIX A: TRANSMISSION THOUGH AN ADULT HIP JOINT

Objectives: The objective of this study is to investigate the following:

- Repeatability at different excitation locations.
- Effect of applying different loads (low, Med, High) at the excitation point.
- Effect of excitation location (i.e., at the patella and greater trochanter).

Methods: The experimental conditions and test protocol steps were the following:

- Participant: One subject (adult male, BMI=23.1) in the sitting position
- Excitation (i.e. stimulus) locations and loading:

Stimulus was applied at the great trochanter or patella.

Different static load levels were applied on the shaker as it transmits the input acoustic excitation to the skin. The loads are believed to be in the 1-3 lb range, but were not measured because a proper load cell was not available. The large shaker was used in this study.

- Sensors: Three uni-axial accelerometers were attached to the skin with a double sided medical tape.
- Sensor locations: One sensor was rigidly attached to the shaker at the excitation point (Sensor1). Two extra sensors were located at the iliac crest (Sensor 2 and 3) (See Figure 73).
- Data acquisition and analysis: A computer-controlled system was constructed to generate and measure acoustic signals. The computer was connected to a data acquisition module (Model: NI USB-6211, National Instruments, Austin, TX). A MATLAB code was written to: (a) generate a band-limited white noise (50-2500 Hz) signal that excites the shaker, (b) acquire three acoustic signals, and (c) calculate the transfer function, phase and coherence between the three acquired signals.

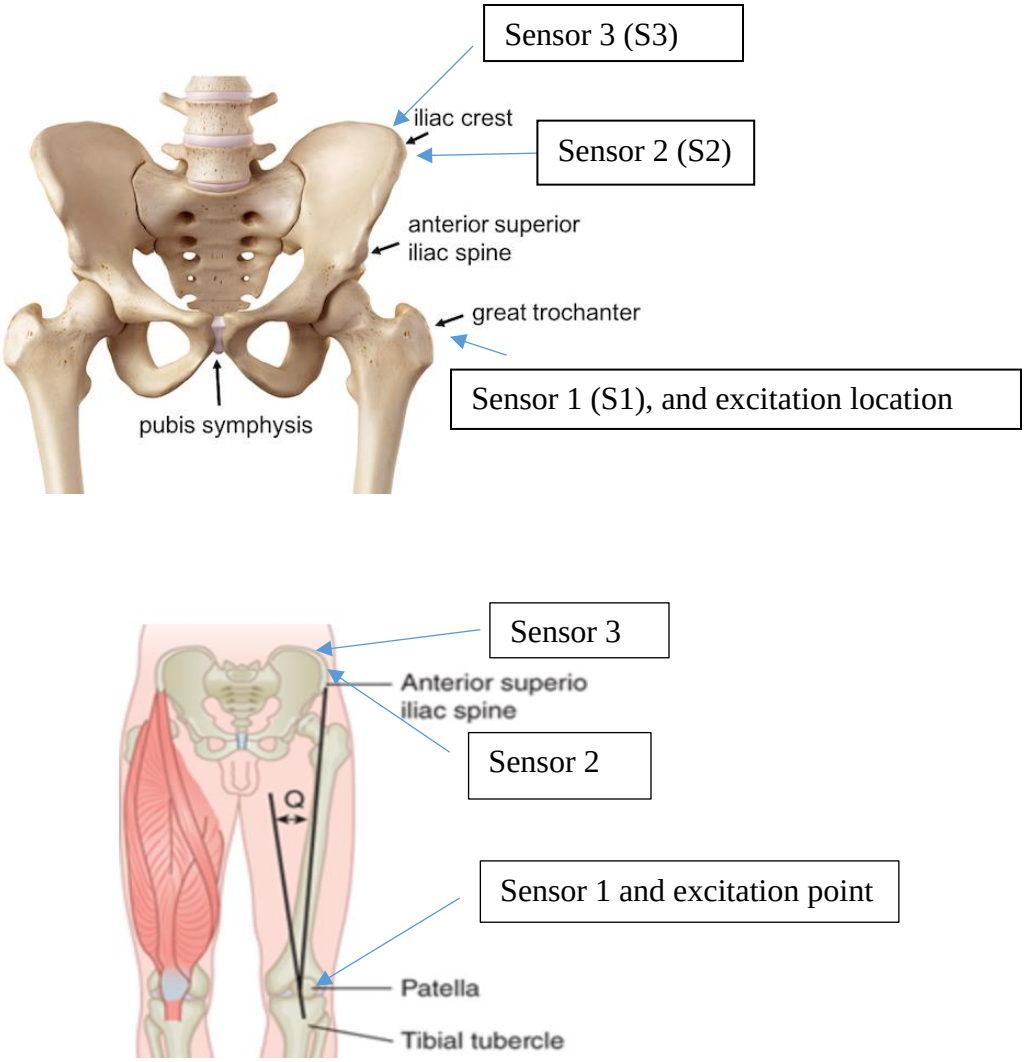

Figure 73: Two accelerometers were placed on the iliac spine. In the first figure, the shaker and one accelerometer were placed at greater trochanter. In the second figure, the shaker and accelerometer (sensor 1) were placed at the patella of the subject.

Results and Findings:

Figure 74 shows transfer function, phase, and coherence for applied light load at patella.

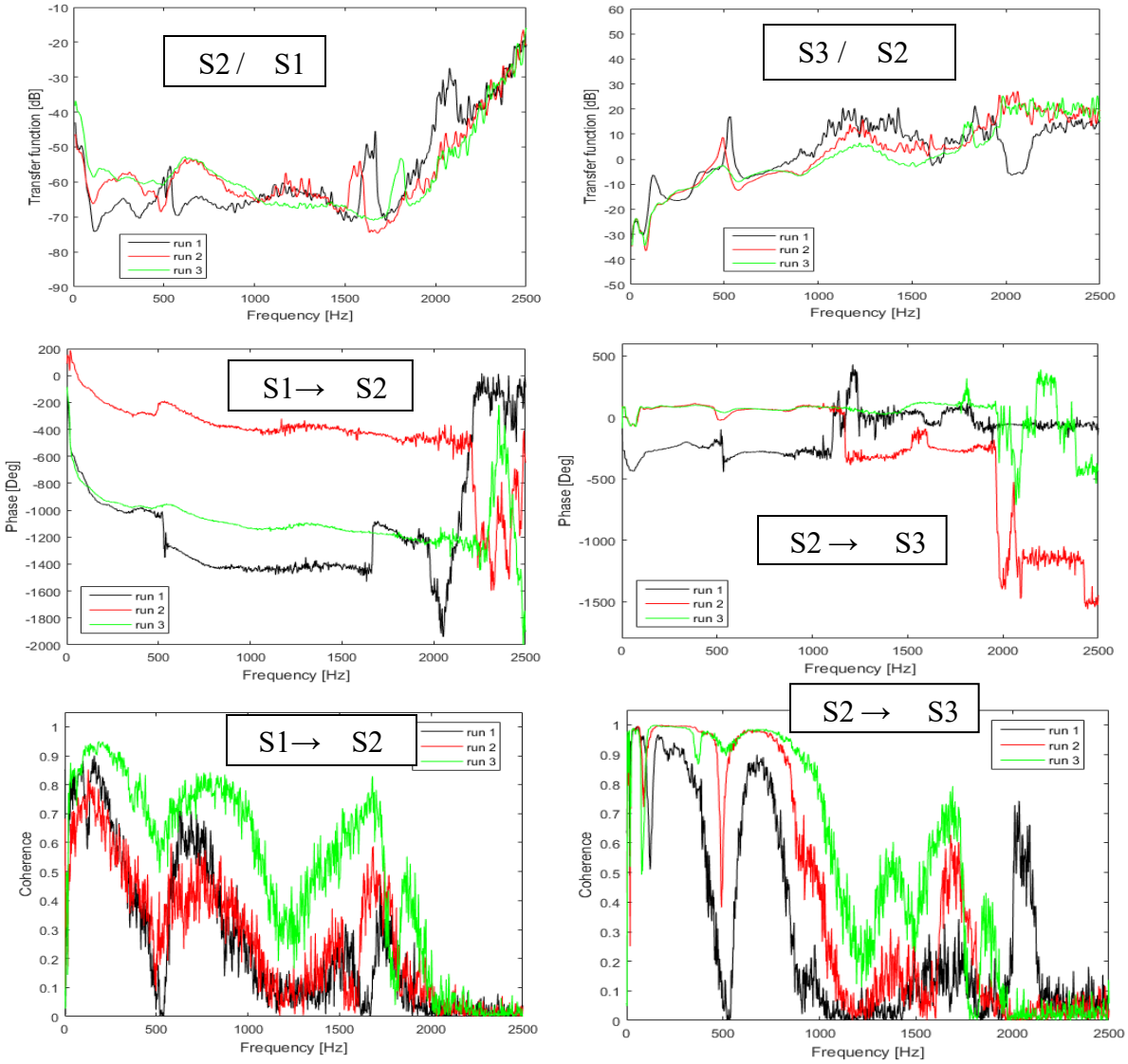

Figure 74: Transfer function, phase and coherence to check repeatability for applying light load at patella.

Findings – Repeatability at patella: The data of Figure 74 suggests the following:

- Transfer function: Run 2 and 3 were similar. Run 1 was different from run 2 and 3. Highest variability is between run 1 on one hand and 2&3 (order of 10 dB).
- Phase: Run 1, 2 and 3 appear shifted by n x 360 degrees.

- Coherence: Higher values were observed for run 3. Hence, data from run 3 is likely more reliable.

Coherence is lowest > ~1500 Hz. Hence, data > 1500 Hz is not very reliable.

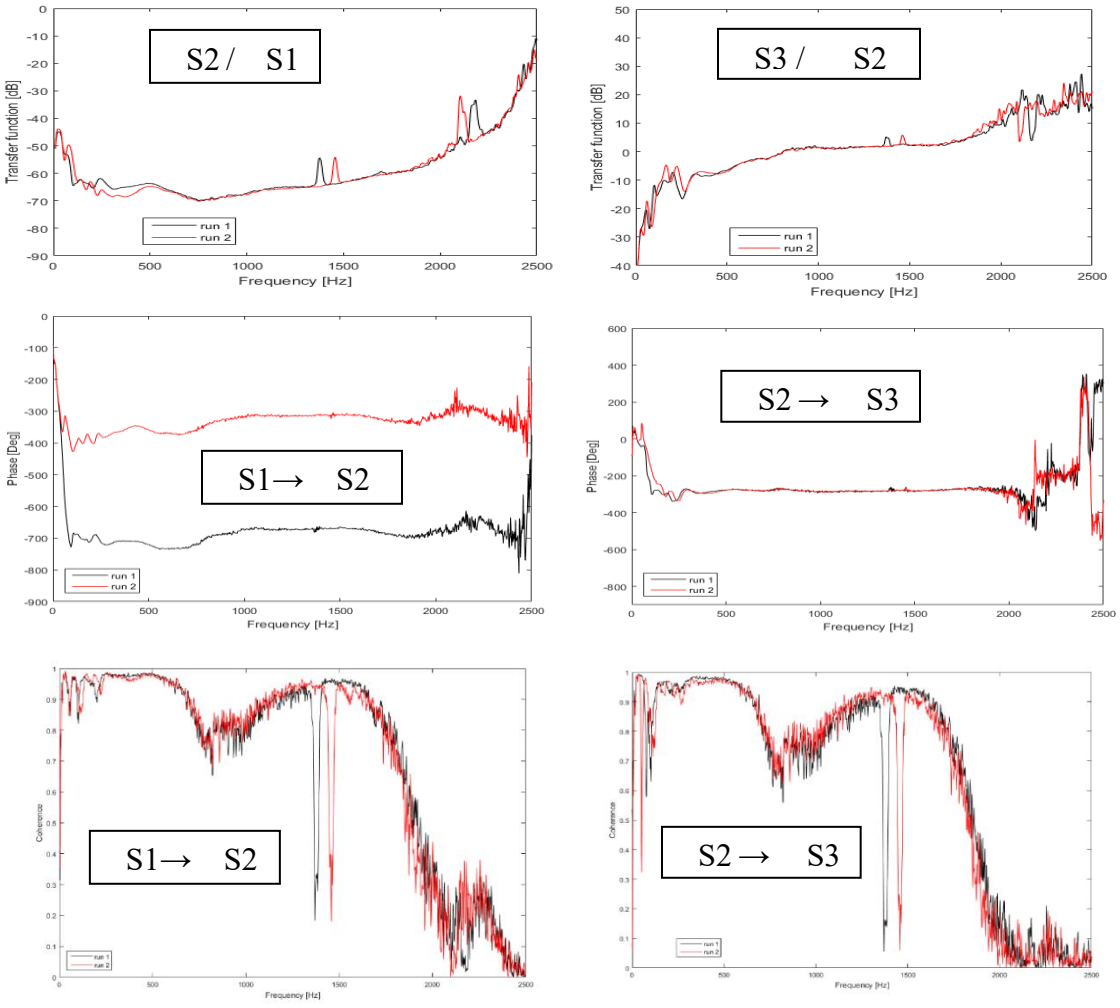

Figure 75: Transfer function, phase and coherence to check repeatability for applying heavy load at greater trochanter

Figure 75 shows transfer function, phase, and coherence for applied heavy load at greater trochanter.

Findings– Repeatability at greater trochanter: The data of Figure 75 suggests the following:

- Transfer function was repeatable for all cases.
- Phase was repeatable.
- Coherence was repeatable.

Figure 76 shows transfer function, Phase and coherence to study the effect of exciting at patella vs greater trochanter.

Findings – Effect of excitation location at patella vs. greater trochanter: The data of Figure 76 suggests the following:

- Higher transfer function (50-1000 Hz) was achieved for patella (light and medium load) compared to the greater trochanter which is unexpected as Patella is further away from greater trochanter.
- Phase difference was minimal for greater trochanter without shorts case.
- Greater trochanter with and without shorts showed the best coherence.

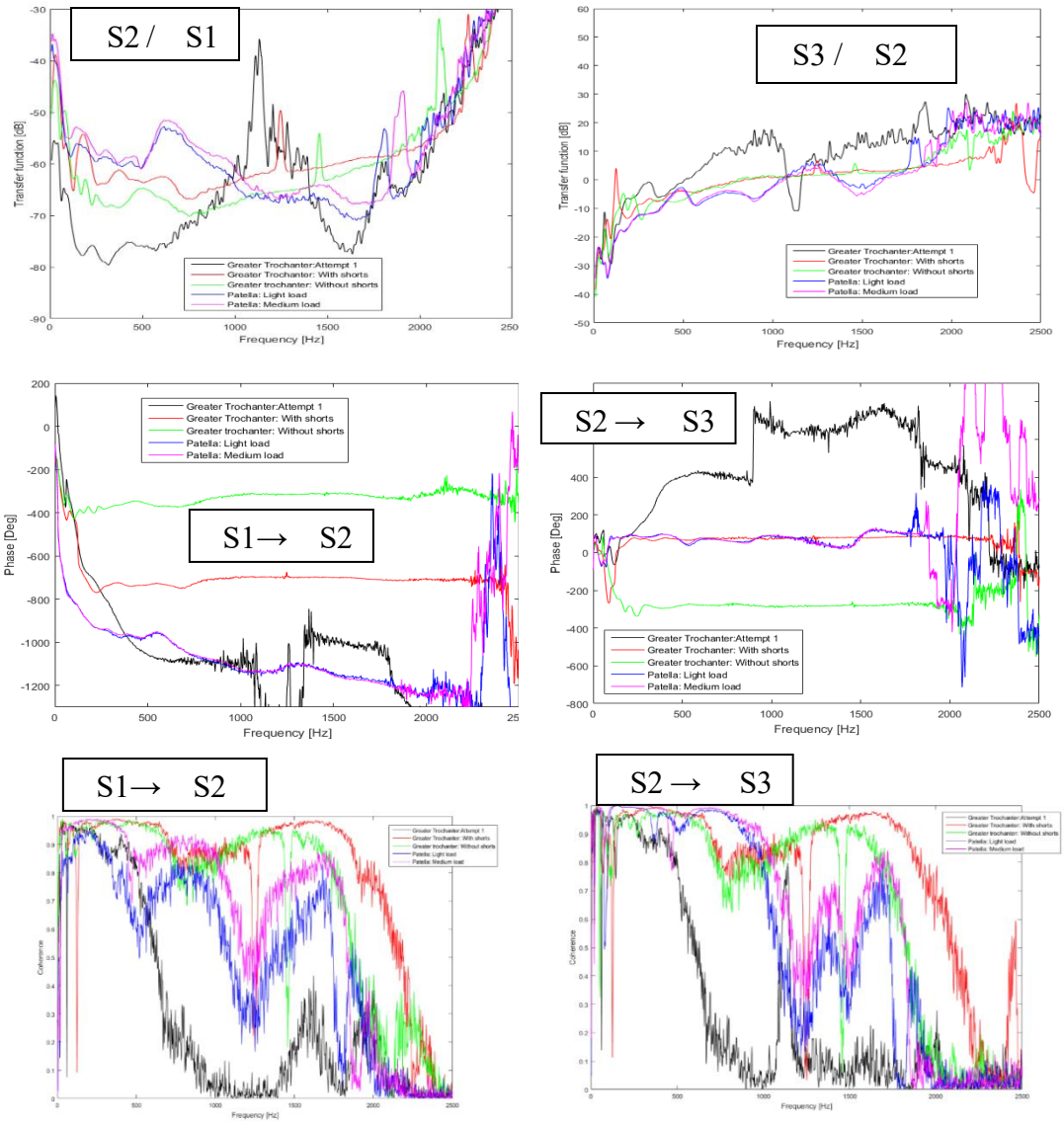

Figure 76: Transfer function, Phase and coherence to study the effect of excitation point (patella vs greater trochanter)

APPENDIX B: TRANSMISSION THOUGH CHICKEN LEGS

Objective: The objective of this study is to investigate the sound transmission across normal hip, dysplastic hip and severely displaced hip in a cooked chicken model.

Methods:

Sensor 1 was rigidly attached to the shaker, which was applied at the excitation point (equivalent to human sacrum). Sensor 2 was placed on the left and right hip, respectively. The experiment was performed during 2 different days. The chicken hips were not symmetrical (one was bend more than the other). Figure 77 shows the sensors, exciter location and experimental set up.

Figure 77: Experimental set up, sensors and exciter location for the chicken experiment.

Day 1 experiments were the following:

1st experiment: Both hips were normal.

2nd experiment: Right hip was displaced (Sensor 3).

Day 2 experiments were the following:

1st experiment: Location of Sensor 3 across displaced right hip was changed to make sure that the sensor is rigidly attached on top of hip bone.

2nd experiment: Now, both right hip and left hip was displaced

3rd experiment: Left hip was severely displaced.

Results and Findings:

Figure 78 shows comparison of transfer function, phase, and coherence between normal hip, displaced right hip (sensor 3 was added with it), displaced right hip where sensor 3 was relocated, displaced right and left hip, displaced right hip and severely displaced left hip.

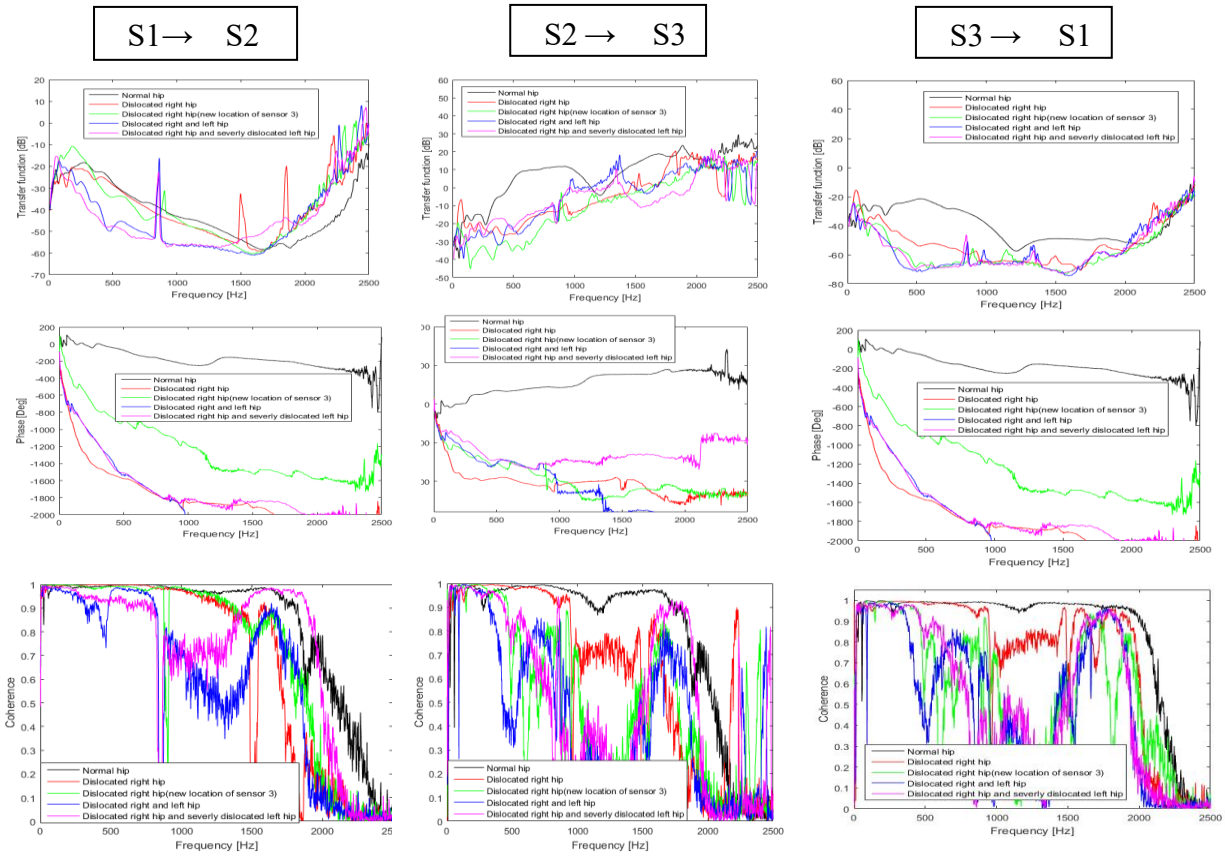

Figure 78: Comparison of transfer function, phase, and coherence between normal left and right hip, normal left hip and displaced right hip, normal left hip and displaced right hip where sensor 3 was relocated, displaced right and left hip, displaced right hip and severely displaced left hip.

Findings: The data of Figure 78 suggests the following:

- Better transfer function (between sensor 2 and 3) was see for normal hips (500-1000 Hz) whereas different degree of dislocated hips showed reduction in transfer function.
- Phase difference increased (between sensor 2 and 3) with dysplasia. Phase difference was at a maximum with dislocated right and left hip.
- Better coherence (between sensor 1&2, 2&3 and 1&3) was achieved with normal hips whereas dislocated right and left hip had lowest coherence.

APPENDIX C: SYSTEM MINIATURIZATION

Objective: The objective of this study is to investigate the ability of a miniaturized set up to detect transmitted signals.

Methods:

A white noise was running using a mp3 file. Then, a piezo disk was used as an exciter. Two sensors were placed into two fingers. Those are also connected to channel 0 and 1. The signal at the stimulus point was not measured. Signals were measured and FFT was calculated using LabVIEW. Figure 79 shows the experimental set up, sensors and exciter location of this study. The following three different cases were considered for the stimulus location:

Case 1: Exciter was in the middle of two fingers.

Case 2: Exciter was placed closer to right finger.

Case 3: Exciter was placed closer to left finger.

Figure 79: Experimental set up, sensors and exciter location for system miniaturization experiment. Case 1, 2, and 3 are shown from left to right in the Figure.

Results and Findings:

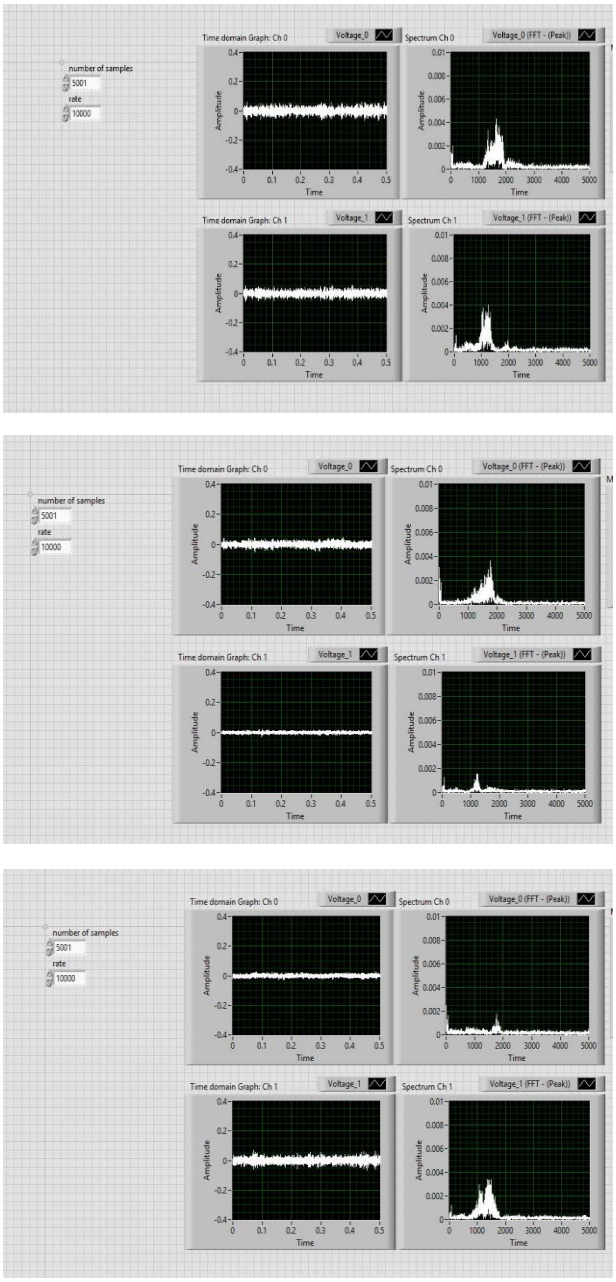

Figure 80: Time domain and frequency domain of 2 sensors for three different exciter positions. The first figure (case 1) shows the results when exciter was in the middle of two fingers. The second figure (case 2) shows the results when exciter was moved to the right relative to case 1. Third figure (case 3) shows the results when exciter was moved to the left relative to case 1. For each case the right signal is shown above the left.

Figure 80 shows time and frequency domain of 2 sensors for three different exciter position.

Findings: The data of figure 80 suggests the following:

- For case 1, when exciter was in the middle of two fingers, the spectrum was similar for channel 0 and 1.
- For case 2, when exciter was moved to the right, channel 0 (i.e., right sensor) spectrum was higher than channel 1 spectrum.
- For case 3, when exciter was moved to the left, channel 1 (i.e., left sensor) spectrum was higher than channel 0 spectrum.

These results show that our miniaturized set up has ability to detect transmitted sound. However, the amplitude of transmitted sounds were very low. Hence, a system that can input higher sound amplitudes is needed.

LIST OF REFERENCES

C. Price and B. Ramo, "Prevention of hip dysplasia in children and adults," *Orthop Clin North Am,* vol. 43, pp. 269-279, 2012.

D. Jones, “Neonatal Detection Of Developmental Dysplasia Of The Hip (DDH),” *J Bone Joint Surg [Br]*, vol. 80, pp. 943-945, 1998.

F. Moore , “Examining infants’ hips-can it do harm?,” *J Bone Joint Surg [Br]*, vol. 7l, pp. 4-5, 1989.

M. Uzel, G. Ergun, and H. Ekerbicer,“The knowledge and attitudes of the primary care physicians on developmental dysplasia of the hip,” *Saudi Medical Journal*, vol. 28, pp. 1430–1434, 2007.

H. Mansy, T. Royston and R. Sandler, "Use of abdominal percussion for pneumoperitoneum detection," *Medical and Biological Engineering and Computing,* vol. 40 (4), pp. 439-446.

H. Mansy, R. Balk, W. Warren, T. Royston and Z. Dai, "Pneumothorax effects on pulmonary acoustic transmission," *Journal of applied Physiology*, 2015.

H. Mansy, S. Hoxie, N. Patel and R. Sandler, "Computerised analysis of auscultatory sounds associated with vascular patency of haemodialysis access," *Medical and Biological Engineering and Computing,* 2005.

F. Khalili, P. Gamage, R. Sandler and H. Mansy, "Adverse hemodynamic conditions associated with mechanical heart valve leaflet immobility," *Bioengineering,* 2018.

Taebi and H. Mansy, "Effect of Noise on Time-frequency Analysis of Vibrocardiographic Signals," *Journal of bioengineering & biomedical science,* 2016.

T. Hassan, L. Mckinney, R. H. Sandler, A. Kassab, C. Price, F. Moslehy and H. A. Mansy, "An Acoustic Approach for Detection of Developmental Dysplasia of Hip," in *IEEE Signal Processing in Medicine and Biology Symposium (SPMB)*, Philadelphia, 2018.

J. Richardson, C. Foo, M. Stone and G. Bennet, "Attenuation of sound transmission in congenital dislocation of the hip," *J Bone Joint Surg*, vol. 69, p. 850, 1987.

K. Kwong, X. Huang, J. Cheng, and J. Evans, "Acoustic transmission in normal human hips: structural testing of joint symmetry," *Medical Engineerng & Physics*, vol. 25, pp. 811-816, 2003.

K. Kwong, X. Huang , J. Cheng , and J. Evans, "New Technique for early screening of developmental dysplasia of the hip: pilot study," *Journal of Pediatric Orthopaedics*, vol. 23, pp. 347-351, 2003.

M. I. S. Kapicioglu and F. Korkusuz, "Diagnosis of Developmental Dislocation of the Hip," *Clinical Orthopaedics and Related Research*, vol. 466, pp. 802-808, 2008.

P. Stoica and R. Moses, Spectral Analysis of Signals, Prentice Hall, 2005.

H. Vold, J. Crowley, and G. T. Rocklin. "New Ways of Estimating Frequency Response Functions," *Sound and Vibration*, vol. 18, pp. 34–38, 1984.

R. N. Bracewell, *The Fourier Transform and Its Applications*.New York, USA: McGraw-Hill , 1983.

J. S. Bendat and A. G. Piersol, Random Data: Analysis and Measurement Procedures, Wiley-Interscience, 1986.

L. Laborie , I. Engesæter , T. Lehmann, F. Sera, C. Dezateux, L. Engesæter, and K. Rosendahl, "Radiographic measurements of hip dysplasia at skeletal maturity—new reference

intervals based on 2,038 19-year-old Norwegians," *Skeletal Radiol*, vol. 42, pp. 925-935, 2013.

U. Narayanan , K. Mulpuri , T. Lehmann, W. Sankar, N. Clarke, H. Hosalkar, and C. Price, "Reliability of a New Radiographic Classification for Developmental Dysplasia of the Hip," *Journal of Pediatric Orthopaedics*, vol. 35, pp. 478-484, 2015.